COHESIVE ZONE MODEL FOR FRACTURE CHARACTERISATION IN COMPOSITES
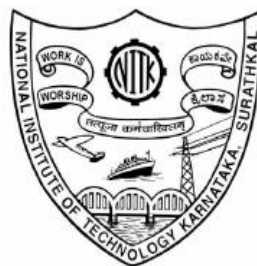
Thesis

Submitted in partial fulfilment of the requirements for the degree of

DOCTOR OF PHILOSOPHY

by

Kesava Rao B.

DEPARTMENT OF CIVIL ENGINEERING
NATIONAL INSTITUTE OF TECHNOLOGY KARNATAKA
SURATHKAL, MANGALURU – 575 025

JULY, 2019

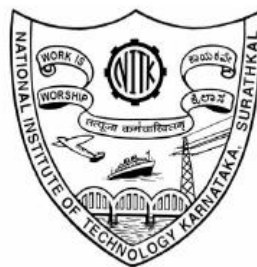# COHESIVE ZONE MODEL FOR FRACTURE CHARACTERISATION IN COMPOSITES

Thesis

Submitted in partial fulfilment of the requirements for the degree of

DOCTOR OF PHILOSOPHY

by

Kesava Rao B.
(CV14F14)

Under the Guidance of
Dr. A. S. Balu

DEPARTMENT OF CIVIL ENGINEERING
NATIONAL INSTITUTE OF TECHNOLOGY KARNATAKA
SURATHKAL, MANGALURU – 575 025
JULY, 2019

DECLARATION

I hereby *declare* that the Research Thesis entitled **"Cohesive Zone Model for Fracture Characterisation in Composites"** which is being submitted to the National Institute of Technology Karnataka, Surathkal in partial fulfilment of the requirements for the award of the Degree of **Doctor of Philosophy** in **Civil Engineering**, is a *bonafide* report of the research work carried out by me. The material contained in this Research Thesis has not been submitted to any University or Institution for the award of any degree.

(Kesava Rao B)
Register No.148056CV14F14
Department of Civil Engineering

Place: NITK, Surathkal
Date: 01-07-2019

CERTIFICATE

This is to *certify* that the Research Thesis entitled **"Cohesive Zone Model for Fracture Characterisation in Composites"** submitted by **Mr. KESAVA RAO B.** (Register Number: **148056CV14F14**) as the record of the research work carried out by him, is accepted as the Research Thesis submission in partial fulfilment of the requirements for the award of degree of Doctor of Philosophy.

Dr. A. S. Balu

Research Guide

(Signature with date and seal)

Prof. K. Swaminathan

Chairman - DRPC

(Signature with date and seal)

ACKNOWLEDGEMENT

ABSTRACT

Delamination between plies is the most common mode of failure in composite laminates, which occurs due to the presence of matrix cracks, free edges and notches. Prediction of such failure poses a challenging task as it overburdens the computational resources. Therefore, cohesive zone model (CZM) was introduced for representing fracture as a material separation across crack surface. In CZM, cracks and other material discontinuities can be represented using zero thickness fracture process zone in a finite element (FE) framework. Hence, it has become one of the most powerful computational models in predicting the crack initiation and propagation in composites. Further to improve the efficiency of the model, metamodel techniques were introduced to capture the delamination strength of composites. Nevertheless, most of the metamodels are inefficient for highly nonlinear problems and sometimes insensitive to the parameters.

Therefore, in this work, a novel CZM is developed based on high dimensional model representation (HDMR) to evaluate the fracture behavior of composites under different mode conditions. The proposed methodology involves the development of CZM using HDMR, implementation of traction-separation laws in FE model using a user-defined subroutine in Abaqus, and minimisation of error using optimisation techniques. An attempt has been made to reduce the computational effort in accurately capturing the delamination strength.

The proposed model is employed for capturing the steady state energy release rate (ERR) of a double cantilever beam (DCB) under Mode-I loading. The FE models have been created using HDMR-based response functions. Initially, the CZM is developed for predicting the delamination strength of 51 mm crack size DCB specimens, and the model is then used to predict the ERR variations of 76.2 mm crack size specimens. Subsequently, the numerical results of the developed DCB models are verified with the available experimental data for unidirectional composites (IM7/977-3). Then, the efficiency of the proposed model is demonstrated by comparing the results with second-order nonlinear regression metamodels.

Further, the proposed methodology is extended to assess mixed-mode (MM) failure behavior of the adhesive joints. As a part of experimental study, the composite single leg bending (SLB) specimens are manufactured by using unidirectional carbon

fiber reinforced material and epoxy resin, and the tests are conducted in TINUS testing machine as per ASTM D790 under the influence of pure mode dominant conditions in order to obtain the cohesive parameters. Optimization techniques are used to minimize the error between the simulation and experimental values. The MM–CZM is then established and implemented in the SLB joint under various mode mixities for analysing the fracture process. Comparison between the numerical and experimental results shows that the proposed HDMR based approach estimates the failure mechanism efficiently.

CONTENTS

LIST OF FIGURES

iv

LIST OF TABLES

ABBREVATION

ANN	Artificial Neural Network
ARSM	Adaptive Response Surface Method
BLUP	Best Linear Unbiased Predictor
CCD	Central Composite Design
CDF	Cumulative Distribution Function
CPT	Classical Plate Theory
CZM	Cohesive Zone Model
DCB	Double Cantilever Beam
DOE	Design of Experiments
ELS	End Load Split
ENF	End Notch Flexure
ERR	Energy Release Rate
FE	Finite Element
FEA	Finite Element Analysis
FPZ	Fracture Process Zone
FRP	Fiber Reinforced Polymer
GA	Genetic Algorithm
GF	Glass Fiber
GHDMR	General-High Dimensional Model Representation
GMDH-PNN	Group Method of Data Handling-Polynomial Neural Network
HDMR	High Dimensional Model Representation
LEFM	Linear Elastic Fracture Mechanics
LH	Latin Hypercube
LHD	Latin Hypercube Designs
LHS	Latin Hypercube Samples
MARS	Multivariate Adaptive Regression Splines

MCS	Monte Carlo Simulation
MLS	Moving Least Square
MM	Mixed Mode
MMB	Mixed-Mode Bending
MM-CZM	Mixed-Mode Cohesive Zone Model
MPA	Multi-Point Approximation
NLFM	Non-Linear Fracture Mechanics
PCE	Polynomial Chaos Expansion
PDF	Probability Density Function
PPR	Park Paulino Roesler
PR	Polynomial Regression
PSO	Particle Swarm Optimization
RBF	Radial Basis Functions
RS-HDMR	Random Sampling High Dimensional Model Representation
RSM	Response Surface Model
SLB	Single Leg Bending
SVM	Support Vector Machine
SVR	Support Vector Regression
TSL	Traction-Separation Law
UEL	User element
VCCT	Virtual Crack Closure Technique

SYMBOLS

δ_w	Center-point deflection in SLB test
δ_0	Characteristic crack separation
Δu_2	Crack initiation opening displacement at the notch root
Δu	Crack opening displacement
G_c	Critical energy release rate
w	Deflection in the z direction
ll	Displacement in the local coordinate
D_T	Effective bending rigidity
λ, ρ	Elastic anisotropy measures
f_N^{el}	Element force vector
δ^*	End-opening of the bridging zone at the notch root
G	Energy release rate
$f\left(x_i, c^i\right)$	First order component function
$f_i\left(x_i\right)$	First order term
a	Initial crack Length
J_0	Initial value of energy release rate
$\mathbf{x}$	Input vector
p	Load
δ	Local crack separation near crack tip in DCB
v_{12}	Major Poisson's ratio
$\mathbf{H}(\xi)$	Matrix containing the quadratic shape functions
$\mathbf{B}$	Matrix containing the shape functions

ν_{21}	Minor Poisson's ratio
E_{11}	Modulus of elasticity in longitudinal directions
E_{22}	Modulus of elasticity in transverse
G_{12}	Modulus of Rigidity
I	Moment of Inertia of double cantilever beam
M_T	Moment on a top face
$\mathbf{d}_N$	Nodal displacement of the vector
$f(\mathbf{x})$	Output of the system response
α	Power law factor
$\mathfrak{c}$	Reference point
$\Delta\mathbf{u}(\xi)$	Relative displacement between the nodes
f_0	Response of the system at mean input parameters
$f_{ij}(x_i, x_j)$	Second order term
$N_i(\xi)$	Shape function for the node pair i
J_{SS}	Steady state crack growth resistance
Δu_0	Steady state crack opening displacement at the notch root
ΔJ_{SS}	Steady state fracture energy
h	Thickness
h	Thickness of the double cantilever beam
Θ	Transformation tensor
b	Width of the double cantilever beam
W	Width of the interface element
B	Width of the single leg bending specimen

x

CHAPTER 1

INTRODUCTION

Composite materials are used in various engineering fields such as aerospace, automobiles, construction, etc. (Mangalgiri 1999). However, due to the presence of flaws in materials, most of the designed components are not able to meet their design strength in service condition. The difference between theoretical and actual strength of the material occurs for various reasons, including lack of knowledge in design and testing, manufacturing defects, types of loading conditions and inadequate maintenance (Maleque and Salit 2013). Figure 1.1 shows the cracks in various structural components. The flaws present in the composite material, mostly as a crack, lead to premature failure of the structure. Therefore, characterising the composite material is very important.

Researchers have studied fracture mechanics principles which assist the linear and nonlinear failure behavior of composite materials (Chaves et al. 2014; Liu et al. 2012; Salih et al. 2019). The linear elastic fracture mechanics (LEFM) principles are used in understanding the linear failure behavior of a defective material though not much appreciated in a plastic failure analysis (Elices et al. 2002). Hence, nonlinear fracture mechanics (NLFM) principles have emerged to describe the crack initiation, propagation and fracture in the materials. Consequently, several methods have been developed using NLFM principles (Pirondi et al. 2014; Stumpf and Le 1990; Wang et al. 1984). A cohesive zone model (CZM) is, therefore, one of such popular computational models which describe the plastic zone in front of the crack tip (Jin and Sun 2006). The available probabilistic CZM's are not much appreciated to analyse the fracture behaviour in composites (Shanmugam et al. 2012). However, it needs further improvement in understanding the failure behavior by using efficient design tools.

Defects in composite material are inevitable due to complex factors involved in the manufacturing processes, and these flaws mainly lead to fracture (Smith 2009; Ghobadi 2017). During continued separation, crack tip moves along a geometric face termed as crack face. The crack tip is the line connecting all adjacent sites where

separation may occur subsequently. Based on the movement of crack faces, the fracture is described in three different modes as shown in Fig. 1.2. In Mode-I, the load is applied normal to the crack plane whereas in mode-II, it is in-plane shear loading. Mode-III is out-of-plane shear, where the crack edges are moved across each other in opposite directions. Likewise, mixed modes (MM) occur as a combination of any two basic modes (Anderson 2017).

1.1 NEED FOR DESIGN TOOL DEVELOPMENT

In most cases, prior to the full scale use of composite components, proper verification and validation have to be performed to fully understand the failure behavior of the material using suitable computational tools. Reliability evaluation of real-size composite components demands constant experimentation, which is highly sensitive and less affordable by the small sectors (Abunima et al. 2018). Furthermore, developing efficient design tools are significant in order to reduce the design and experimentation cost for certifying a composite material. Therefore, the use of advanced computational tools is gaining much consideration in composite material testing (Shymchenko et al. 2017).

| (a) | (b) | (c) |
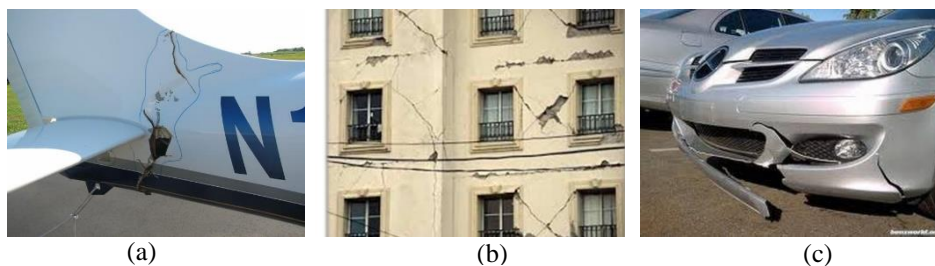
Fig. 1.1 Cracks in (a) aerospace structure (b) buildings and (c) automobile parts (source: https://www.google.com)

Mode-I   Mode-II   Mode-III
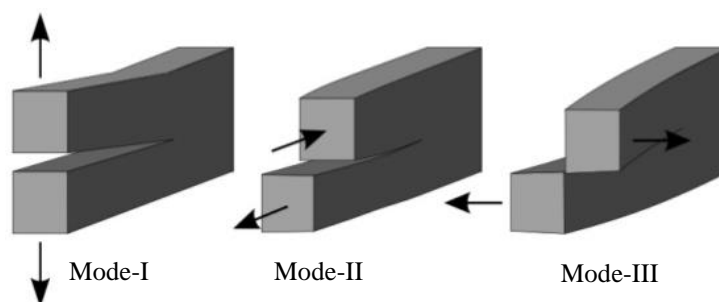
Fig. 1.2 Types of mode fractures

2

The process of conducting tests using computer applications is called virtual testing. If composite life under service condition is effectively predictable, then there is a scope of increasing the application of composites as structural components in many fields.

Several factors affect the testing and analysis of composite components. Neither test nor analysis alone is enough to adequately verify and validate the models. Therefore, to increase the reliability and decrease the computational effort, test and analysis have to be performed simultaneously. This synergistic process helps the composite material from lamina developmental stage to the real size component stage. Moreover, each development stage is based on the knowledge obtained from a previous low-level complex situation. The process starting with the low-level complex situation and finally dealing with highly complex situations is known as the "Building Block" approach as shown in Fig. 1.3 (Turon 2006). Therefore, the advanced knowledge of technology and design tools assists in improving the performance and efficiency of the composite materials.

1.2 DELAMINATION

Laminated composite materials experience various types of damages during testing and in-service life condition. Generally, the most commonly observed type of damage is delamination. Delamination is a process of layer separation in the composite that occurs due to the presence of voids in the resin and misalignment of the layers (Di Landro et al. 2017). Internal and surface delamination are the two significant types of delamination often observed in composites (Bolotin 2001).
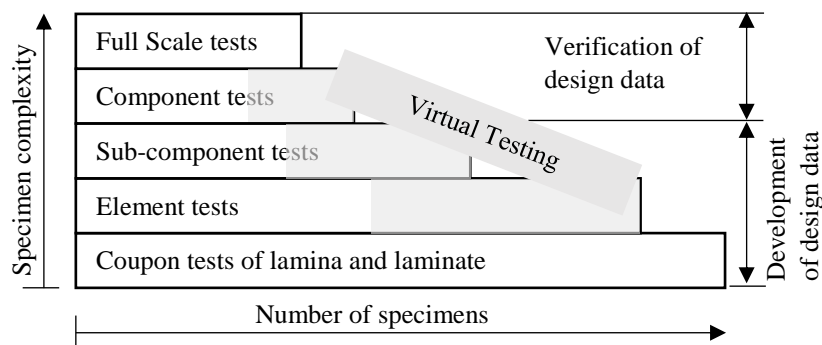
Fig. 1.3 Building block integration and reduction on the test requirement through virtual testing (Turon 2006)

Various reasons are involved in delamination process such as sudden changes in sections, sharp edges, thermal variations, shrinkage of the matrix, formation of resin-rich areas etc (Bolotin 1996). During interlaminar delamination in unidirectional fiber reinforced composites as shown in Fig. 1.4, fiber cross over bridging occurs, thereby interaction between laminates takes place. Owing to fiber bridging, variation in strength can be observed (Shanmugam et al. 2013). Therefore, the behavior of the laminate subjected to fiber bridging is crucial in predicting the life of the composite materials. Moreover, delamination damage mode is essential for the structural integrity of composite structures, because it is difficult to detect during the inspection.

There are various approaches available to deal with delamination. LEFM approach has been used in the early stages of numerical simulation for predicting the delamination growth. Based on the LEFM principles, different techniques such as virtual crack closure technique (VCCT) (Irwin 1957; Krueger 2002; Raju 1987; Rybicki and Kanninen 1977; Zou et al. 2001;), *J*-integral method (Rice 1968), and stiffness derivative (Parks 1974) are used for energy release rate (ERR) calculations. Hence, the delamination growth in the composite material can be predicted when the ERR is equal to or greater than a critical value (Griffith 1921). However, the techniques face difficulties in using finite element (FE) codes unless nodal variable and topological information from the nodes ahead and behind the crack front is available for stationary crack.

Another approach is developed based on cohesive or damage mechanics which follows cracks, progressively within the framework, starting from the crack initiation to the complete failure. CZM concept is the popular technique in damage modeling for predicting the delamination growth in both linear and NLFM (Gain et al. 2011).

Fig. 1.4 Uni-directional fiber bridging (Robinson and song 1992)

Cohesive elements, which depends on constitutive laws or traction-separation law (TSL) with zero volume or zero surface area, are used to simulate the interfacial failure between material. In a CZM, damage propagation studies can be carried out without the presence of initial crack, and it is possible to embed in FE codes for static and fatigue damage studies. The drawback of the CZM is on selection of the appropriate TSL, because this affects the efficiency of the simulation process (Desai et al. 2016;) Zou et al. 2003).

1.3 COHESIVE TRACTION-SEPARATION LAWS

Experimental methods and/or phenomenological studies (with predefined functional assumption and estimated parameters) have been used in the development of TSLs. Though some tests are performed in laboratories to determine the TSLs, no standard approch exists for measuring the traction-separation performance (Tan et al. 2005). The TSLs measured will have a typical feature, i.e., the value of the cohesive traction increases until it reaches the critical peak value, then starts decreasing and finally reaches to zero as the separation still advances. The descending traction indicates the material softening with fracture proceeds.

The CZM approach assumes a certain TSL for defining the cohesive region failure, and the values of cohesive parameters (the cohesive strength, the cohesive energy and characteristic length) are adjusted to fit the experimental results. The cohesive strength indicates the maximum resistance to fracture and is typically associated with the yield stress of the composite material in use, whereas the cohesive energy represents the transformation of energy associated with the material separation. On the other hand, the characteristic length refers to the magnitude of displacement that corresponds to the cohesive strength. The parameters are determined after fixing the shape of the TSL. Specifically, shape of the TSL and the value of the cohesive parameters are the important features of CZM. Many studies indicate that the shape of TSL has no significant effect on the numerical results of fracture simulations (Alfano 2006; Hutchinson and Evans 2000; Jin and Sun 2005; Needleman 1990; Tvergaard and Hutchinson 1992).

The CZM represents the toughness at the crack tip and describes the whole deformation process including the initiation and propagation of the crack. The presence

of an initial crack is not essential as required in conventional fracture mechanics. The CZM is a phenomenological model which does not describe exactly the real physical processes of fracture, however it has been used in several applications. The effective practicality of the CZM in studying and justifying crack growth simulation has been well known since 1960 in various materials such as metals, concretes, ceramics, polymers, and their composite counterparts. Likewise, several studies have been conducted using CZM to describe the micro-mechanical separation processes such as void growth and nucleation, atomic separation, interfaces fracture, composite delamination, and fibre bridging (Alfano and Crisfield 2001; Needleman 1987; Shanmugam et al. 2013; Tvergaard and Hutchinson 1993). In addition, CZM has been used in numerical modeling for understanding the propagation of earthquake ruptures (Andrews 1976; Lu et al. 2010; Rosakis 2002; Shi et al. 2010). Furthermore, the CZM has also been used in different modes of fracture studies under bonded specimen (Li et al. 2005; Roe and Siegmund 2003).

1.4 METAMODELS

Metamodels have been widely used in many scientific and engineering areas in order to analyse and model the intricate real-world systems. They essentially aim at establishing certain relationships between input variables and the output of the system. Therefore, it is evident that metamodels can govern any of the physical parameters present in the real-word problems. Nevertheless, the precision of the metamodel should be enhanced to reflect the real system and simulate the performance of a product or system, which has the preferred design configurations and set of design parameters, by choosing a better model. Performance is generally measured as a vector quantity and may encompass components such as part deflection, weight, noise, cost, reliability, etc. In general, the better the model is, the more accurate it represents the real system.

Numerous interactive computer modules have been developed using mathematical representation to establish the input-output relationship which helps to understand the underlying physical phenomenon in composite materials. However, system-level design based on computational models is difficult to develop and predict the overall system behaviour, because the requirement of integration of different sub-system modules is not an easy task. Furthermore, the individual components of the

6

computer model are often computationally expensive, thus researchers have examined the use of different approximation strategies (for instance, response surface methods) as alternative inexpensive simulation models. Usually, the metamodels are used as alternatives for the genuine simulation or experimental models when vast number of assessments are required. Accordingly, a large number of likely combinations of all design parameters can be established for each set of variables by assuming analogous predictive metamodel analysis. The use of well designed and developed metamodels allows a faster analysis and reliable information about the composite materials than the original complex engineering models.

The metamodel development approach is characteristically a three-step procedure. The first step refers to selection of typical representative sample points in order to acquire optimal data on the whole design space depending on the kind of metamodel established. In the second step, outputs corresponding to each sample points are assessed and then used to obtain set of design points and corresponding responses. Finally, the third step is the building of the mathematical model which maps the input-output relationship (Dey et al. 2017).

Currently, many studies have incorporated the metamodeling techniques in design and optimization models. Some of research areas include sampling approaches (Giunta et al. 2003), metamodels development (Koziel and Yang 2011), model fitting techniques, model validation and verifications (Jin et al. 2001; Kim et al. 2009; Li et al. 2010), design space exploration, and optimization methods in support to diverse types of problems. The classical design of experiments (DOE) theory is being applied during the metamodel development process, in which polynomial functions are introduced as response surfaces. The response surfaces are typically a second-order polynomial models with inadequate ability to precisely simulate nonlinear functions of random shape. Evidently, higher-order response surfaces are required to adequately simulate the nonlinear design space.

Despite the fact that several sampling techniques and various metamodel formation methods are readily available for use, the selection of suitable DOE method and metamodeling technique is the key concern in choosing the efficient one among the existing fracture analysis approaches. Since the entire sampling approaches and metamodeling techniques have their unique properties, no universal metamodel is

considered as a best choice for all types of problems. Therefore, the sampling method and metamodeling technique for a specific type of problem has to be decided based on the degree of model complexity, existence of error in sample data, type and extent of input variables, anticipated level of precision and computational effectiveness. Moreover, it is crucial to rigorously check the quality of fitting and estimation capability of the available data beforehand using a particular metamodeling technique. Table 1.1 summarises the different metamodeling methods and sampling techniques applicable for fracture analysis studies. Furthermore, the sampling techniques and particular metamodeling methods shown in Figure 1.5 can be adopted to choose best likely performance of each model.

High Dimensional Model Representation:

High dimensional model representation (HDMR) is a dimension-reduction technique widely used in chemistry and structural reliability areas. It is a tool which shows the relationship between input variables and output solutions in the form of hierarchical correlated functional expansions (Balu and Rao 2012; Balu and Rao 2014; Li et al. 2001; Rabitz et al. 1999). Also, HDMR tools have been employed for constructing a model from laboratory data, FE modeling, inverse reliability problems, structural damage identification, and so on (Balu and Rao 2011). An efficient uncertainty quantification scheme for frequency responses of laminated composite plates was investigated by bottom up metamodel-based approach using general-high dimensional model representation (GHDMR) for achieving computational efficiency in quantifying uncertainty (Dey et al. 2016). There are few studies on the application of response surface methods (RSM) to simulate the fracture behaviour. However, the proposed HDMR based methodology is computationally efficient as evidenced in the results and discussion. In the present work, CZM is developed based on the HDMR technique to simulate the fracture in composites.

1.5 SIGNIFICANCE OF THE PRESENT WORK

Few studies have used second-order nonlinear regression based CZMs to characterise the delamination strengths in laminated composites. However, the computational efficiency and the prediciton capabilty of such models are not much appreciable.

8

Table 1.1 Metamodel techniques

Modeling Methods	Sampling Techniques
❖ Polynomial Regression (PR)	❖ Classic methods
❖ High dimensional model representation (HDMR) (Li et al. 2002)	▪ Factorial design
❖ Polynomial chaos expansion (PCE) (Ghanem and Spanos 1990)	▪ Central composite design (CCD)
❖ Splines [linear, cubic] (Durrleman and Simon 1989)	▪ Box-Behnken
❖ Multivariate adaptive regression splines (MARS) (Friedman 1991)	▪ Optimal designs
❖ Gaussian process	▪ Plackett-Burman
❖ Kriging (Myers 1982)	❖ Space-filling methods
❖ Radial basis functions (RBF) (Park and Sandberg 1991)	▪ Simple grids
❖ Least interpolating polynomials (moving least square) (MLS) (Lancaster and Salkauskas 1981)	▪ Latin Hypercube (LH)
❖ Artificial neural network (ANN) (Yao 1999)	▪ Sobol sequence
❖ Group method of data handling - polynomial neural network (GMDH - PNN) (Lee and Jeng 1998)	▪ Orthogonal arrays (Taguchi)
❖ Knowledge base or decision tree (Cramer et al. 1976)	▪ Hammersley sequence
❖ Support vector machine (SVM) (Suykens and Vandewalle 1999)	▪ Uniform designs
❖ Weighted least squares regression (Ruppert and Wand 1994)	▪ Minimax and maximin
❖ Best linear unbiased predictor (BLUP) (Goldberger 1962)	❖ Hybrid methods
❖ Multi-point approximation (MPA)	❖ Random or human selection
❖ Sequential or adaptive metamodeling (Dear and Brager 2001).	❖ Importance sampling
❖ Hybrid models (Atluri et al.1975)	❖ Directional simulation
	❖ Discriminative sampling
	❖ Sequential or adaptive methods

In the present work, HDMR based CZM is introduced to improve the computational efficiency and accuracy of the unidirectional fiber reinforced composite material under different mode conditions using TSLs in FE models.
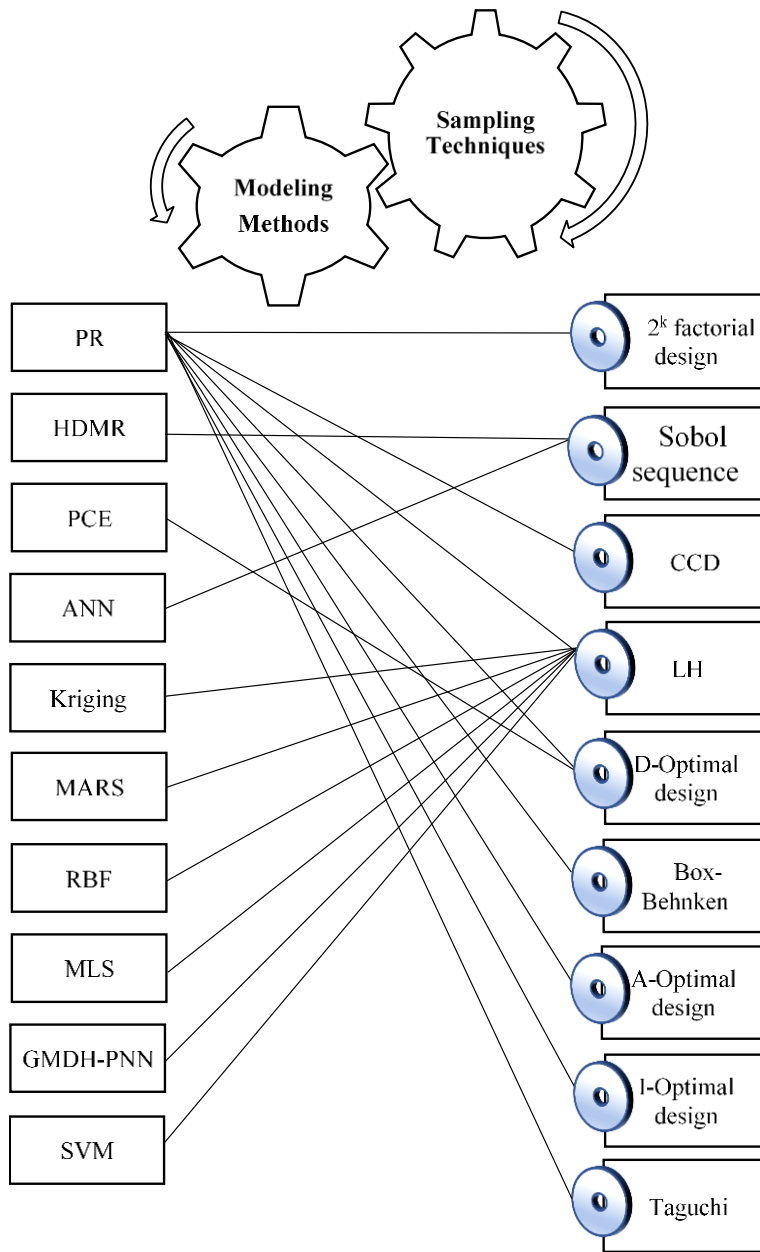
Fig. 1.5 Metamodeling methods and corresponding sampling techniques

Moreover, the HDMR based CZM is also applied for single leg bending (SLB) joint failure analysis of an arbitrary initial crack in composite materials. Accordingly, experiments have been conducted on SLB joints to find the fracture toughness. In addition, comparisons between the numerical and experimental results have proved that the HDMR based approach can efficiently estimate the failure mechanisms in composite materials.

1.6 THESIS ORGANISATION

In this work, HDMR-based CZM is developed for predicting the failure charactaristics in composite materials. Experimental studies have been carried out for evaluating the fracture toughness under MM conditions. The thesis is organised as follows.

i) The first chapter describes a brief introduction to fracture, need for developing design tools, delamination and delamination methods. In addition, characteristics of cohesive TSL have been discussed. Furthermore, the use of metamodels and their importance to analyse and simulate complex real-world systems have been described along with the significance of the present study.

ii) The second chapter presents a detailed review of relevant literature on CZMs, and metamodels, followed by summary of literature and objectives of the proposed research work.

iii) The third chapter demonstrates the development of HDMR based CZM to capture the steady state ERR of a Double Cantilever Beam (DCB) under mode-I loading. The efficiency of the proposed model is compared with the available experimental data.

iv) The fourth chapter describes the determination of inter facial fracture toughness using SLB test setup. Various composite thickness test results are also demonstrated.

v) The fifth chapter demonstrates the simulation of MM-CZM.

vi) The last chapter presents the conclusions based on the findings from the present work, and also scope for the future work.

CHAPTER 2

LITERATURE REVIEW

2.1 GENERAL

The prediction of failure behavior of composite materials using LEFM principles has gained attention since 1960. Such ability to predict fracture has provided a basis for assessing the safety and reliability of composite elements. Furthermore, it evaluates the product quality in a series of manufacturing processes, and also provides the basis for failure analysis. However, the nonlinear failure behaviour is not efficiently predicted despite its success in LEFM.

Advanced development in computer technology contributes to provide the solution for analysing the nonlinear structures using computational fracture mechanics. In limited cases, it is possible to obtain a closed-form analytical solution. Consequently, numerical modeling has become a potential tool in fracture analysis. A variety of numerical techniques have been applied to problems in solid mechanics, including finite differences, FE methods and boundary integral equation methods. Recently, the FE based CZM has gained much attention in cracked bodies studies. In CZM, fracture is characterised by a TSL relation across a specified set of cohesive surfaces. The cohesive constitutive relation embodies a description of the mechanical effects of the separation process as well as any dissipation associated with it.

A detailed review of relevant articles in the field of fracture mechanics is presented in this chapter. Also, the importance of CZM in fracture studies with respect to various techniques is explored. Metamodels and their developments in different studies are reviewed. HDMR and its contribution as a metamodel or surogate model has been presented. The literature study is mainly focused on CZM, metamodel and HDMR. Summary of the literature is provided and also research gaps are highlighted. Finally, the objectives of the present work are derived.

2.2 COHESIVE ZONE MODEL

The CZM has gained a lot of attention in crack nucleation and propagation modeling, and is widely adopted in nonlinear failure mechanism studies. Therefore, several studies has been developed to charaterise the cohesive region in composite materials. The distribution of cohesive forces near the crack tip region is quite complicated in characterising the behavior of failure. Therefore, a phenomenological distribution has been introduced for brittle fracture, which shows peak value at the crack tip thereby decreases rapidly (Barenblatt 1959, 1962). Similarly, analysis to calculate the extent of yielding in steel sheets containing cracks is carried out by considering the uniform stress distribution in the cohesive region (Dugdale 1960).

A fictitious crack model was developed for characterising the fracture behavior in concrete structures (Hillerborg et al. 1976). The application was limited to the concrete fracture community for more than a decade. The cohesive concepts were used to generate the mathematical framework. Despite the fact that the model was focused on brittle fracture studies, the computational formulation of the cohesive region facilitates to describe the nonlinear materials behavior. Cohesive surfaces were introduced to assess the void nucleation at the interface of particle and matrix material, crack growth in brittle material under dynamic loading, and dynamic crack growth along the interface of composites. Constitutive relations were specified independently for the matrix, the inclusion, and the interface. Constitutive equation for the interface was similar to that of CZM concept. To describe mechanical response of the interface, critical interfacial strength and displacement are the necessary input parameters. Dimensional considerations have introduced a characteristic interface length into the model. The key advantage of the model is the ability to predicit the ductile to brittle fracture without any initial crack (Needleman 1987, 1990; Xu and Needleman 1994).

Cohesive constitutive relationships can be classified as either nonpotential-based models or potential-based models. The fracture behavior has been characterised by the TSL in potential based models. The TSL relations are usually derived based on direct (Gowrishankar et al. 2012; Sørensen and Jacobsen 2000; Sorensen et al. 2008; Victor et al. 1987) or indirect methods (Gowrishankar et al. 2012; Manshadi et al. 2014; Pappas and Botsis 2016; Sorensen et al. 2007;). In the direct method, calculation of the *J*-integral (Rice 1968) and measurements of crack opening displacement at the end of

the bridging zone, are required for obtaining the tractions. Effective usage of such method generally requires the data points quality to be exactly fit, particularly at the commencement of the fracture process, the description of maximum deflection, and the displacement at which the tractions disappear (Heidari-rarani et al. 2013; Sorensen et al. 2008). In the indirect method, the bridging zone traction parametrs were identified using an inverse optimisation technique, which requires the objective function experimental data set. Iterative procedures were adopted in the indirect methods to derive the TSL using measured strain data set along the specimen (Cox and Marshall 1991; Gowrishankar et al. 2012; Sorensen et al. 2007). Both the direct and indirect methods were used to extract the TSL of various types of composites (Frossard et al. 2017; Gowrishankar et al. 2012; Manshadi et al. 2014; Pappas and Botsis 2016; Pappas et al. 2017; Sørensen and Jacobsen 2000;). Moreover, Feih et al. (2005) developed adjusted bridging law for the composites subjected to fiber bridging. Furthermore, Shanmugam et al. (2013) used adjusted bridging law for simulating delamination in composites.

The CZMs have been efficiently simulating not only the interfacial delamination (Feraren and Jensen 2004; Li et al. 2005a; Valoroso and Champaney 2006; Parmigiani and Thouless 2007), but also a plethora of other interface problems such as crack nucleation at bimaterial corners (Mohammed and Liechti 2000), plastic dissipation in thin debonding films (Shirani and Liechti 1998), and delamination of composites (Högberg et al. 2007; Li et al. 2005b; Li and Thouless 2006; Moroni and Pirondi 2011; Sørensen and Jacobsen 2000). However, CZMs require specific material parameters in order to make meaningful predictions.

Delamination of fiber reinforced composite material under mode-I loading condition has been studied mostly by the DCB specimen test (Kim and Mai 1991; Ivens et al. 1995; O'Brien 1998; Sela and Ishai 1989; Sørensen and Jacobsen 2000). In the DCB specimens test, the fracture toughness or ERR in mode-I failure (ASTM D5528) for unidirectional composites has been measured. However, many tests using the DCB specimen are plagued by fiber bridging. Despite the fact that the fiber-bridging is undesirable, the researchers try to describe the structure at the occurrence of fiber-bridging during failure (Johnson and Mangalgiri 1987). Spearing and Evans (1992) conducted experiments on DCB specimens to understand the sensitivity of the fibre

bridging on the inter-laminar fracture. As a result, the energy plot showed a steadily raising pattern in ERR with advance in crack length, and such increasing phenomenon is known as R-curve effect (Anderson 2017). Sørensen and Jacobsen (1998) proved that the feature of R-curve is purely dependent on the geometry of the model if large scale bridging takes place in the material at the time of failure, hence it cannot be considered as a material property. In most of the cases, fiber breakage occurs in unidirectional composite since the fibers migrate into other laminates during the curing process. Rafiee and Ghorbanhosseini (2018) developed a computational model to predict the material properties of a composite covering all involved scales from nano to macro. Shanmugam et al. (2013) conducted tests on unidirectional composite DCB specimens to understand the R-curve effect. Response surface model had been constructed by using Latin hypercube samples (LHS) on various combinations of adjusted bridging law parameters for capturing steady state ERR.

Generally, predicting the failure behavior of the adhesive is cumbersome during numerical simulations, because they are influenced by adhesive properties and interface characteristics. In most cases, modeling methods use FEs for representing the adhesive layer and assume that the adhesive and adherent bondage without any flaws, which indirectly state that the strength of the adhesive is weaker than the interface strength (Sheppard et al.1998). To model failure behavior of the bonded joints, several modeling methods are proposed (Tong and Steven 1999). In many cases, partial cohesive failure occurred in bonded joints. Therefore, analysing the failure behavior of bonded joints is having more importance in composites (Chen and Baker 2005).

For NLFM problems, CZM is commonly applied to understand failure behavior of bonded joints (Ouyang and Wan 2009). In VCCT the fracture is modelled using stiff spring elements, but in the CZM, cohesive laws are implemented (Shet and Chandra 2002). The role of the TSL is to define progressive failure of the bonded layer (Shabir et al. 2011). Bilinear TSL can be easily described by three parameters (the initial stiffness, critical cohesive strength and fracture toughness) (Song et al. 2008). To determine cohesive parameters there is no standard procedure, but one can estimate by conducting the experiments on the given material fracture toughness (Lee et al. 2010). The remaining parameters are obtained by matching the simulation and experimental results respectively (Li et al. 2005a).

The CZM in pure modes I and II is constructed using the Double Cantilever Beam (DCB) test and the End Notched Flexure (ENF) test, respectively. On the other hand, the SLB joint has an inherent mode-mixity because of its geometry and its mode-mixity can be controlled by specimen thicknesses. For simplicity, three-point bending tests of mode I and II-dominant SLB joints can be performed instead of pure mode tests by controlling the composite thickness of the SLB specimen.

2.3 METAMODEL

Metamodels (also referred as apporximation models) are used as a preferable approach for the studies demanding repetitive model assessment to successfully substitute the expensive models in a computationally efficient manner (Baran et al. 2017; Kleijnen 1987). Consequently, metamodeling approaches have been extensively implemented in the design appraisal and optimization processes of numerous engineering activities (Arregui-mena et al. 2016). Most important metamodeling techniques such as polynomial regression (PR), Kriging, HDMR, polynomial chaos expansion (PCE), artificial neural network (ANN), moving least square (MLS), support vector regression (SVR), multivariate adaptive regression splines (MARS), radial basis function (RBF) and polynomial neural network (PNN) are available in many areas of research.

Conventional DOE concepts are used in the development of metamodels using polynomial functions as response surfaces. Sacks et al. (1989a; 1989b) suggested Kriging models for treating deterministic variables in order to realise the random function with respect to the real system response. ANNs have also been used in establishing the response surfaces for system approximation (Papadrakakis et al. 1998). Other types of models include rational basis functions (Dyn et al. 1986), MARS (Friedman 1991), and inductive learning (Langley and Simon 1995). Besides, Varadarajan et al. (2000) have reported works involving both the polynomial functions and ANNs. So far, there is no distinctive approach to choose the appropriate model for superior performance. However, much more insight on various models has been gained through a number of studies (Giunta and Watson 1998; Jin et al. 2001; Koch et al. 1999; Simpson et al. 2001b; Simpson et al. 2001c). The Kriging and second-order polynomials are the most intensively studied models. The Kriging model is, generally, considered as a more precise model for nonlinear problems, but difficult to develop and

apply. In contrast, the polynomial model is easy to develop, good in parameter sensitivity, and inexpensive to work with, but is less precise than the Kriging model (Jin et al. 2001; Simpson et al. 2001c).

Clarke et al. (2005) introduced SVR, a novel metamodel technique with higher precision compared to other models. However, the vital reasons for the SVR to win out are yet unclear. Mullur and Messac (2005) established an enhanced RBF model including additional terms to the basic RBF model to improve the flexibility. It is claimed that this extended RBF applies to almost all problems. The interests on Kriging remain high with more in-depth studies (Van Beers and Kleijnen 2003; Martin and Simpson 2005).

Similarly, a reliable and inexpensive gradient data can be employed in metamodeling applications (Morris et al. 1993; Koehler 1998). Furthermore, multipoint approximation (MPA) approach has also gained some attention by several researchers (Toropov et al. 1993; Wang et al. 1996; Rasmussen 1998; Shin and Grandhi 2001). It uses blending function to join several local approximations in metamodels. Based on the aforementioned studies, a flexible and generic metamodels are required as alternative to the expensive models. Such metamodels may include mixed metamodels, metamodels of irregular reliability, tuneable metamodels, and so on (Leary et al. 2003).

From the practical view, there is always uncertainty issues originating from sampling and difference in model functions, regardless to the type of model used. Moreover, the accuracy of the metamodel is also associated with design space. Hence, an iterative-based metamodels have been established to improve the accuracy in the metamodel (Dennis and Torczon 1997). Several methods were developed aiming at reducing the design space in metamodels to improve the modeling accuracy. Based on the available literatures, two types of design space reduction approaches were observed.

The first one corresponds to dimensionality reduction of the design space by decreasing the number of design parameters. This has been explained in the early works of several scholars foucsing on refining the response surfaces to accurately predict the actually system by minimising the input parameters. (Welch et al. 1992; Giunta et al. 1997; Balabanov et al. 1999). Dimensionality reduction is highly significant as it aims at breaking the "curse of dimensionality", though it is not easy to bring such significant reduction particularly for multidisciplinary design problems (Koch et al. 1999). The

second approach of design space reductions tends to decrease the size of the design space with the assumption that the dimensionality cannot be further decreased. The size of the design space is contolled by the collective range of design parameters.The smaller the range of design parameters, the smaller the size of the design space, and viceversa. However, having larger design space leads to cumbersome and expensive metamodel construction. In other hand, sequential metamodeling technique was promoted by several scholars by means of move limits or trust regions (Alexandrov et al. 1998; Wujek and Renaud 1998a; Wujek and Renaud 1998b; Booker et al. 1999). Renaud and Gabriele (1994), have detailed the importance of data generated during concurrent subspace optimization in developing response surface approximations of the design space, which inturn forms a basis for the subspace coordination procedure.

In order to achieve the model accuracy, itreratively generated samples are required to update the response surface approximations. Thus, the approximation precisions of the model were sequentially updated and enhanced with multistage Kriging strategies using additional sample points (Osio and Amon 1996). Wang (2003) developed the adaptive response surface method (ARSM), which systematically decreases the size of the design space by removing sample points with values greater than to the threshold value at each optimization iterations. Therfore, the design space is progressively reduced near to the optimal design value.

In general, the systematic justification of the interrelatedness between design variables is used to characterise the design space reduction techniques. The enhanced ARSM uses inherited latin hypercube designs (LHD) for sampling purpose. This largely decreases the quantity of samples required (Wang 2003). Moreover, Wang and Simpson (2004) established a heuristic hierarchical metamodeling approach to improve the drawabcks of both polynomial and Kriging models.

Physical experiments and simulations performed during engineering design are the time consuming tasks, in addition with increase in design cost. High dimensional or large number of input variables makes the design problem complex. HDMR is a powerful method in approximating high dimensional and expensive problems (Rabitz et al. 1999). It is a set of quantitative model assessment and analysis tools for improving the efficiency of deducing high dimensional input–output system behavior. HDMR is a tool, which expresses the input and output relationships of complex and

computationally expensive models to form a function having hierarchical correlation expansions. Various studies concluded that, responses of a system have influence from the lower order input variables interaction.

Stochastic free vibration analysis of angle-ply composite plates using random sampling high dimensional model representation (RS-HDMR) approach has been carried out (Dey et al. 2016) by developing a metamodel to express stochastic natural frequencies of the system, and performance of RS-HDMR has been compared with full-scale Monte Carlo simulation results. Mukhopadhyay et al. (2015) introduced an efficient hybrid method based on RS-HDMR and genetic algorithm (GA) coupled with a local unconstrained multivariable minimization function for optimization of fiber reinforced polymer (FRP) composite web core bridge deck panels. The application of HDMR in stochastic multiscale modeling in conjunction with multielement least square approach has been carried out by Jiang and Li (2015). HDMR tools have been employed for constructing a model from lab data, FE modeling, inverse reliability problems, structural damage identification etc (Mukhopadhyay et al. 2016). Further in order to construct an efficient HDMR expansion, concepts of support vector regression adopted by Li et al. (2017) enabled efficient construction of high dimensional models with satisfactory prediction accuracy from a modest number of samples.

2.4 SUMMARY OF LITERATURE REVIEW

Experimental results attribute to evaluate material properties like yield strength, shear strength, ultimate strength and fracture toughness values used in structural design. Nevertheless, there are no precise assessments designed to calibrate the CZM bridging variables so as to measure their scatter information when transforming from traditional failure analysis technique to the new CZM based technique. Therefore, RSMs have been developed to characterise the load and crack length distribution in terms of adjusted bridging law variables.

The existing methodologies using RSM techniques have ability to precisely estimate the energy and load variations, but are not effective in predicting the crack length variations in uni-directional composites. This can be attributed to lack of information significant in associating steady state energy and load values to a specific crack length. Hence RSMs play a vital role in predicting the fracture parameters.

Composite materials are used as base materials in most of the advanced products. The use of composites in main structural components is still limited owing to the difficulty in predicting the service life. The presence of material defects or manufacturing defects in composites is highly uncertain to diagnose, and hence fracture phenomenon is unpredictable. Many studies have been carried out both experimentally and numerically to understand the failure behavior and factors influencing the fracture process using the concepts of LEFM. However, the available techniques developed based on LEFM are not readily applicable to nonlinear problems. Therefore, as an alternative approach, the application of CZM has become prevalent due to the advantages such as the ability to adequately predict the behavior of uncracked structures, and suitability in the conceptual framework for interfaces. CZM is a computational model in which fracture formation is regarded as a gradual phenomenon where separation of the surfaces occurs across an extended crack tip, and is opposed by cohesive tractions. Cohesive elements have been proven to be an excellent approach in computational fracture mechanics. Nevertheless, massively parallel computations are required in order to capture the damage-patterns and evolutions precisely in composites.

Computationally efficient metamodels were employed in evaluating large number of model outputs with limited set of algorithmically selected input variables. As a result, a corresponding mathematical model is developed to simulate the fundamental input-output relationship of the system based on efficient metamodels. The need of integrating the metamodels has significant demand for assessing the response characteristics of composites by accounting the uncertainties in the models. Different metamodels are developed to understand the responses of a laminated composite structures. Compared to all the other methods, models developed based on HDMR are promising towards the computational efficiency.

2.5 OBJECTIVES OF RESEARCH WORK

Based on the literature review, the objectives of the present research work are as follows:

i) To develop the high dimensional model representation based cohesive zone model for representing the effects of toughening behavior in composites.

ii) To conduct the single leg bending tests for obtaining the cohesive parameters under different mode dominance conditions.

iii) To validate the methodology in mixed mode conditions.

2.6 SCOPE OF THESIS

i) To develop HDMR based CZM for capturing the steady state energy in uni-directional DCB specimens, based on the experimental data.

ii) To conduct experiments on the uni-directional composite specimens under three point bending test using Tinus testing machine for obtaining load-displacement curves on different mode dominant conditions.

iii) To determine the optimal cohesive parameters form the experimental data and simulation, and

iv) To verify the developed method in different mixed mode conditions.

CHAPTER 3

MODELING DELAMINATION IN COMPOSITE USING HDMR BASED COHESIVE ZONE MODEL

3.1 COHESIVE BRIDGING LAW

Generally, cohesive elements are embedded by the TSL for defining the crack tip. Based on TSL, the CZM which signifies fracture process zone (FPZ), starts separation as the load increases and this separation will continue till it reaches the critical limit. Traction-separation failure mechanism follows three steps: (i) Damage initiation: It signals when the element starts the damage, (ii) Damage evolution: It is the rate of change of stiffness of the element when damage occurs, and (iii) Element removal: It happens when the traction reaches zero at a critical normal separation value. Due to active participation of fibers in the crack advancement, the crack growth resistance will take place in delamination process.

In General, delamination takes place between matrix interfaces. During crack propagation in laminates, fiber interaction is inevitable due to their misalignment of the fibers at the time of curing process. Hence, these type of fiber interactions rely on the geometry of specimen and loading mixity at the time of fracture resistance (Spearing and Evans 1992). Due to the fiber bridging in composites, increase in ERR is observed. Therefore, the crack initiation and crack propagation energies need to be considered in TSL, which is not possible with the existing bilinear or park paulino roesler (PPR) CZM. To estimate the progressive delamination of composites, different TSLs were used in the literature.

With the help of *J*-integral concepts, the bridging law parameters are measured to understand the features of the unidirectional fiber composites (Rice 1968; Spearing and Evans 1992). Suo et al. (1992) developed an analytical expression for evaluating the global *J*-integral on the outer layers of the specimen beneath mode-I loading as follows.

$$J = \frac{p^2 a^2}{b\, E_{11}\, I} \left[1 + \xi(\rho)\, \lambda^{\frac{1}{4}} \left(\frac{h}{a} \right) \right]^2 \qquad (3.1)$$

where, λ is an elastic anisotropy measure, $\lambda = E_{22}/E_{11}$, in which, E_{22} is modulus of elasticity in transverse, and E_{11} is in the longitudinal directions, and ρ is also an elastic anisotropy measure, $\rho = \left(\sqrt{E_{11}E_{22}}/2G_{12}\right) - \sqrt{\nu_{12}\nu_{21}}$, G and ν are shear moduls and Poisson's ratio, while p is load, a is crack length, and b & h are the dimensions of the specimen. I is the moment of inertia of the DCB model expressed as, $I = bh^3/12$. The coefficient ξ has been evaluated numerically (Bao et al. 1992) as: $\xi = 0.677 + 0.146(\rho - 1) - 0.0178(\rho - 1)^2 + 0.00242(\rho - 1)^3$.

Generally, when the unidirectional composite DCB specimen is subjected to a load, fiber bridging occurs across the crack faces near the crack tip for the growth of the crack in pure mode-I, assuming that the stresses corresponding to closure/bridging are dependent on the local crack separation, δ. Due to this nature, bridging law $\sigma = \sigma(\delta)$ is taken as equal over the bridging zone length. Therefore, the relationship between bridging stress, σ and local crack separation, δ is used to define the bridging law. The fibers will carry the load till it reaches the characteristic crack separation δ_0, and once this stage is reached, the closure traction disappears. Then locally estimated J-integral is represented as (Suo et al. 1992)

$$J = \int_0^{\delta^*} \sigma(\delta)\,d\delta + J_0 \tag{3.2}$$

where, first term is the energy dissipation in the bridging zone and J_0 is the initial value of ERR evaluated around the crack tip, and δ^* is the end-opening of the bridging zone. Also, the bridging law is obtained by

$$\sigma(\delta^*) = \frac{\partial J_R}{\partial \delta^*} \tag{3.3}$$

where J_R is the ERR during crack growth. At the beginning, the crack is unbridged, and the crack growth initiation takes place when $J_R = J_0$. As the crack develops, the value of J_R goes up, and the R-curve reaches steady state crack growth resistance J_{ss}, whereas the end-opening of the bridging zone δ^* reaches δ_0.

Feih et al. (2005) found that the following analytical equation will be valid for all the test data curves of crack growth resistance against crack separation data.

24

$$J_R\left(\delta^*\right) = J_0 + \Delta J_{SS}\left(\frac{\delta^*}{\delta_0}\right)^{\frac{1}{2}} \tag{3.4}$$

where, ΔJ_{SS} is the steady state fracture energy, $\Delta J_{SS} = \left(J_{SS} - J_0\right)$, which indicates that the presence of fiber bridging results in increased value of crack growth resistance. Differentiating Eq. (3.4) yields the results in bridging law.

$$\sigma\left(\delta^*\right) = \frac{\Delta J_{SS}}{2\delta_0}\left(\frac{\delta}{\delta_0}\right)^{-\frac{1}{2}} = \frac{\Delta J_{SS}}{2\sqrt{\delta_0 \delta}} \quad 0 < \delta^* < \delta_0 \tag{3.5}$$

Feih (2006) compared bridging laws for different fiber systems and concluded that the bridging law is independent of specimen geometry. Figure 3.1 shows the bridging law for a typical material system , and it can be considered as a material property (Spearing and Evans 1992; Sørensen and Jacobsen 1998).

3.2 IMPORTANCE OF ADJUSTED BRIDGING LAW

The bridging law in Eq. (3.5) has a simple form, but if the crack opening displacement is zero, then the singularity will take place, and the bridging stress leads to infinity and also after differentiation of Eq. (3.4), there is no crack initiation (J_0) term. To address these two important points during the numerical adjustment, finite stress value and zero stress value are the two different methods implemented (Feih 2006). The simplest approach is to divide the two components J_0 and ΔJ_{ss} within the bridging law and use the initial increase up to Δu_2 for introducing J_0. The adjusted bridging law is shown in Fig. 3.2.
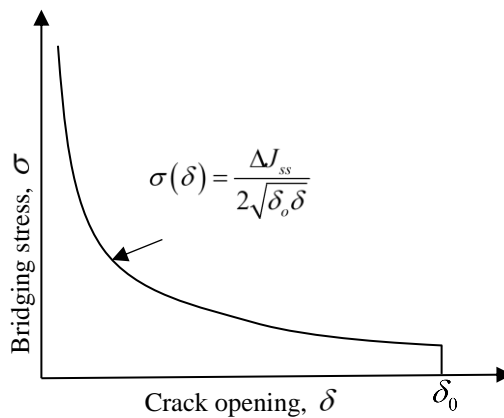
Fig. 3.1 Typical bridging law (Shanmugam et al. 2013)

The power law factor α helps to maintain the tangent close to zero at the peak of the bridging law, in turn, assists to an improved numerical behavior by means of convergence. The physical interpretation of the cohesive law parameters is advantageous in splitting of the bridging law into an initial fracture and damage control part. Accordingly, the bridging law variables (J_0, ΔJ_{SS}, Δu_0 and Δu_2 except Δu_1) are measured on the basis of the experimental data. Hence, the crack initiation J_0 and steady state energy J_{SS} values can be designated using the R-curve as shown in Fig. 3.3 (obtained from the experiments), and with the help of these two values, the difference in fracture energy, $\Delta J_{SS} = \left(J_{SS} - J_0 \right)$ is calculated. Figure 3.4 shows the relationship between crack opening displacement and crack growth resistance, and both the crack opening displacements Δu_2 and Δu_0 are measured at J_0 and J_{SS}, respectively. Hence, only the value of Δu_1 is to be adjusted in the bridging law to fit the experimental data points.
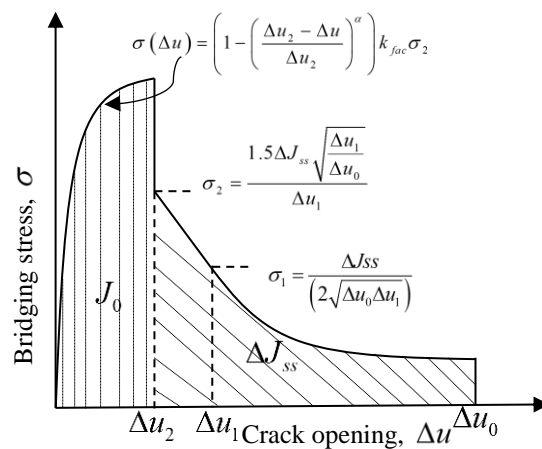
Fig. 3.2 Adjusted bridging law (Shanmugam et al. 2013)
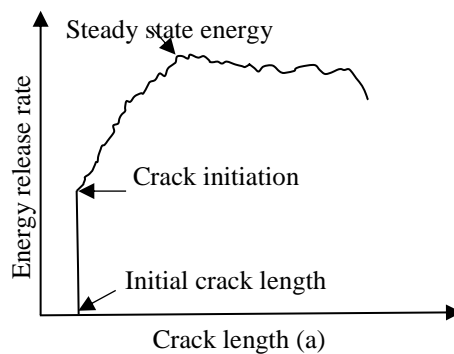
Fig. 3.3 Energy vs crack length (Shanmugam et al. 2013)

26

3.3 APPLICATION OF THE USER ELEMENT

Several possible techniques are used in applying the cohesive laws in the FE codes. The development and coding of cohesive elements based on the cohesive laws is among the most adoptable one (Schellekens and Borst 1993; Chen et al. 1999; Spring and Paulino 2014). A stress, based on a relative nodal spacing is recommended in most cases, presumably known with zero thickness choesive elements. Likewise, efforts asscociated with simplifications have also been employed in VCCT in order to compute the corresponding nodal spring forces from the surrounding elements. However, VCCT is not directly applicable for nonlinear shape functions, such as eight-noded elements (Jacobsen and Sorensen 2001).

Basic Equations:

Two-dimensinal and three-dimensional interface elements are illustrated in Figure 3.5.
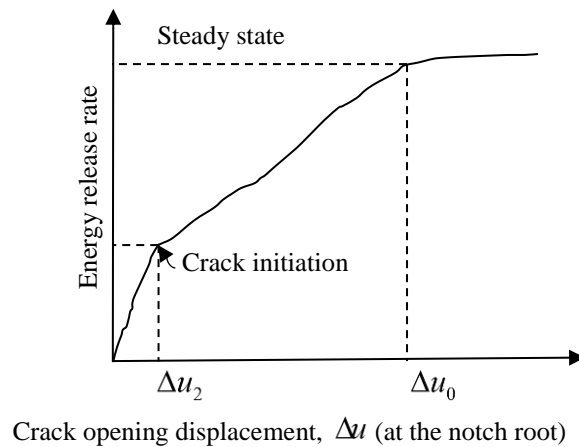
Fig. 3.4 Energy vs crack opening displacement (Shanmugam et al. 2013)
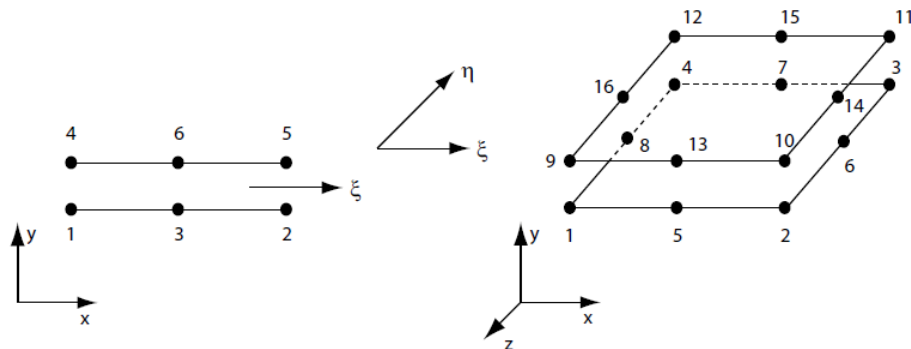
Fig. 3.5 Quadratic line and plane interface elements

The interface element encompasses two quadratic line elements or two quadratic two-dimensional plane elements. During the fracture growth, the faces of adjacent elements are connected with the interface elements. Segurado and Llorca (2004) have studied the application of user elements. Accordingly, quadratic solid elements are selected as a cantilever beam, which in most cases distorts under bending. Overlaying the quadratic element with interface element requires the interface element nodes to fit perfectly. Therefore, the node numbering is selected based on ABAQUS conventions of two-dimensional and three-dimensional quadratic solid elements.

In unstressed deformation state, the two interface element surfaces lie together and separate as the adjacent elements start to deform. The relative separations of the element face create both normal and shear movements, which in turn create element stresses based on the constitutive equations of the material. The application of a general interface element for the quadratic line element (for two-dimensional models) is explained as follows.

The line interface element has 12 (i.e., 2×6) degrees of freedom, where as the vector (12×1) of the nodal displacements $(\mathbf{d}_N)$ in the global coordinate system is given as:

$$\mathbf{d}_N = \left(d_x^1 \ d_y^1 \ d_x^2 \ d_y^2 \ \ldots d_x^6 \ d_y^6 \right)^{\mathrm{T}} \tag{3.6}$$

where, T stands for transpose of the matrix.

The nodal difference between the top and bottom displacements , (u) gives the opening of the interface element and expressed as:

$$\Delta u = \{u\}^{\mathrm{top}} - \{u\}^{\mathrm{bottom}} \tag{3.7}$$

thus leading to the subsequent description of the interface opening $\Delta \mathbf{u}_N$ in terms of nodal separation of paired nodes:

$$\Delta \mathbf{u}_N = \boldsymbol{\Phi} \mathbf{d}_N = \left[-\mathbf{I}_{6 \times 6} \ \middle| \ \mathbf{I}_{6 \times 6} \right] \mathbf{d}_N \tag{3.8}$$

where $\mathbf{I}_{6 \times 6}$ represents an identity matrix with six rows and six columns, and $\mathbf{u}_N$ is a 6×1 vector.

The crack opening is interpolated to the integration points from the nodal locations with the help of standard shape functions. Let $N_i(\xi)$ be the shape function for the node pair i ($i = 1-3$), where ξ stands for the local coordinate of the element with $-1 \leq \xi \leq 1$. The

relative displacement between the nodes for each point within the element is then given by:

$$\Delta\mathbf{u}\left(\xi\right) = \begin{pmatrix} \Delta u_x\left(\xi\right) \\ \Delta u_y\left(\xi\right) \end{pmatrix} = \mathbf{H}\left(\xi\right)\Delta\mathbf{u}_N \tag{3.9}$$

where $\mathbf{H}\left(\xi\right)$ is a 2×6 matrix containing the quadratic shape functions. From the line element,

$$\mathbf{H}\left(\xi\right) = \begin{pmatrix} N_1\left(\xi\right) & 0 & N_2\left(\xi\right) & 0 & N_3\left(\xi\right) & 0 \\ 0 & N_1\left(\xi\right) & 0 & N_2\left(\xi\right) & 0 & N_3\left(\xi\right) \end{pmatrix} \tag{3.10}$$

thus results in,

$$\Delta\mathbf{u}\left(\xi\right) = \mathbf{H}\left(\xi\right)\mathbf{\Phi}\mathbf{d}_N = \mathbf{B}\left(\xi\right)\mathbf{d}_N \tag{3.11}$$

where, $\mathbf{B}\left(\xi\right)$ is of the dimension 2×12 and $\Delta\mathbf{u}\left(\xi\right)$ is of the dimension 2×1; thereby describing the continuous displacement field in both directions within the element.

A local coordinate system is required by the user element, inorder to measure local deformations in normal and tangential directions during large deformations. The coordinate system obtained from the middle points of the two element faces is, therfore, considered as one of the best common choice, which thereby coincides with the nodal positions in the undeformed state.

If the coordinates of the initial configuration are given by the vector $\mathbf{X}_N$ and the deformation state is defined by the vector $\mathbf{d}_N$, the reference surface coordinates $\mathbf{X}_N^R$ are computed by linear interpolation between the top and bottom nodes in their deformed state:

$$\mathbf{x}_N^R = \frac{1}{2}\left(\mathbf{I}_{6\times6} \mid \mathbf{I}_{6\times6}\right)\left(\mathbf{x}_N + \mathbf{d}_N\right) \tag{3.12}$$

The coordinates of any specific reference plane can be derived similar to Eq.(3.9).

$$\mathbf{x}^R\left(\xi\right) = \begin{pmatrix} x^R\left(\xi\right) \\ y^R\left(\xi\right) \end{pmatrix} = \mathbf{H}\left(\xi\right)\mathbf{x}_N^R \tag{3.13}$$

This local coordinate vector, with unit length, is obtained by differentiating the global position vector with respect to the local coordinates:

$$t_1 = \frac{1}{\left\| \frac{\partial \mathbf{x}^R}{\partial \xi} \right\|} \left(\frac{\partial x^R}{\partial \xi}, \ \frac{\partial y^R}{\partial \xi} \right)^{\mathrm{T}} \tag{3.14}$$

The normal vector (also with unit length) of the local coordinate element needs to be perpendicular to the vector t_1:

$$t_n = \frac{1}{\left\| \frac{\partial \mathbf{x}^R}{\partial \xi} \right\|} \left(\frac{-\partial y^R}{\partial \xi}, \ \frac{\partial x^R}{\partial \xi} \right)^{\mathrm{T}} \tag{3.15}$$

and the derivatives are determined as follows:

$$\frac{\delta \mathbf{x}^R(\xi)}{\delta \xi} = \begin{pmatrix} x^R_{,\xi} \\ y^R_{,\xi} \end{pmatrix} = \frac{\delta(\mathbf{H}(\xi))}{\delta \xi} \mathbf{x}^R_N = \mathbf{h}(\xi)\mathbf{x}^R_N \tag{3.16}$$

with

$$\mathbf{h}(\xi) = \begin{pmatrix} N_{1,\xi}(\xi) & 0 & N_{2,\xi}(\xi) & 0 & N_{3,\xi}(\xi) & 0 \\ 0 & N_{1,\xi}(\xi) & 0 & N_{2,\xi}(\xi) & 0 & N_{3,\xi}(\xi) \end{pmatrix} \tag{3.17}$$

The length of the vector is given by the standard definition:

$$\left\| \frac{\partial \mathbf{x}^R}{\partial \xi} \right\| = \sqrt{\left(\frac{\partial x^R}{\partial \xi} \right)^2 + \left(\frac{\partial y^R}{\partial \xi} \right)^2} \tag{3.18}$$

The components t_1 and t_n indicate the direction cosines of the local coordinate system to the global one, thus defines the 2×2 transformation tensor Θ as

$$\Theta = [t_1, t_n] \tag{3.19}$$

which relates the local and global displacements as follows:

$$\Delta \mathbf{u}_{\mathrm{loc}} = \Theta^{\mathrm{T}} \Delta \mathbf{u} \tag{3.20}$$

where, the local matrices are designated by the subscript (loc) as in Eq. 3.20 above, else the expressions refer to the global values.

t_{loc} is the 1×2 vector governing the bridging stresses in the local coordinate system and relates to the local relative displacement through constitutive equation for the interface element:

$$\mathbf{t}_{\mathrm{loc}} = \begin{pmatrix} \sigma_1 \\ \sigma_n \end{pmatrix} = \mathbf{C}_{\mathrm{loc}}(\Delta \mathbf{u}_{\mathrm{loc}}) \ \Delta \mathbf{u}_{\mathrm{loc}} \tag{3.21}$$

where, $\mathbf{C}_{loc}$ is the constant not depend on the displacements. The constitutive equation can be described either with a linear displacement term for $\Delta\mathbf{u}$ as shown above, or with a coupled form, where $\Delta\mathbf{u}$ is encompassed with nonlinear dependence. Nonetheless, the ideal alternative depends on the form of the constitutive expression. For the equation introduced in Eq. (3.5) , a coupled form is preferable:

$$\mathbf{t}_{loc} = \mathbf{C}_{loc}\ \Delta\mathbf{u}_{loc}^{-\frac{1}{2}} \tag{3.22}$$

In comparison with Eq. (3.5), δ has been substituted with the general numerical terminology for the opening, $\Delta\mathbf{u}_{loc}$. This convention will be used in the following descriptions. Note that, the UEL subroutine in ABAQUS needs the element stiffness matrix and the right hand side nodal force vector.

The element force vector is of size 12×1. Its role to the global force vector is given by

$$\begin{aligned}\mathrm{f}_N^{el} &= \int_{A_{el}} \mathbf{B}^T\mathbf{t}\ dA \\ &= W\int_{-1}^{1}\mathbf{B}^T\Theta\mathbf{t}_{loc}\ \det\mathbf{J}\ d\xi\end{aligned} \tag{3.23}$$

where W is the width of the interface element and, as in most cases of 2-D modeling, also the width of the FE model, and $\det\mathbf{J}$ is the Jacobian defined by the transformation of the global coordinates (x, y) to the current element coordinate (ξ), and results, for the line element, in the same expression as previously used for calculating the length of the unit vector in Eq. (3.18):

$$\det\mathbf{J} = \sqrt{\left(\frac{\partial x^R}{\partial\xi}\right)^2 + \left(\frac{\partial y^R}{\partial\xi}\right)^2} \tag{3.24}$$

In most studies, the Jacobian matrix is not considered as constant but depends on the local element coordinates. Therefore, it requires derivations for each integration point. Hence, the tangent stiffness matrix (i.e., 12×12) is accordingly defined as

$$\mathbf{K}^{el} = -\frac{\partial\mathbf{f}_N^{el}}{\partial\mathbf{d}^{el}} \tag{3.25}$$

with the derivation from Eq. (3.23), this results in:

$$\begin{aligned}\mathbf{K} &= -\int_{Ael} \mathbf{B}^T\Theta\frac{\partial\mathbf{t}_{loc}}{\partial\mathbf{d}^{el}}\ dA \\ &= -W\int_{-1}^{1}\mathbf{B}^T\Theta\mathbf{D}_{loc}\Theta^T\mathbf{B}\ \det\mathbf{J}\ d\xi\end{aligned} \tag{3.26}$$

31

The stiffness matrix $\mathbf{D}$ is defined as:

$$\mathbf{D}_{\text{loc}} = \frac{\partial \mathbf{t}_{\text{loc}}}{\partial \Delta \mathbf{u}_{\text{loc}}} \qquad (3.27)$$

It can also be expressed in terms of the constitutive equation in Eq. (3.21) with a linear dependence on $\Delta \mathbf{u}$:

$$\mathbf{D}_{\text{loc}} = \frac{\left[\partial \mathbf{C}(\Delta \mathbf{u}) \Delta \mathbf{u} \right]}{\partial \Delta \mathbf{u}} = \frac{\left[\partial \mathbf{C}(\Delta \mathbf{u}) \right]}{\partial \Delta \mathbf{u}} \Delta \mathbf{u} + \mathbf{C}(\Delta \mathbf{u}) \qquad (3.28)$$

The local traction matrix $\mathbf{S}$ is then given by

$$\mathbf{S}_{\text{loc}} = \begin{pmatrix} D_1 & D_c \\ D_c & D_n \end{pmatrix} \qquad (3.29)$$

Finding derivations of Eq. (3.27) yields the terms D_1 and D_n values. The D_c elements are possible coupling terms, which are typically attained by the TSLs derived from an elastic potential for the cohesive law. For mode-I loading cases, the relative displacement in u_1 direction will be zero, and thus leads to zero traction stresses. Therefore, the coupling terms can then be set to zero as they do not impact the overall results. However, a dummy value for D_1 has to be assumed to prevent likely numerical errors attributable to a singular stiffness matrix.

3.4 COHESIVE ELEMENT VERIFICATION

The process of implementing the cohesive elements in to the ABAQUS is shown in Fig. 3.6. A simple two element model with user element is shown in Fig. 3.7. Accordingly, the nodes 1 to 6 (in Fig. 3.7) for the user element primarily coincide in their position (here, the nodes are shown far from each other for a good understanding of the node numbering). The input deck for the two-element problem is as shown in Appendix-A.

Figure 3.8 reveals the values for the test case as created by ABAQUS. As the stiffness of the top element is high compared to the bridging stress input, the stress distribution in loading direction appears constant.
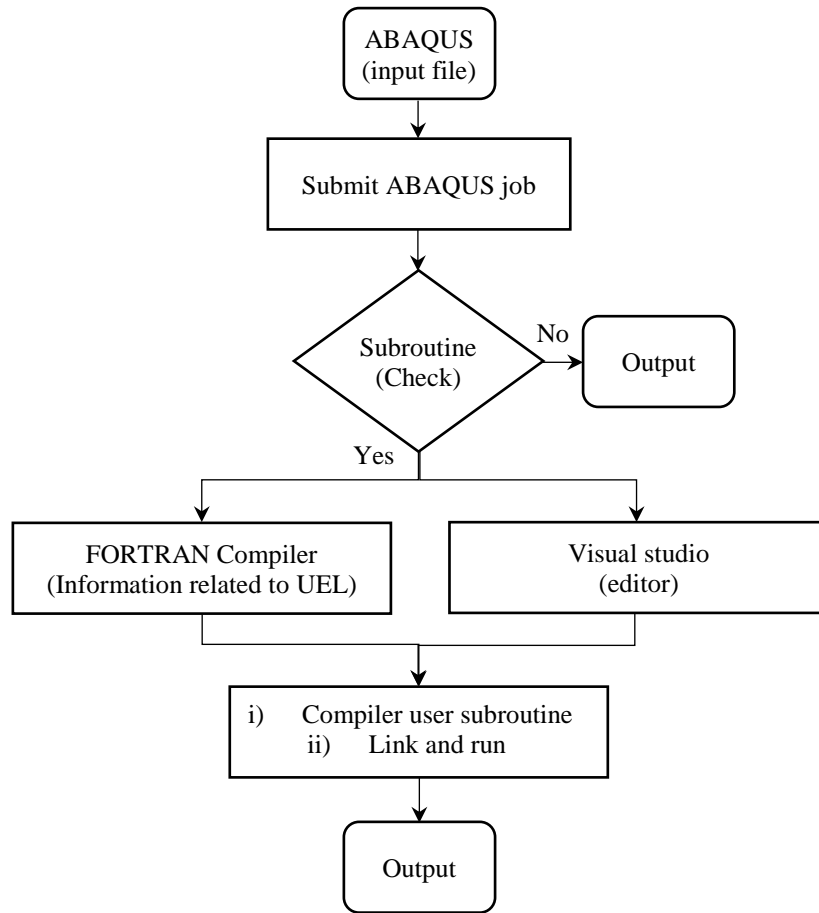
Fig. 3.6 Implementation process
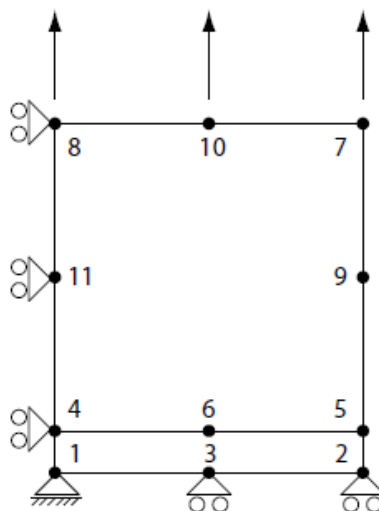
Fig. 3.7 2-D user element

Besides, the displacement field caused by the Poisson's effect in x-direction varies linearly with the loading stress. Consequently, the reaction forces, element area and the opening of the element are used to form the original bridging law for simple case of

uniform deformation (i.e., constant displacement boundary conditions on the entire top nodes). Meanwhile, the sensitivity of results use the crack opening, crack length and crack shape among the information related to fracture data to the presumed bridging law shape. Furthermore, numerical estimates are used in refining the bridging law fit of the shapes.
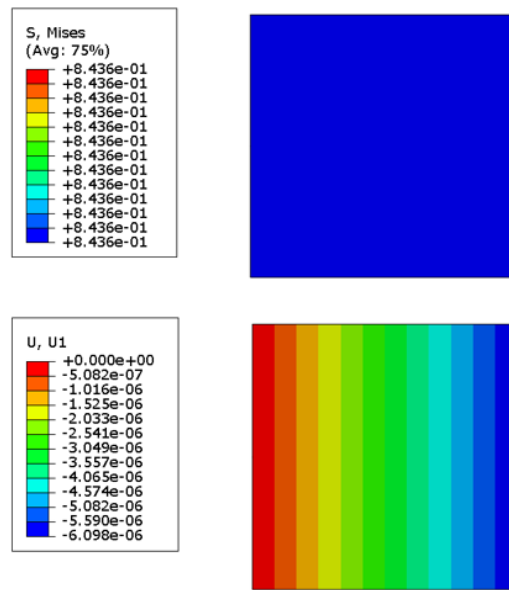
(a)
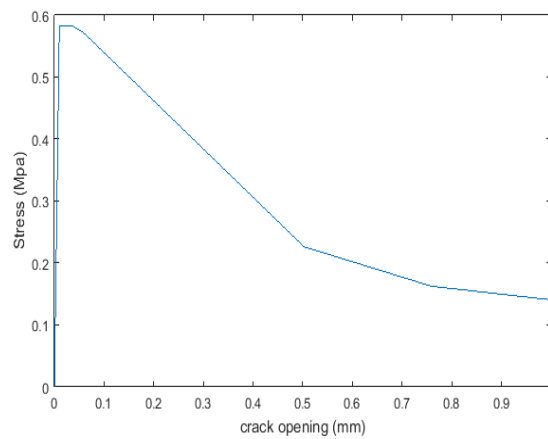
(b)

Fig. 3.8 (a) Contours of stress and displacement; (b) Stress at crack tip

3.5 HIGH DIMENSIONAL MODEL REPRESENTATION

HDMR is the method of multivariate functions (Balu and Rao 2013). It is having high command on the system response, starts with constant term and gradually includes higher order terms. In most of the cases, by using only lower order terms, the entire physical system can be captured. The HDMR methodology has been applied to even nonlinear models to get accurate reduced model of the original system (Wang et al. 1999; Alış and Rabitz 2001; Chowdhury and Adhikari 2010; Li et al. 2001; Balu and Rao 2012; Gao et al. 2015; Naveen and Balu 2017)

To understand the relationship among the input parameters and output response, consider $f(\mathbf{x})$ as the output of the system response, which is a function of input vector $\mathbf{x} = \{x_1, x_2, ..., x_N\}$. The output response will have the effect of the input in terms of individual or cooperative, therefore the output of the HDMR is expressed as follows.

$$f(\mathbf{x}) = f_0 + \sum_{i=1}^{N} f_i(x_i) + \sum_{1 \le i \le j \le N} f_{ij}(x_i, x_j) + ... + f_{12...N}(x_1, x_2, ..., x_N) \quad (3.30)$$

where f_0 denotes the response of the system at the mean input parameters. The term $f_i(x_i)$ is a first-order of variable x_i on the output $f(\mathbf{x})$, and $f_{ij}(x_i, x_j)$ is a second-order term having the influence of the both the variables x_i and x_j in the cooperative manner on $f(\mathbf{x})$. If all the component functions in Eq. (3.30) are obtained, then it is efficient to calculate the output responses of the system. Hence, expensive methods can be replaced with the HDMR for calculations.

To represent the output $f(\mathbf{x})$ exactly in the given variable space, cut-HDMR method will be helpful. The initial step in this method is selecting the reference point $\mathbf{c} = \{c_1, c_2, ..., c_N\}$ for the variables, but in the convergence limit, the selection of reference point $\mathbf{c}$ is invariant. Generally, $\mathbf{c}$ is chosen within the region of interest in the input space. Once the selection process is finalised, need to determine the expansion functions with the help of input–output responses of the system relative to the defined reference point $\mathbf{c}$ along the cuts in the input variable space. Hence the component functions in Eq. (3.30) are as follows.

$$f_0 = f(\mathbf{c}) \quad (3.31)$$

$$f_i(x_i) = f(x_i, c^i) - f_0 \qquad (3.32)$$

where $f(x_i, c^i) = f(c_1, c_2, \dots c_{i-1}, x_i, c_{i+1}, \dots c_N)$ represents that except x_i the other input parameters are at their reference point values. Finally, to get the value for f_0 evaluate all the input parameters at the reference point $\mathbf{c}$.

To get the final output response $f(\mathbf{x})$, the following steps are followed.

Step 1: Select the first-order component function $f(x_i, c^i) = f(c_1, c_2, \dots, c_{i-1}, x_i, c_{i+1}, \dots, c_N)$. If for $x_i = x_i^j, n$ function values

$$f(x_i^j, c^i) = f(c_1, c_2, \dots c_{i-1}, x_i^j, c_{i+1}, \dots c_N), \quad j = 1, 2, \dots, n \qquad (3.33)$$

are given at n sample points along the variable axis x_i. The function value is thus evaluated as follows.

$$f(x_i^j, c^i) = \sum_{j=1}^{N} \phi_j(x_i) f(c_1, \dots, c_{i-1}, x_i^j, c_{i+1}, \dots, c_N) \qquad (3.34)$$

where, N is number of variables involved. By using Eq. (3.34), $f_i(x_i)$ can be generated if n function values are available. Repeat the same procedure for the remaining component functions.

Step 2: By adding the above functions, we get the first-order expansion $f(\mathbf{x})$ as follows.

$$\tilde{f}(x) = \sum_{i=1}^{N} \sum_{j=1}^{n} \phi_j(x_i) f(c_1, \dots, c_{i-1}, x_i^j, c_{i+1}, \dots, c_N) - (N-1) f_0 \qquad (3.35)$$

where the Lagrange interpolation function $\phi_j(x_i)$ is defined as

$$\phi_j(x_i) = \frac{(x_i - x_i^1) \dots (x_i - x_i^{j-1})(x_i - x_i^{j+1}) \dots (x_i - x_i^n)}{(x_i^j - x_i^1) \dots (x_i^j - x_i^{j-1})(x_i^j - x_i^{j+1}) \dots (x_i^j - x_i^n)} \qquad (3.36)$$

The total number of original function evaluation is obtained by

$$\sum_{s=0}^{l} \frac{N!}{(N-1)! s!} (n-1)^s \qquad (3.37)$$

where, s is the order of the component function, n is the number of sample points. As compared to the other sampling schemes, HDMR sampling scheme is significant because, with minimum component functions, more accurate results can be achieved.

36

3.6 HDMR BASED CZM

For generating the FE model, the details of the model are chosen from the tests conducted to determine the interlaminar fracture toughness of the unidirectional composite DCB under mode-I loading (Shanmugam et al. 2013). The dimensions of the 2-D FE model are 254 mm long with a width of 25 mm which has two 6 mm thickness arms, and also having an initial crack of 51 mm and 76.2 mm, which are similar to the test specimens. The material properties of the composite are shown in Table 3.1. Each FE model (Fig. 3.9) comprises of 6 node cohesive elements with zero thickness and 0.5 mm element size 8 node elements (i.e., CPE8). In the FE model, cohesive elements are placed ahead of crack tip at the interface of model arms.

In this work, to capture the steady state ERR variation, following procedure is adopted.

i. From the available experimental data of 51 mm crack size (Table 3.2), the load, crack length and steady state energy are represented in cumulative distribution function (CDF) format.

ii. The HDMR response surface functions are developed for crack length and load distribution from bridging law parameter bounds.

iii. Monte carlo simulations (MCS) are performed to get the load, crack length and the corresponding energy (J).

iv. To minimize the error between the experimental and calculated values, optimization is performed using Eq. (3.38) and statistical characteristics (mean, standard deviation, skewness and kurtosis) are determined for the adjusted bridging law parameters.

$$Error = \sqrt{\left(J_{cal} - J_{test}\right)^2} \tag{3.38}$$

Figure 3.10 shows the flowchart for the procedure adopted in calculating the ERR.

Cohesive element (user subroutine)
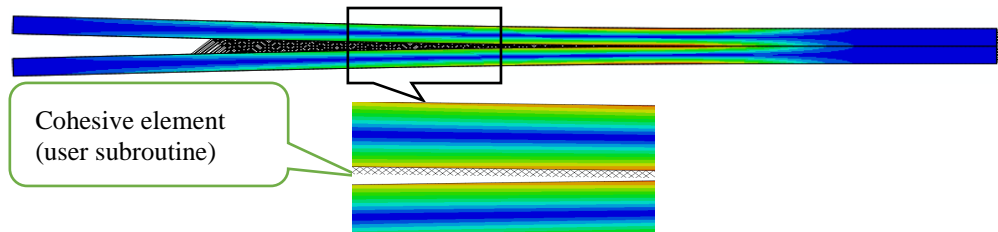
Fig. 3.9 DCB finite element model

Table 3.1 Material properties (Shanmugam et al. 2013)

Description	Value
E_{11} (GPa)	146
E_{22} (GPa)	8.214
G_{12} (GPa)	4.53
v_{12}	0.332
v_{21}	0.012
$J_{0\text{-Initiation}}$ (J/m^2)	213

Table 3.2 Test data for 51mm initial crack (Shanmugam et al. 2013)

Test number	Crack length, a (m)	Load (N)	J_{ss} (J/m^2)
Test 1	0.1314	243.863	653.0
Test 2	0.1614	220.741	800.6
Test 3	0.1746	204.248	800.3
Test 4	0.1203	236.659	517.5
Test 5	0.1251	221.788	490.6
Test 6	0.1509	223.733	721.3
Test 7	0.1689	197.728	702.8
Test 8	0.1740	203.795	791.7
Test 9	0.1689	197.867	702.4
Test 10	0.1880	193.867	833.7
Test 11	0.1829	176.798	656.8
Test 12	0.1421	201.575	519.9
Test 13	0.1509	216.157	672.7
Test 14	0.1560	198.514	605.6
Test 15	0.1558	200.236	614.6

Using the experimental data, bounds for each bridging law parameter are estimated as presented in Table 3.3 (Shanmugam et al. 2013). For these bounds, the HDMR techniques are implemented to generate the component functions. Accordingly, HDMR was constructed using 21 component functions for the adjusted parameters.

The magnitudes of the crack length and load, where the steady state crack propagation starts, were determined for the developed component functions using the ABAQUS. Figure 3.11 presents a flow chart for generating the response surface using HDMR.

From the Finite Element Analysis (FEA), the details of crack length and load are calculated for the component functions, and their results are shown in Table 3.4.

Table 3.3 Lower and upper bounds

Parameter	Lower bound	Upper bound
$\Delta J_{ss}\ (\mathrm{J/m^2})$	100	700
$\Delta u_0\ (\mathrm{mm})$	1	7
$\Delta u_1\ (\mathrm{mm})$	0.01	0.09
$J_0\ (\mathrm{J/m^2})$	190	230
K_{fac}	5	12

Figure 3.12 shows the captured steady state energy and load for the corresponding crack length for the third component function. Using the FEA data, two individual HDMR response surfaces were created for crack length and load as they are necessary inputs for steady state ERR calculation. After substituting the available material properties in Eq. (3.1), it becomes easy to calculate the steady state ERR as shown in Eq. (3.39).

$$Energy, J = \frac{p^2 a^2}{1.6425}\left[1 + \frac{0.00291}{a}\right]^2 \qquad (3.39)$$
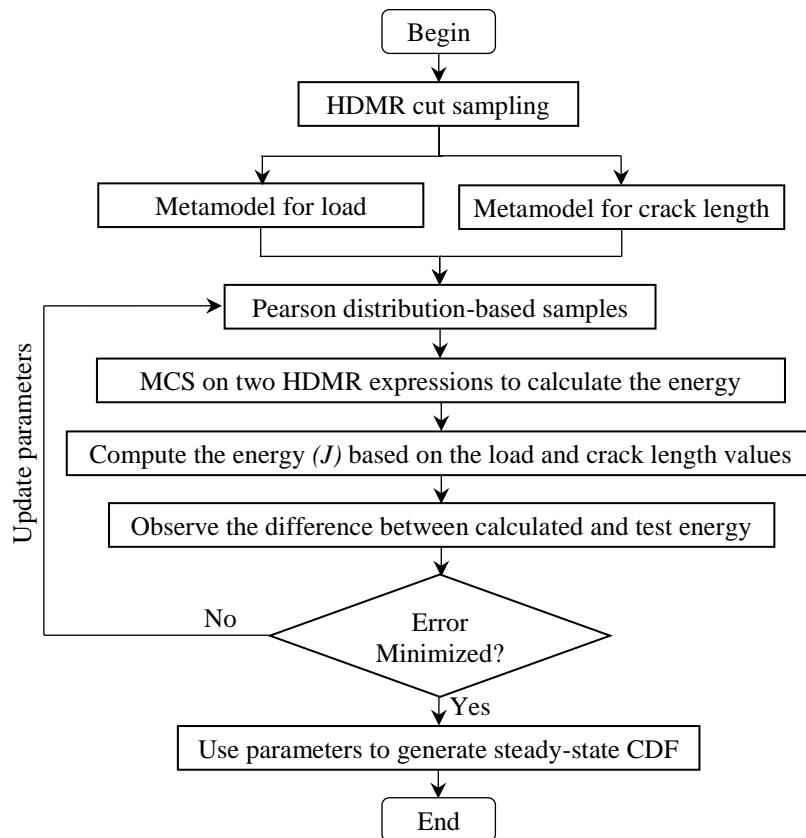
Fig. 3.10 Flowchart for determining CZM parameters

39

Table 3.4 Cut-HDMR sampling and corresponding FEA results for 51 mm initial crack

Component functions	Load (N)	Crack length (m)
f(100, 4, 0.455, 210, 8.5)	127.26	0.1522
f(250, 4, 0.455, 210, 8.5)	171.92	0.1523
f(400, 4, 0.455, 210, 8.5)	208.67	0.1489
f(550, 4, 0.455, 210, 8.5)	243.50	0.1440
f(700, 4, 0.455, 210, 8.5)	275.26	0.1417
f(400, 1, 0.455, 210, 8.5)	312.26	0.0940
f(400, 2.5, 0.455, 210, 8.5)	243.50	0.1252
f(400, 4, 0.455, 210, 8.5)	208.67	0.1489
f(400, 5.5, 0.455, 210, 8.5)	187.23	0.1680
f(400, 7, 0.455, 210, 8.5)	170.69	0.1860
f(400, 4, 0.01, 210, 8.5)	213.36	0.1510
f(400, 4, 0.2325, 210, 8.5)	209.41	0.1495
f(400, 4, 0.455, 210, 8.5)	208.67	0.1489
f(400, 4, 0.6775, 210, 8.5)	207.25	0.1489
f(400, 4, 0.9, 210, 8.5)	207.37	0.1482
f(400, 4, 0.455, 190, 8.5)	203.11	0.1515
f(400, 4, 0.455, 200, 8.5)	205.43	0.1550
f(400, 4, 0.455, 210, 8.5)	208.67	0.1489
f(400, 4, 0.455, 220, 8.5)	209.96	0.1487
f(400, 4, 0.455, 230, 8.5)	212.37	0.1417
f(400, 4, 0.455, 210, 5)	207.34	0.1472
f(400, 4, 0.455, 210, 6.75)	209.14	0.1469
f(400, 4, 0.455, 210, 8.5)	208.67	0.1489
f(400, 4, 0.455, 210, 10.25)	209.63	0.1487
f(400, 4, 0.455, 210, 12)	209.78	0.1495

The MCS was implemented on the response functions generated using HDMR with Pearson family of distributions. The selected distribution requires only four statistical parameters to represent probability density function (PDF). From each iteration of the MCS, the particular response surface generates one set of crack length and load values to estimate the CDF of steady state ERR using Eq. (3.39). The use of four statistical parameters facilitates the determination of each of the five CZM parameters in the HDMR owing to Pearson systems. The resulting 20 variables are adjusted for the purpose of simulation so as to match the scatter level in ERR with the experimental values.
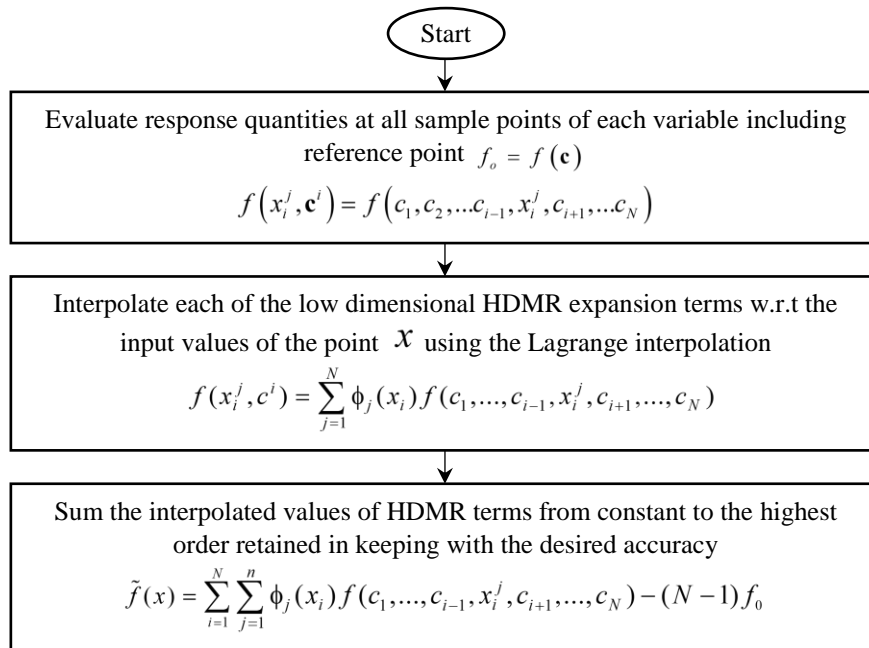
Fig. 3.11 Flow chart of HDMR based response surface generation

The flow chart contains the following boxes:

Start

Evaluate response quantities at all sample points of each variable including reference point $f_o = f(\mathbf{c})$

$$f\left(x_i^j, \mathbf{c}^i\right) = f\left(c_1, c_2, \ldots c_{i-1}, x_i^j, c_{i+1}, \ldots c_N\right)$$

Interpolate each of the low dimensional HDMR expansion terms w.r.t the input values of the point x using the Lagrange interpolation

$$f(x_i^j, c^i) = \sum_{j=1}^{N} \phi_j(x_i) f(c_1, \ldots, c_{i-1}, x_i^j, c_{i+1}, \ldots, c_N)$$

Sum the interpolated values of HDMR terms from constant to the highest order retained in keeping with the desired accuracy

$$\tilde{f}(x) = \sum_{i=1}^{N} \sum_{j=1}^{n} \phi_j(x_i) f(c_1, \ldots, c_{i-1}, x_i^j, c_{i+1}, \ldots, c_N) - (N-1)f_0$$

Fig. 3.12 Variation of energy and load with crack length (for 3rd sample point)

3.7 RESULTS AND DISCUSSION

In order to simulate the scatter in the delamination process, the cohesive bridging law variables have to be adjusted. This process involves minimisation of error between the expected and actual scatter in the steady state ERR. The error between the computed CDF and actual CDF from the experimental data is optimized by implementing the particle swarm optimization (PSO) using lower and upper bounds as presented in Table 3.3. The CDF plots of the steady state ERR for both experiment and simulation based obtained results are shown in Fig. 3.13. The statistical moments of the CZM parameters are well predicted by the implemented optimization process as observed from Fig. 3.13 and the maximum error occurred is 0.105. In Table 3.5 the optimal values of the CZM bridging parameters are exhibited. Using the available optimized values of the CZM, with an arbitrary initial crack size of DCB specimens, the steady state energy can be anticipated. Similarly, the load and crack length scatters have also been captured in the simulation as shown in Figs. 3.14 and 3.15, respectively. The load plot is in good agreement with the experimental data and the maximum error occurred is 0.149. However, the crack length prediction has shown some contradiction due to the inconsistent definitions, and the maximum error is 0.252. An average ERR can be obtained throughout steady state crack propagation and it remains constant. In the same way, it is clearly identified where the steady state crack propagation is approaching for a particular load. Nonetheless, the crack length may take many values. Hence, the scatter in crack lengths is inappropriate for adjusting the CZM parameters.
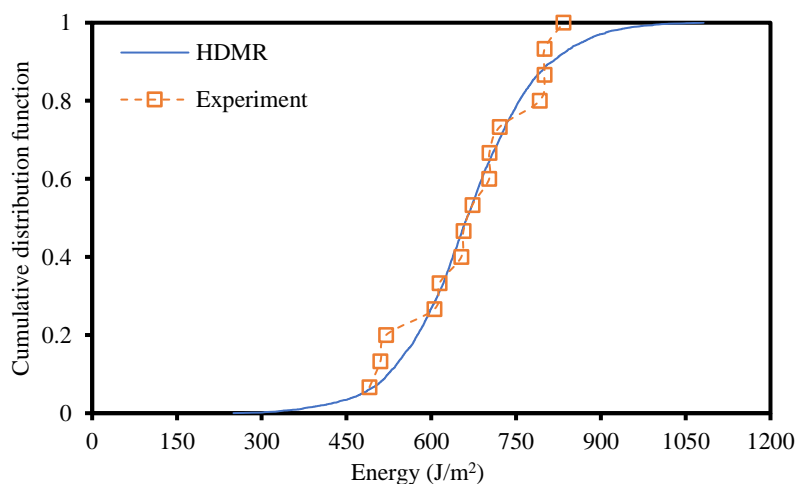
Fig. 3.13 Cumulative distribution function obtained by HDMR with respect to steady state energy for 51 mm crack

Table 3.5 Bridging law distribution results

Bridging law parameters	Pearson distributions	Optimal
ΔJ_{ss}	Mean (J/m^2)	396.749
	Std. dev.(J/m^2)	96.311
	Skewness	0.285
	Kurtosis	6.310
Δu_0	Mean (mm)	4.026
	Std. dev.(mm)	0.342
	Skewness	-0.412
	Kurtosis	3.784
Δu_1	Mean (mm)	0.285
	Std. dev.(mm)	0.106
	Skewness	-0.047
	Kurtosis	7.000
J_0	Mean (J/m^2)	203.460
	Std. dev.(J/m^2)	6.396
	Skewness	0.250
	Kurtosis	4.323
K_{fac}	Mean	7.764
	Std. dev.	0.803
	Skewness	-0.123
	Kurtosis	6.658

Fig. 3.14 Cumulative distribution function obtained by HDMR with respect to load for 51 mm crack
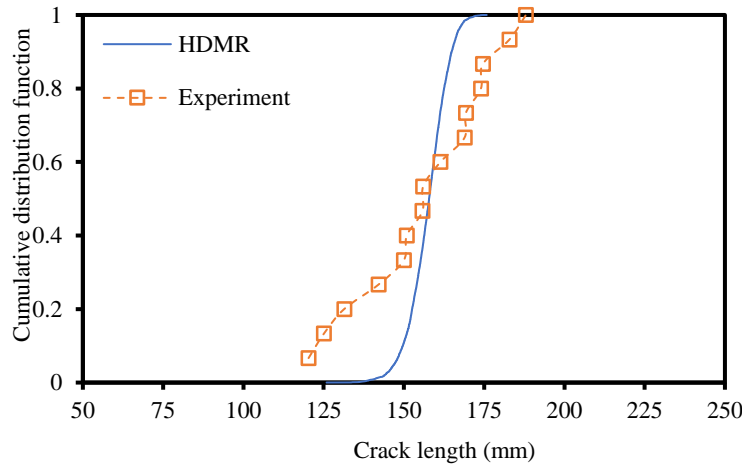
Fig. 3.15 Cumulative distribution function obtained by HDMR with respect to crack for 51 mm crack

To show the predictive potential of newly developed CZM, a FE model with 76.2 mm crack size is created. Similar to the 51 mm initial crack, two individual HDMR response surfaces were created for crack length and load. Table 3.6 shows the FEA results obtained for the 76.2 mm initial crack component functions. Considering the bridging parameters as the material property, the determined optimal cohesive parameters for 51 mm model are directly taken for 76.2 mm model with no further minimisation process.

The MCS was performed on the HDMR expressions and their results are compared with the experimental data for load, crack length and steady state energy as presented in Table 3.7. Figure 3.16 presents the details of crack propagation and identification of load. It has predicted the values exactly matching with the one obtained through the experiments, hence the proposed technique has the capability to model the delamination strength efficiently. As observed for the 51 mm initial crack length specimens, the crack length scatter (Fig. 3.17) between the test and simulation was not comparable even for the 76.2 mm specimens. As the 51 mm and 76.2 mm models possess the identical ERR, the information can be combined to make a single plot as presented in Fig. 3.18.

Table 3.6 Cut-HDMR sampling and corresponding FEA results for 76.2 mm initial crack

Component functions	Load (N)	Crack length (m)
$f(100,\ 4,\ 0.455,\ 210,\ 8.5)$	113.365	0.1780
$f(250,\ 4,\ 0.455,\ 210,\ 8.5)$	150.165	0.1750
$f(400,\ 4,\ 0.455,\ 210,\ 8.5)$	180.786	0.1720
$f(550,\ 4,\ 0.455,\ 210,\ 8.5)$	209.988	0.1675
$f(700,\ 4,\ 0.455,\ 210,\ 8.5)$	235.445	0.1650
$f(400,\ 1,\ 0.455,\ 210,\ 8.5)$	254.272	0.1171
$f(400,\ 2.5,\ 0.455,\ 210,\ 8.5)$	206.133	0.1486
$f(400,\ 4,\ 0.455,\ 210,\ 8.5)$	180.786	0.1720
$f(400,\ 5.5,\ 0.455,\ 210,\ 8.5)$	182.969	0.1750
$f(400,\ 7,\ 0.455,\ 210,\ 8.5)$	156.145	0.2027
$f(400,\ 4,\ 0.01,\ 210,\ 8.5)$	181.692	0.1725
$f(400,\ 4,\ 0.2325,\ 210,\ 8.5)$	180.598	0.1713
$f(400,\ 4,\ 0.455,\ 210,\ 8.5)$	180.786	0.1720
$f(400,\ 4,\ 0.6775,\ 210,\ 8.5)$	177.616	0.1733
$f(400,\ 4,\ 0.9,\ 210,\ 8.5)$	179.699	0.1720
$f(400,\ 4,\ 0.455,\ 190,\ 8.5)$	182.764	0.1710
$f(400,\ 4,\ 0.455,\ 200,\ 8.5)$	184.855	0.1700
$f(400,\ 4,\ 0.455,\ 210,\ 8.5)$	180.786	0.1720
$f(400,\ 4,\ 0.455,\ 220,\ 8.5)$	180.681	0.1710
$f(400,\ 4,\ 0.455,\ 230,\ 8.5)$	181.703	0.1718
$f(400,\ 4,\ 0.455,\ 210,\ 5)$	182.124	0.1718
$f(400,\ 4,\ 0.455,\ 210,\ 6.75)$	113.365	0.1780
$f(400,\ 4,\ 0.455,\ 210,\ 8.5)$	180.786	0.1720
$f(400,\ 4,\ 0.455,\ 210,\ 10.25)$	150.165	0.1750
$f(400,\ 4,\ 0.455,\ 210,\ 12)$	209.988	0.1675

Table 3.7 Test data for 76.2 mm initial crack (Shanmugam et al. 2013)

Test number	Crack length, a (m)	Load (N)	J_{ss} (J/m^2)
Test 1	0.1535	195.306	567.8
Test 2	0.1599	179.193	518.2
Test 3	0.1722	179.608	602.0
Test 4	0.1596	173.628	484.5
Test 5	0.1585	184.528	540.3
Test 6	0.1725	173.947	566.9
Test 7	0.1708	179.904	594.5
Test 8	0.1600	198.845	638.6
Test 9	0.1799	164.193	548.5

Fig. 3.16 Cumulative distribution function obtained by HDMR with respect to load for 51 & 76.2 mm initial crack

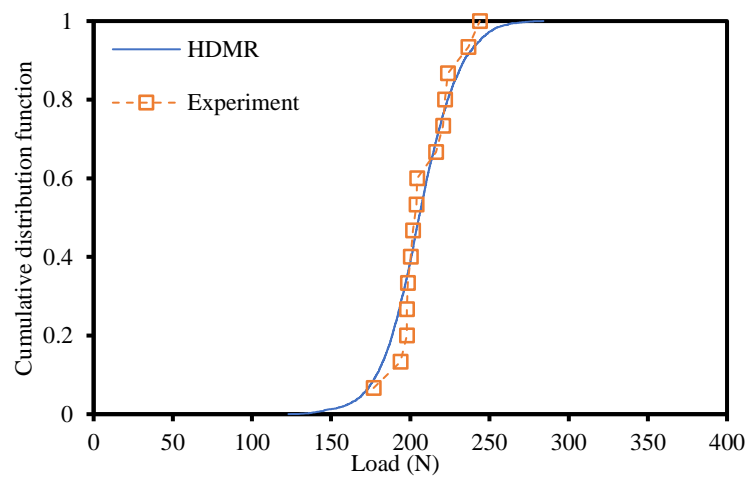Fig. 3.17 Cumulative distribution function obtained by HDMR with respect to crack for 51 & 76.2 mm initial crack
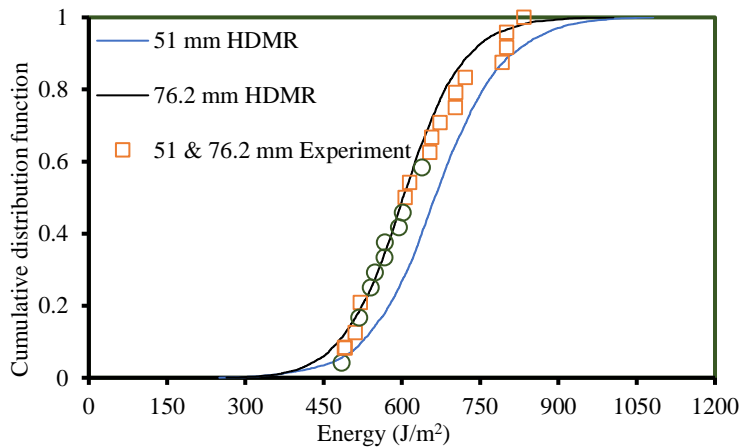
Fig. 3.18 Cumulative distribution function obtained by HDMR with respect to steady state energy for 51 & 76.2 mm initial crack

Comparison Between HDMR, RSM and Experimental Data

The results of HDMR based CZM are compared with the RSM based probabilistic CZM reported in the literature (Shanmugam et al. 2013). The comparative study is carried out for 51 mm initial crack among the RSM, HDMR and experimental data. Figure 3.19 shows the scatters obtained from RSM, HDMR and the experiment. It is also observed that the HDMR sampling scheme is having much significance as compared to the LHS sampling scheme owing to the accurate results in minimum component functions. From the Fig. 3.19, it is observed that the maximum error occurred for predicting the load, based on RSM and HDMR, is 0.159 and 0.149, respectively compared to the experimental data. The efficiency of the HDMR can be seen in Fig. 3.20, where the crack length of the specimen captured using first-order HDMR is much better than the second order nonlinear regression model (Shanmugam et al. 2013). When compared the RSM and HDMR in Fig. 3.20, the error is 0.265 and 0.252 respectively.

Figure 3.21 shows the effectiveness of the HDMR while capturing the delamination strength of the DCB specimen. Finally, in the energy plot shown in Fig. 3.21, the error obtained using RSM and HDMR is 0.148 and 0.105, respectively. In the similar way the predictive capability of the HDMR based CZM was compared to the 76.2 mm initial crack. As discussed earlier, all the data are combined into one data set and plotted.
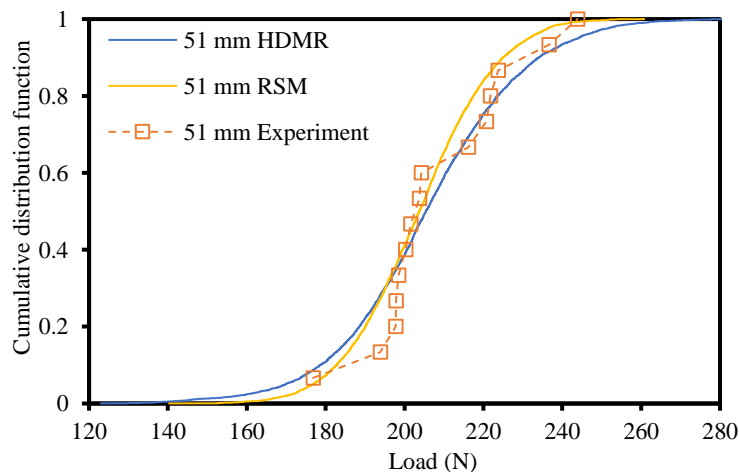
Fig. 3.19 Cumulative distribution function obtained by HDMR, RSM and test data with respect to load for 51 mm crack

Figure 3.22 shows the CDF plots of the load corresponding to the steady state crack propagation. In the same way, the plots for crack length and energy are respectively shown in Figs. 3.23 and 3.24. Due to the reasons mentioned earlier, while capturing the steady state crack length, the application of HDMR improves the efficiency of the model compared to the nonlinear regression model.
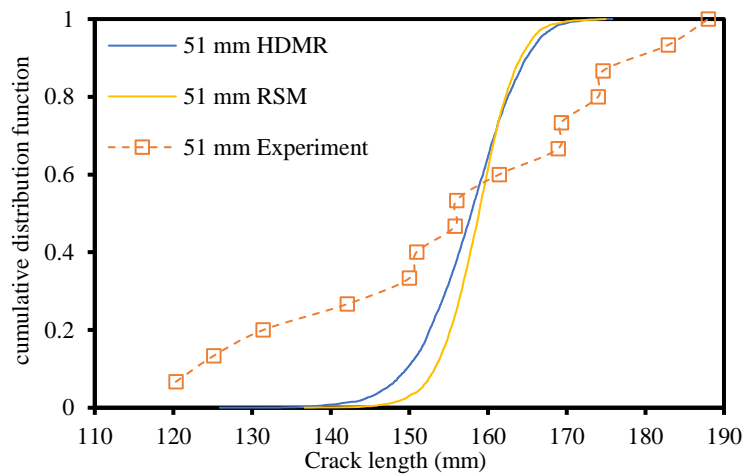
Fig. 3.20 Cumulative distribution function obtained by HDMR, RSM and test data with respect to crack for 51 mm crack
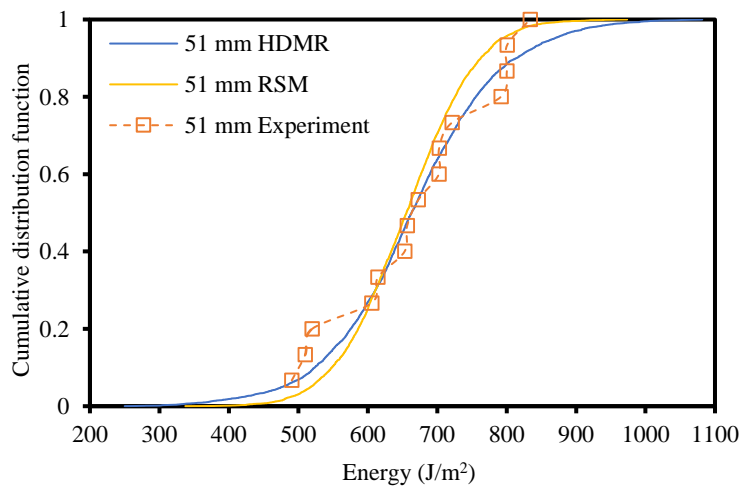
Fig. 3.21 Cumulative distribution function obtained by HDMR, RSM and test data with respect to steady state energy for 51 mm crack
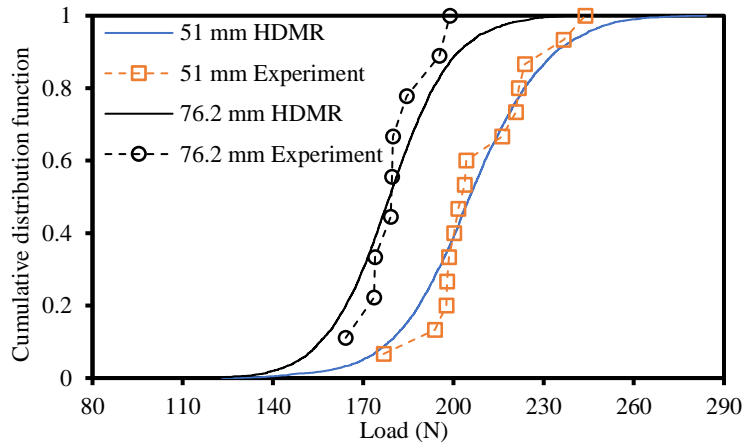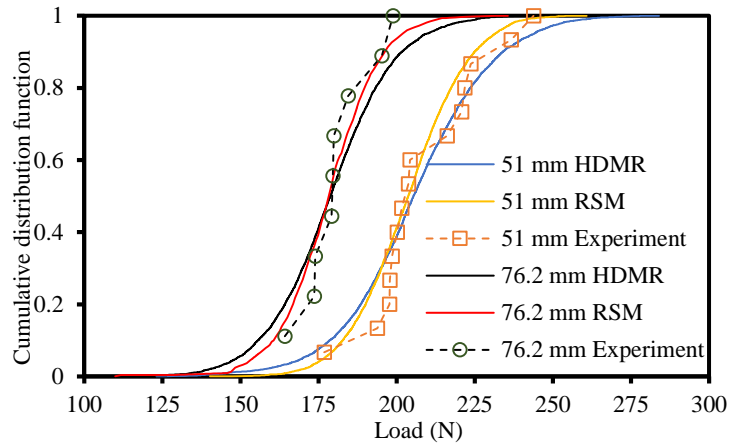
Fig. 3.22 Cumulative distribution function obtained by HDMR, RSM and test data with respect to load for 51 & 76.2 mm crack
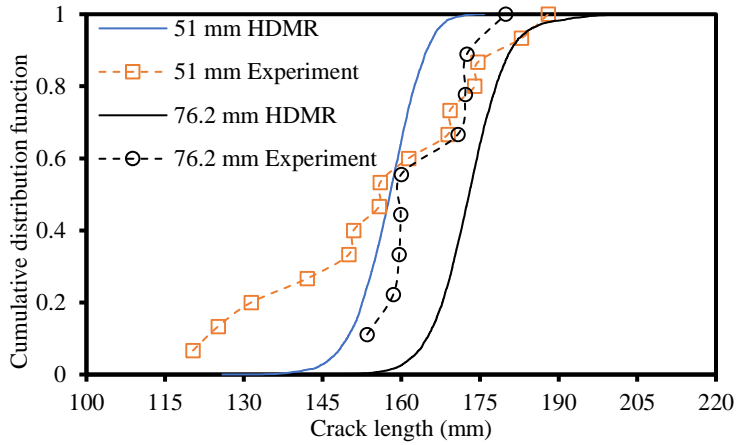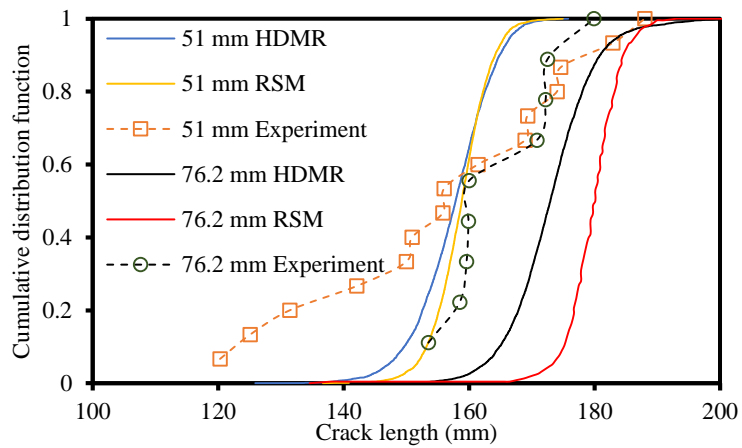

Fig. 3.23 Cumulative distribution function obtained by HDMR, RSM and test data with respect to crack for 51 & 76.2 mm crack
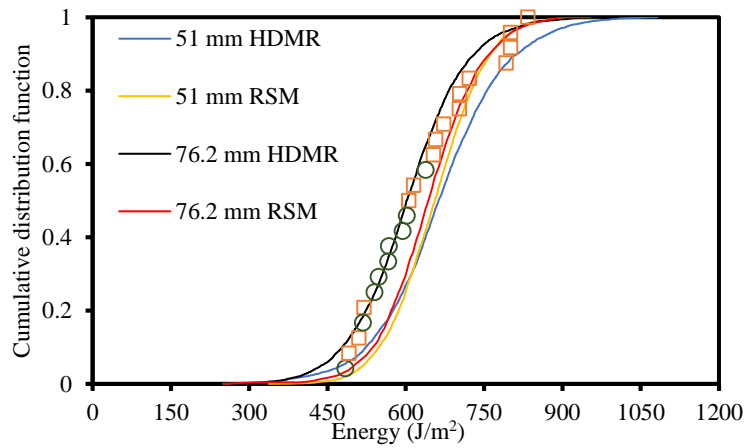
Fig. 3.24 Cumulative distribution function obtained by HDMR, RSM and test data with respect to steady state energy for 51 & 76.2 mm crack

49

Moreover, the HDMR based CZM is effective in capturing the delamination strength of any arbitrary initial crack length. Therefore, the novel method implemented to capture the steady state energy using HDMR based CZM depicts a good agreement between the predicted and the actual scatter. In fact, a marginal deviation is observed in the plots from the experimental data in comparison with the present model using HDMR. This deviation can be further reduced with the use of higher-order HDMR expressions, but with additional computational effort.

CHAPTER 4

EXPERIMENTAL STUDY FOR FRACTURE TOUGHNESS

4.1 GENERAL

Experimental investigations are necessary to understand the failure behavior of composites. Shih (1991) and Hutchinson and Suo (1991) developed a valuable theoretical work on the interfacial fracture. For understanding the interfacial fracture, a well-defined experimental setup with suitable load fixtures and effectively designed specimens are required. The experimental setup should be able to perform the test on different types of material pairs, and has to form different mode mixities. For non-oscillatory singular fields, the test techniques are principally driven by the need to analyse the delamination toughness of laminated materials. The DCB (Devitt 1980) and end notch flexure (ENF) tests (Carlsson et al. 1986) are well recognized for usage of such materials under pure mode-I and mode-II conditions, respectively. Several MM experiments have been employed over the past years (Whitney and Pagano 1989). The mixed-mode bending (MMB) test is found to be the widely recognized method by different researchers in the recent times (Reeder and Crews 1990; Reeder and Crews 1992; Oliveira et al. 2009; Razavi et al. 2018). However, the MMB test requires a nonlinear analyses for most of the bimaterial specimen geometries, as reported by Sundararaman and Davidson (1997).

In this chapter, a brief description is given on the SLB test, and also a suitability analysis is made on the interfaces between materials, in order to determine the fracture toughness. It is shown that the SLB test, along with other tests such as the asymmetric DCB and ENF test, provides a way to determine the fracture toughness of most bimaterial interfaces over an entire range of mode mixities (Sundararaman and Davidson 1997). Besides, these tests use somewhat simple specimen geometries, loading fixtures, and data reduction approaches. As will be elucidated afterwards, the key benefit of the SLB test is the use of compliance calibration procedure to directly obtain the whole ERRs from test data. Thus, any uncertainties resulted from

inappropriate description of material properties, geometric properties, and/or the effect of finite width are controlled.

4.2 THE SLB TEST

Figure 4.1 represents a distinctive SLB test and specimen schematic diagram. Consequently, the sample has a beam-type geometry which comprises different materials attached in some manner. Accordingly, Davidson et al. (1995) have made a standard three-point bending fixture with loading pins. In the experiment, a portion of the lower material has been removed in order to transfer the entire reaction force at the cracked end to the upper end material.

4.2.1 Classical Plate Theory Analysis

Classical Plate Theory (CPT) analysis is used to relate the in-plane load and moment resultants in a sample to its in-plane strains and curvature (Szekrényes and Uj 2006). It is believed that CPT is valid for the measurement of strain ERR (Davidson and Sundararaman 1996a). From the SLB geometries shown in Fig.4.1, the section on top of the crack plane is termed as the top plate and the region beneath the crack plane is the bottom plate. The origin of system lies along the plane defined by the geometric centre of the uncracked region. For the upper cracked region, the moment curvature relationship is given by (Davidson and Sundararaman 1996a).

$$M_T = -BD_T \frac{d^2 w}{dx^2} \qquad (4.1)$$

where M_T is the moment on a face expressed by a normal vector in the positive or negative x direction, B is the width, w is the deflection in the z direction, and D_T is the effective bending rigidity of the top plate. As the bending rigidity depends upon the constraint conditions, the term 'effective' is used in the description. Moreover, a standard sign convention is used for M_T, i.e., a positive moment generates a positive stress in positive z.

For the uncracked section, a similar functional relationship is also applied, in such cases the subscript 'T' will be omitted. Applying the CPT assumptions, the bending rigidity of the top plate is expressed as

$$D_T = \frac{E_T' t_T^3}{12} \tag{4.2}$$

and for the uncracked region

$$D = D_{11} - \frac{B_{11}^2}{A_{11}} \tag{4.3}$$

where

$$D_{11} = \frac{E_1' t_1 \left(t_1^2 + 3t_2^2 \right) + E_2' t_2 \left(t_2^2 + 3t_1^2 \right)}{12} \tag{4.4}$$

$$B_{11} = \frac{\left(E_2' - E_1' \right) t_1 t_2}{2} \tag{4.5}$$

$$A_{11} = \frac{E_1' t_1 + E_2' t_2}{2} \tag{4.6}$$

where, $E_i' = E_i$, for plane stress conditions and $E_i' = E_i / \left(1 - v_i^2 \right)$. for plane strains.

In the above expressions, the terms E_i and v_i corresponds to the Young's modulus and Poisson's ratio, respectively, of material 'i', and t_i is the thickness (Fig. 4.1). The E_T' term used in Eq. (4.2), is similarly can be expressed using the above equation by substituting the subscript the 'i' term in the E_i' by 'T'. The expression for D in Eq. (4.3) represents the reduced bending rigidity as shown by the uncracked region, that does not have a midplane symmetry. This equation is derived from the standard CPT equation by considering the fact that, the in-plane load is zero for the SLB geometry and loading.
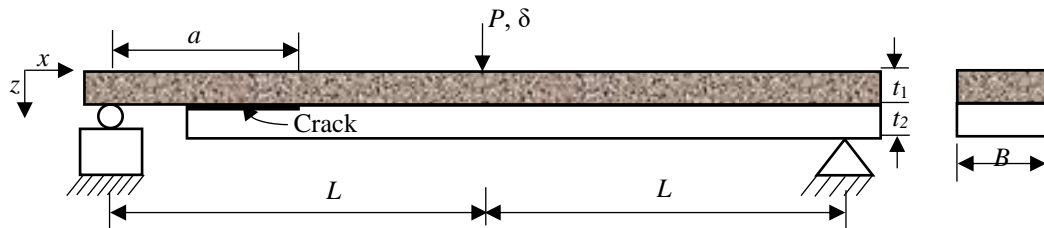
Fig. 4.1 SLB test and specimen geometry

The moment-curvature relationship expressed in Eq. (4.1) and its equivalent for the uncracked region are used in the derivation of the equation of compliance of the SLB specimen using CPT as

$$C^{CPT} = \frac{2L^3 + a^3(R-1)}{12BD} \quad (4.7)$$

where the compliance (C) is defined as the centre-point deflection divided by the load. Also, the crack length, (a) and half-span length, (L) are as defined in Fig. 4.1, and R is the ratio of the flexural rigidity of the uncracked region to that of the top plate, i.e., $R = D/D_T$. Assuming a specimen production process with no contribution of the residual thermal stresses to the ERR, Eq. (4.7) may be substituted into the relation between ERR (G) and the derivative of compliance with respect to crack length;

$$G = \frac{P^2}{2B} \frac{\partial C}{\partial a} \quad (4.8)$$

to obtain

$$G^{CPT} = \frac{P^2 a^2 (R-1)}{8B^2 D} \quad (4.9)$$

Or, substituting Eq. (4.7) into Eq. (4.9)

$$G^{CPT} = \frac{3P\delta_w a^2}{2B} \left[\frac{R-1}{2L^3 + a^3(R-1)} \right] \quad (4.10)$$

where δ_w is the center-point deflection and P is the applied load. Equation (4.9) with the critical load or Eq. (4.10) with the critical load and deflection, can be used to determine the critical ERR, (G_c). Equation (4.10) is more precise, as there is less effect of errors in material properties on G_c. Hence, the compliance calibration method is found to be the most preferable and more precise data reduction technique for obtaining G_c. In such approaches, the compliance of the specimen should be first measured with proper assignment of the specimen in the loading point as a function of crack length. The specimen is then examined to failure at the crack length of interest. Likewise, the critical load together with the experimentally measured compliance and the crack length relations are applied in Eq. (4.8) to get G_c.

4.2.2 Laboratory Test

In general, the fracture toughness of the materials is obtained by performing the laboratory test on DCB for mode-I, and ENF for mode-II (Tsai et al. 2014; Kossakowski 2007). Lee et al. (2010) conducted co-cured SLB joint tests to evaluate the fracture toughness of the composite materials under mode-I and II dominant conditions. In SLB joint, the mode mixity can be controlled by modifying the specimen thickness. For the homogeneous SLB, the values of the mode mixity ranges may precisely be acquired from the values reported in Davidson et al. (1995). Hence, SLB joint has been studied in the present work by applying three-point bending tests on the composite specimens. The composite specimens have been prepared with mild steel and unidirectional carbon fiber reinforced materials.

An alternative to the DCB and ENF tests, the SLB joint specimens have been utilized by changing the thickness of the composite specimens. Figure 4.2 shows the SLB specimen with dominant conditions of mode-I and mode-II. The composite thickness was adjusted in order to develop different mode conditions. The details of the composite specimens are as follows: the thickness of the composite for mode-I dominant case is $t_{1a} = 0.7$ mm and for mode-II dominant case is $t_{1b} = 2.2$ mm, and the length and breadth of the composites are 40 and 5 mm, respectively. The dimensions of the steel are $26 \times 1 \times 5$ mm; the distance between supports, $2L = 35$ mm; the initial crack, $a = 12.5$ mm from the left support; $t_2 = 1$ mm and $B = 5$ mm. Table 4.1 presents the details of the materials. The experiments were conducted in TINUS Olsen testing machine as per ASTM D790 as shown in Figs. 4.3 and 4.4.
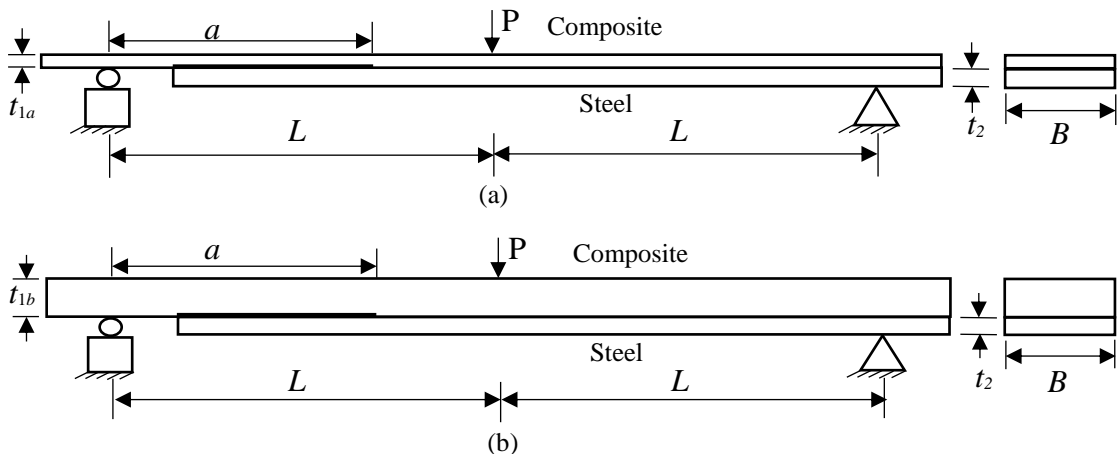
Fig. 4.2 SLB joint dominant cases (a) Mode-I, (b) Mode-II

Table 4.1 Material properties

Material	Property	Value
Composite	E_1 (GPa)	130.20
	E_2, E_3 (GPa)	8.00
	G_{12}, G_{13} (GPa)	4.50
	ν_{12}, ν_{13}	0.28
	ν_{23}	0.46
Steel	E (GPa)	200.00
	ν	0.30

The load-displacement (P-δ) curves obtained from the experiments for the mode-I and mode-II dominant conditions are shown in Figs. 4.5 and 4.6, respectively. In mode-I case the maximum force noticed is 21.34 N and in mode-II case is 144.32 N. Due to the thickness variation in the composite arms, maximum deflection occurred before failure in the mode-I is 0.669 mm and in the case of mode-II is 0.207 mm. The link between the P-δ curve during crack propagation and the fracture energy is usually represented by the compliance method (Whitney and Pagaon 1989). The fracture toughness was measured and mode-mixity was determined experimentally by using the classical beam theory (Davidson and Sundararaman 1996a)

Fig. 4.3 Experimental set up for bending test

Many experimental observations in MM delamination specimens reveal that the fracture energy globally involved in the fracture process strongly depends on the percentage of participation of different fracture modes. The fracture toughness for pure mode-I and mode-II conditions were determined by linear extrapolation as shown in Fig 4.7 (Allix and Corigliano 1996; Lee et al. 2010).

(a)

(b)
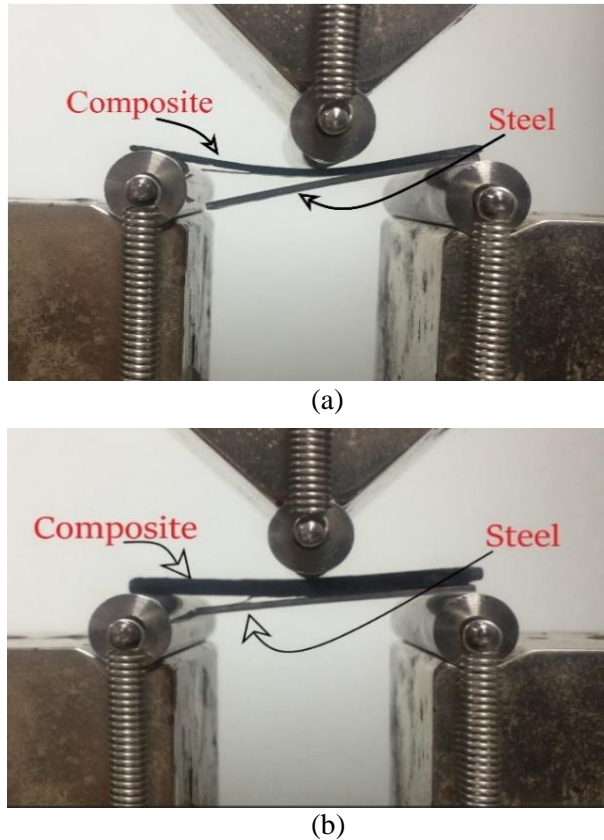
Fig. 4.4 Three-point bending test for (a) Mode-I and (b) Mode-II
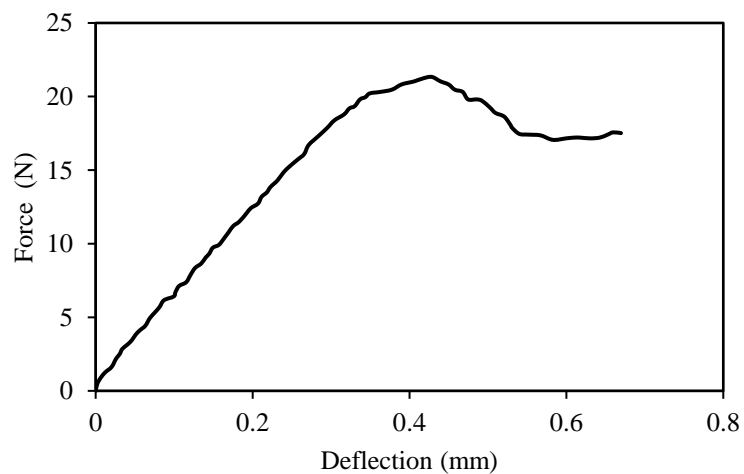
Fig. 4.5 P-δ curve for mode-I dominant condition
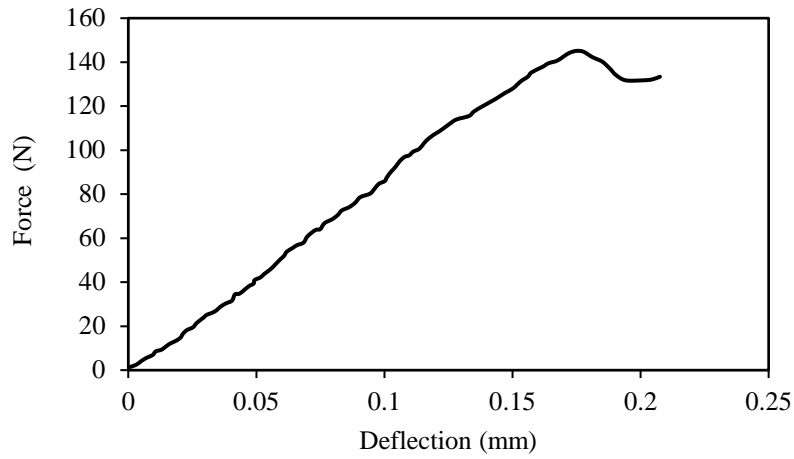
Fig. 4.6 *P*-δ curve for mode-II dominant condition
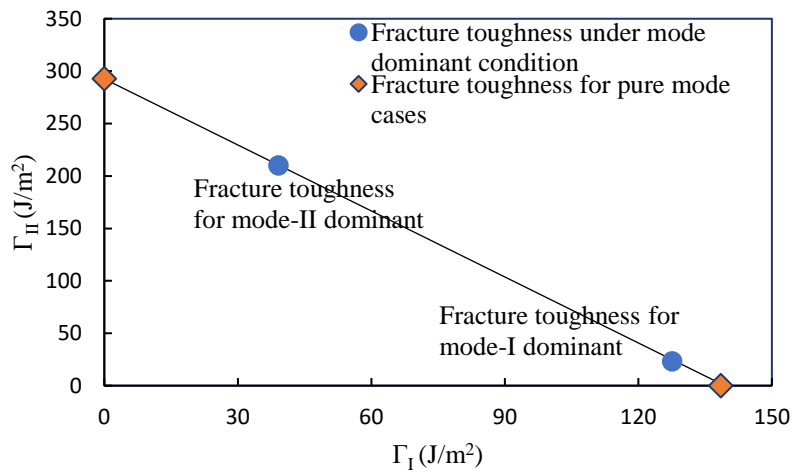
Fig. 4.7 Fracture toughness as a function of the mode mixity by linear extrapolation

The circular dots are the fracture toughness for each mode dominant condition and the diamond dots are the fracture toughnesses for each pure mode obtained by linear extrapolation. The mode decomposition values obtained from calculation are $\Gamma_I^c = 138.5$ J/m² and $\Gamma_{II}^c = 292.6$ J/m² for each pure mode, respectively.

CHAPTER 5

SIMULATION OF MIXED MODE COHESIVE ZONE MODEL

5.1 GENERAL

Generally, predicting the failure mechanism of adhesive joints using simulation is challenging task due to the complexity in characterising the interface between adhesive and adherend joints (Chang et al. 1998). Thus, FE models are used to effectively represent the adhesive layer, and the bonding between adhesive and adherent of the composite, which states that the strength of the adhesive is weaker than interface strength (Sheppard et al. 1998). However, in many cases, partial cohesive failures occur in adhesive joints, and hence analysing the failure mechanism is of more importance in composites (Behroozinia et al. 2018).

The VCCT is a basic modeling technique which depicts the failure mechanism of adhesive joint based on LEFM (Alfano and Crisfield 2001). In VCCT, the crack propagation depends on the displacement of the internal nodal forces at the crack tip, and the ERR is calculated based on the relative displacements of the nodes. If the calculated ERR exceeds the fracture toughness of the material, then the crack propagation will take place (Wei et al. 2017).

In contrast to VCCT, where stiff spring elements are used, the cohesive laws are implemented in CZM to infer the failure mechanism of the adhesive layer (Shet and Chandra 2002). The TSL such as bilinear, trilinear, PPR , etc., defines the progressive failure of the adhesive layer (Shabir et al. 2011; Park and Paulino 2012). The bilinear TSL can be described by three parameters (initial stiffness, critical cohesive strength and fracture toughness). To determine the cohesive parameters, as there is no standard method available, experiments need to be conducted on the given material for fracture toughness (Lee et al. 2010). Using the simulation and experimental data, the remaining parameters can be obtained. From the P-δ curves, the observed load deviation is considered as an error which is used to construct a metamodel, and then the error is minimized using optimization techniques. However, the choice of the metamodel will eventually affect the sensitivities in the optimization algorithm (Kim et al. 2006).

Generally, two methods are considered in the extraction process of TSLs: *a direct method* and *an iterative method*. In the direct method, in general, primarily measured displacement variables were used to deliver results without repetition on extensive numerical analysis (Sørensen and Jacobsen 2000; Sorensen et al. 2008; Zhu et al. 2009). In this approach, however, resolution issues control the extraction of TSLs in deciding the crack front and determining the crack opening displacements. Conversely, the iterative method categorizes parameters based on comparison results of numerical solutions and measurements (Cox and Marshall 1991; Li et al. 2005a; Mello and Liechti 2006; Sorensen et al. 2008).

In most cases, fracture energies use a specific equipment, loading fixture, or a number of different specimen configuration for assessing the mode mixity effect of bonded joints. For instance, a bi-axial fracture test was performed by Liechti and Chai (1992), to describe the fracture energy envelope under full range of mode mixity for a brittle epoxy/glass interface. Accordingly, as the mode mixity closes to the pure mode-II condition, the fracture energy abruptly increases. In addition, has made an attempt to determine the fracture energy on asymmetric constant thickness DCB specimen up to a phase angle of 38° using a simplified wedge test, where the phase angle is defined by $\psi = \tan^{-1}\left(K_{II}/K_{I}\right)$ and K_{II} and K_{I} are the mode-II and mode-I stress intensity factors, respectively. During such test, the fracture energy was observed to rise as the value of the phase angle approximately reaches 27°. Furthermore, an asymmetric DCB test was performed by Sundararaman and Davidson (1997) on a glass/epoxy interface to assess a mode mixity up to 30°.

Russell and Street (1985) have also developed a MM flexure test (also referred to as the SLB test), to determine the fracture energy in bonded joints. An identical sample to that of the DCB configuration was used during SLB test, except that the load is applied to only one of the debonded arms of the sample, as the bonded end remains fixed. Any variation in the ratio of the adherend thicknesses in the SLB test leads to a limited mode mixity state, similar to that of the DCB test. For the case of identical adherends, the SLB provides a mode mixity of 41°.

In general, all the aforementioned test configurations are used to evaluate the fracture energy at a single mode mixity adherends with set of uniform thicknesses. Park

and Dillard, (2007) suggested asymmetric tapered beam samples to give a range of such thicknesses, in which one adherend is of uniform thickness and the other is contoured. The relative toughness of the two adherends varies as the debond propagates, resulting in a systematic variation in fracture mode mixity. Sundararaman and Davidson (1997) have documented values of the asymmetric tapered specimens tested as DCB specimens.

Nevertheless, hybrid adherend arrangements, such as the end load split (ELS) or ENF specimens, could also be applied to the SLB loading configuration or to other configurations. In this case, the mode mixity can change from 0° to the limiting value of approximately 40° if the DCB specimen is used, with one adherends being much firmer than the other.

5.2 MIXED-MODE COHESIVE ZONE MODEL (MM-CZM)

CZM is one of the specialised models to predict the crack growth in damage region. In the CZM, the damage region is accumulated into one cohesive layer before it is placed ahead of the crack tip. Here, the TSL characterises the fracture mechanism, and the intrinsic fracture energy (Γ) influences on the propagation of the crack. Hence, the TSL constitutes the microscopic and macroscopic features of the composite specimens (Vossen et al. 2014). Both the energies of adhesive and adherent of the composites are incorporated into the cohesive zone. An advantage of the SLB joint is the development of normal and shear behaviors occuring simultaneously in the damage zone with the existing MM condition.

The damage initiation for MM condition is evaluated as follows.

$$\left(\frac{\sigma_{\mathrm{I}}}{\sigma_{\mathrm{I}}^{\mathrm{c}}}\right)^2 + \left(\frac{\sigma_{\mathrm{II}}}{\sigma_{\mathrm{II}}^{\mathrm{c}}}\right)^2 = 1 \tag{5.1}$$

where $\left(\sigma_{\mathrm{I}}, \sigma_{\mathrm{II}}\right)$ are the stress elements, and $\left(\sigma_{\mathrm{I}}^{\mathrm{c}}, \sigma_{\mathrm{II}}^{\mathrm{c}}\right)$ are the cohesive strengths at critical state. Similarly, the propagation of the cohesive layer is estimated as follows.

$$\left(\frac{G_{\mathrm{I}}}{\Gamma_{\mathrm{I}}}\right) + \left(\frac{G_{\mathrm{II}}}{\Gamma_{\mathrm{II}}}\right) = 1 \tag{5.2}$$

in which $\left(G_{\mathrm{I}}, G_{\mathrm{II}}\right)$ are the ERR, and $\left(\Gamma_{\mathrm{I}}, \Gamma_{\mathrm{II}}\right)$ are the fracture toughness. Once the

cohesive elements satisfy Eq. (5.1) criterion, the damage initiation will occur in the model and the complete separation is guided by Eq. (5.2). The bilinear TSL as shown in Fig. 5.1 is considered to define the fracture process of the SLB joint with three cohesive parameters.

5.3 DETERMINATION OF COHESIVE PARAMETERS

Generally, CZMs are used to describe the interfacial mechanism of the composite joints. To understand fracture mechanism using CZM, cohesive parameters must be known in advance. The iterative method, in contrast, measures the parameters by distinguishing numerical results and measurements, which has been frequently employed in the past. The research on the systematic way to find the cohesive parameters is scarce. In the present study, the cohesive parameters are determined based on HDMR techniques as outlined in the flow-chart shown in Fig. 5.2.

Application of HDMR for Cohesive Parameters:

In this study, it is observed that the critical cohesive strength and initial stiffness are responsible to efficiently define the failure mechanism of SLB joint. The limits on the affecting variables are obtained by relating the experimental data with the simulation results. Table 5.1 shows the limits of the variables.
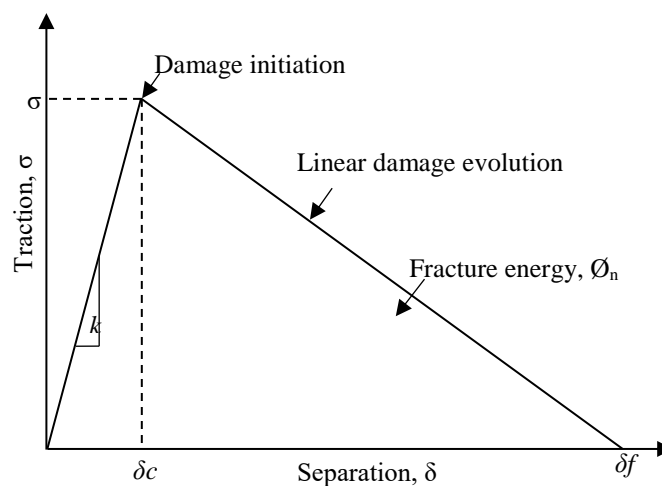
Fig. 5.1 Bilinear TSL

Based on the limits, HDMR sampling scheme is implemented to generate the component functions, and the corresponding P-δ curves are obtained through FEA. Using the FEA data, two individual HDMR expressions were developed for mode-I and mode-II dominant cases, as they are necessary input for predicting the optimal values of the cohesive parameters. Therefore, to obtain the optimal cohesive parameters for predicting the MM-SLB joint failure, the error observed from the experiment and simulation P-δ curves should be minimized. To minimize the error, a nonlinear algorithm-based optimization technique has to be implemented.

Using lower and upper limits as presented in Table 5.1 and the developed HDMR expressions, the GA is implemented. From this process the obtained optimal cohesive parameters are $\sigma_I^c = 8.5\text{MPa}$, $\sigma_{II}^c = 57\text{MPa}$, $E_1 = 50\text{MPa}$, and $E_{II} = 350\text{MPa}$. Based on the obtained cohesive parameters, MM-SLB joint failure is determined.
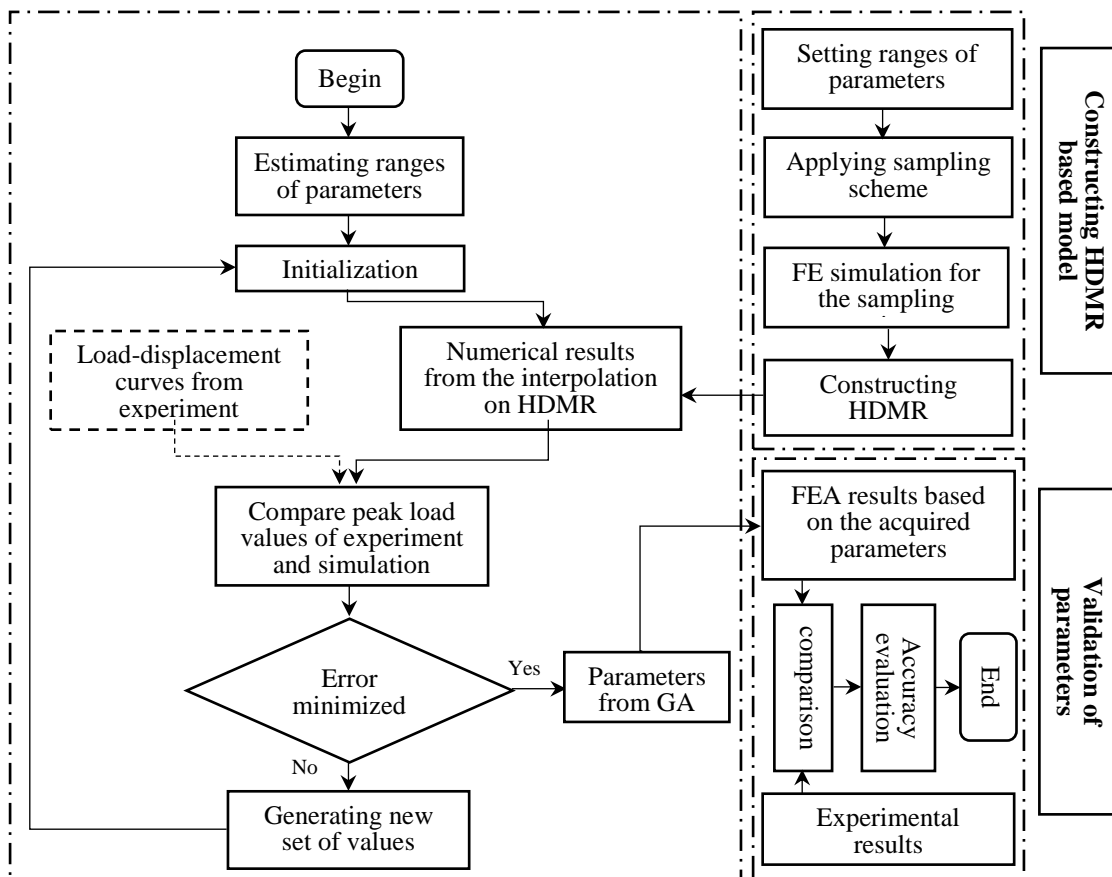
Fig. 5.2 Flowchart for determining the CZM parameters

Table 5.1 Lower and upper limits

Parameter	Lower limit	Upper limit
E_{I} (N/mm^2)	50.0	300.0
E_{II} (N/mm^2)	200.0	350.0
$\sigma_{\text{I}}^{\text{cr}}$	6.5	8.5
$\sigma_{\text{II}}^{\text{cr}}$	48.0	58.0

5.4 ANALYSIS OF SLB JOINT

The numerical model utilized to predict the failure mechanism of SLB joint is shown in Fig. 5.3. In the FE model, the cohesive elements are used in the FPZ, and for the remaining portion, four-node elements are provided. Figure 5.3 also shows the FPZ from the crack head to the loading point of the specimen. The entire model was constructed with the help of FEA software. The total number of elements used for mode-I and mode-II model are 5032 and 6598, respectively. Moreover, Fig. 5.4 shows the discretised version of the SLB geometry near the crack tip. CPE4R type of element are adopted. The mesh dimensions are adopted based on the models created by Davidson et al. 1995. Thus, the output acquired from the FEA is then evaluated with the experimental values. The obtained optimal cohesive parameters were implemented to verify the developed method in the mode-I and mode-II dominant SLB joint models. FEA results of these models are compared with the experiment results as shown in Figs. 5.5 and 5.6. The relative errors of 6.5% and 5.3% for mode-I and mode-II dominant conditions are observed between the peak failure load of the experimental and simulated P-δ curves.
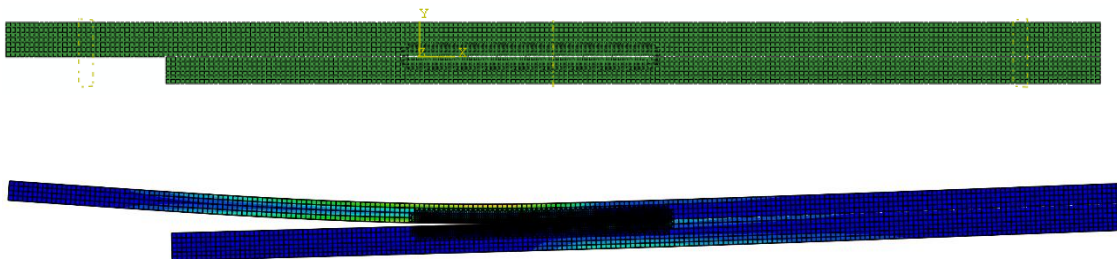
Fig. 5.3 FE model of SLB joint
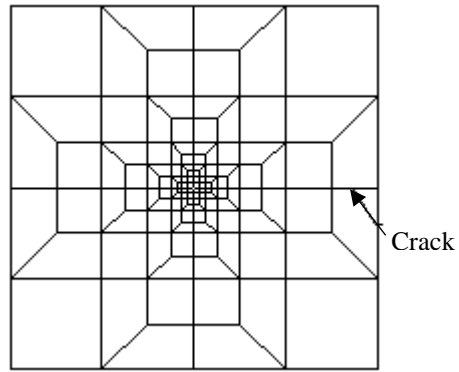
Fig 5.4 Finite element mesh in the crack tip neighborhood
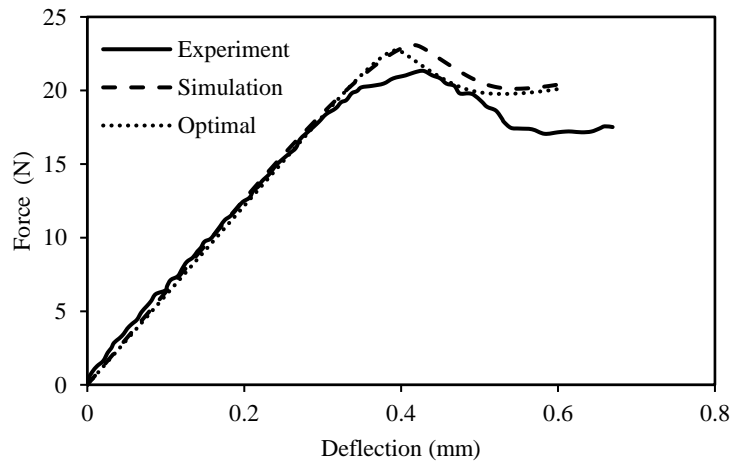
Fig. 5.5 P-δ curves for mode-I
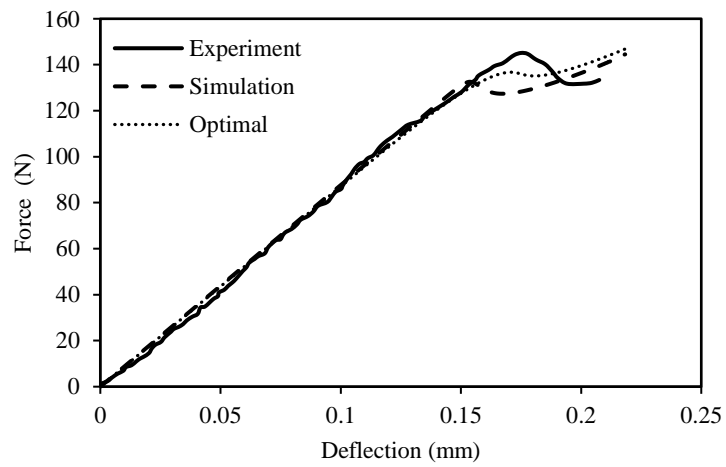
Fig. 5.6 P-δ curves for mode-II

Hence, the determined cohesive parameters are implemented in the MM-CZM. For different thicknesses of the composite varying from 1.28 to 1.48 mm, the FEA is carried out by implementing the developed cohesive parameters. Due to the variation in thickness of composite, different mode-mixities will develop in the specimens. In Fig. 5.7 and Fig. 5.8 the P-δ curves obtained from the simulation and the experiment for composite thickness of 1.28 and 1.48 mm are respectively presented.
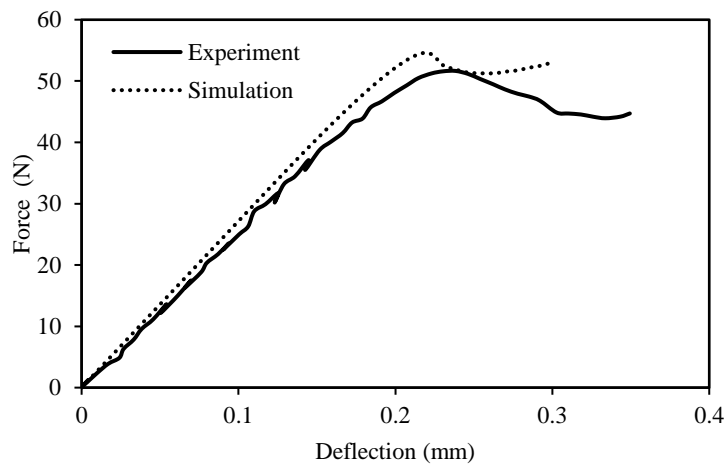
Fig. 5.7 P-δ curve ($t = 1.28$ mm)
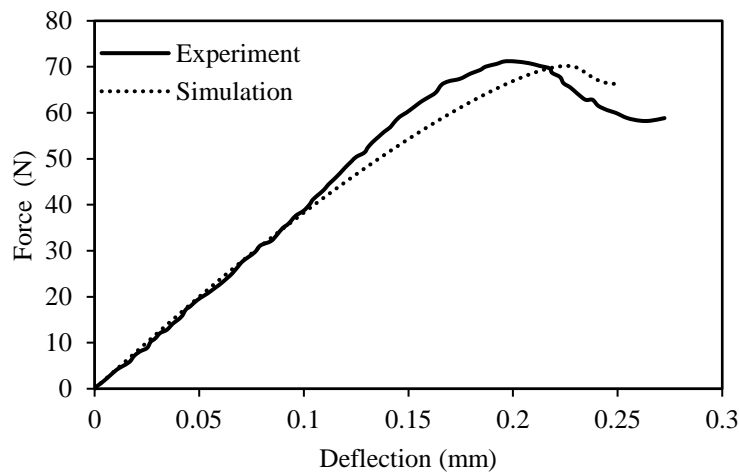
Fig. 5.8 P-δ curve ($t = 1.48$ mm)

The relative error between the experiment and simulation for the 1.28 mm and 1.48 mm is 5.8% and 7% respectively. The error can be further reduced by refining the cohesive elements size.

66

CHAPTER 6

SUMMARY AND CONCLUSION

6.1 SUMMARY AND RESEARCH FINDINGS

Compared with metals, composites have high demand due to their elevated strength to weight. Many justifications are presumed for the failure behaviour of the composite materials. One of such major reason of failure is the delamination. The cracks due to the delamination interact with misaligned or inclined fibers especially in unidirectional composites. Usually, such interactions lead to fiber bridging, which inturn causes the nominal delamination resistance to rise as the crack spreads. The key objetive of study in this area is to evaluate the behavior of composites when fiber bridging occurs during structural failure. In general, mode-I inter-laminar fracture toughness and critical ERRs of unidirectional composites are determined using DCB specimens. To understand the energy variations in unidirectional composites, several crack dimensions of DCB samples are tested, and the variations in ERR are observed.

CZM represents the fracture as a material separation. Nowadays, the use of CZM has grown largely due to the accessibility of computational power. For this reason, the probablistic model development process requires the determination of the CZM parameter distributions. Furthermore, the fiber bridging zone has to be simulated as a discrete method on its own. As a result, the link between the crack opening separation and the local bridging tractions emanating from the bridging ligaments is characterized by a bridging law, which in turn defines the failure process.

The order of correlations amongst the input parameters is revealed by a systematic mapping technique between the inputs and outputs. Only a relatively low-order relationships of the input parameters are expected for most well-defined physical systems in order to have an impact upon the output. The HDMR utilize this property to present an exact hierarchical representation of the physical system. The HDMR approximates multivariate functions in such a way that the component functions of the approximations are well-organized, beginning with a constant trend and later steadily approaches to multivariates as it progresses along process such as first-order, second-

order and so on. The HDMR applications includes building a computational model directly from experimental/field data, making an efficient comparable operational model that replaces an existing time-intensive mathematical model, identifying the main model parameters, comprehensive uncertainty studies, efficient quantitative risk analysis, etc. It is specified that a few lowest-order terms are often sufficient to represent the model in equivalent form to good accuracy.

In this work, bridging laws have been applied into an interface element using the user subroutine in ABAQUS. The efficient implementation of a cohesive user element into ABAQUS is carried out. This element type is proved to be a flexible tool for estimation of opening crack length and crack profiles as a function of the crack growth resistance. The distinct benefit of cohesive element is that it has a number of integration points which can be used to advance the numerical performance for a given mesh density. Therefore, a novel HDMR based CZM has been developed to capture the steady state ERR of an initial crack of 51 mm unidirectional composite specimen.

To understand the fracture characteristics in the FPZ, the adjusted bridging law has been employed in the FE model. Based on the cohesive parameter limits, two first-order HDMR expressions are developed for capturing the load and crack length, and then the objective function was built-up using the residuals between the experimental and the predicted responses. Optimization techniques are used to get the optimal values from the developed HDMR expressions. The simulation of delamination for 51 mm initial crack is carried out with the help of the optimal values. MCS is applied to the HDMR expressions with the Pearson family distributions of bridging law parameters. From each iteration of the MCS, the particular HDMR generates load and crack length values to estimate steady state ERR. The results showed that the developed HDMR based CZM is effective in capturing the delamination strength. In order to substantiate the effectiveness of the developed model, the delamination strength of 76.2 mm initial crack specimens is predicted without any further optimization. The comparison of the simulation and experimental results showed good agreement.

Finally, the developed procedure has been adopted for determining the cohesive parameters of an MM-CZM. Instead of DCB and ENF tests for finding the fracture toughness in pure modes, SLB joint with different thickness of the composite are manufactured and tested in the laboratory using TINUS testing maching. The critical

cohesive strength and initial stiffness are selected as the variables which affect the behaviour of the SLB joints, and the limits of these variables are decided based on the simulation and the experimental results. The two HDMR expressions are, then constructed for mode-I and mode-II dominant conditions. From the observation of P-δ curves obtained from the experiments and the simulation, the variation in peak loads is considered as an error. Using the cohesive parameter limits and HDMR expressions, the optimization was carried out to minimize the error. The MM-CZM is developed based on the optimal values and utilized in predicting the failure behavior of the MM-SLB joint.

For different mode-mixities, the constructed model has been implemented in the FEA. The effectiveness of the model has been validated using experimental results. The results obtained from the FEA indicate that the failure behaviour was well predicted for different mode-mixities. The maximum relative error observed between the experimental and the simulation failure loads is around 7% for all the cases. It is observed that the other models exhibited the error of about 15% as reported in the literature. Hence, the developed model using HDMR is computationally efficient, and it can be implemented in different types of adhesive joints.

6.2 FUTURE SCOPE

i.   In the present work, based on first order HDMR expansions the CZM has been developed. Further, the accuracy for capturing the delamination strength can be significantly improved by employing the second order HDMR with a little increased computational effort.

ii. In the present study, Lagrange interpolation functions are utilized. Further, other interpolation techniques can be used for improving the computational efficiency.

iii. The present model has been developed for crack growth studies under static loads. However, further studies using the HDMR based CZM need to be employed for fatigue crack growth propagation analysis.

APPENDIX A

INPUT FILE FOR 2D ELEMENT

*HEADING
*NODE
1, 0.0, 0.0
2, 1.0, 0.0
3, 0.5, 0.0
4, 0.0, 0.0
5, 1.0, 0.0
6, 0.5, 0.0
7, 1.0, 1.0
8, 0.0, 1.0
9, 1.0, 0.5
10, 0.5, 1.0
11, 0.0, 0.5
*NSET, NSET=ALL
8, 10, 9
*user element, type=U6, nodes=6, coordinates=2, i properties=2, properties=7,
variables=15
1, 2
*ELEMENT, TYPE=U6, ELSET=ALL
1, 1, 2, 3, 4, 5, 6
*ELEMENT, TYPE=CPS8, ELSET= ALL
2, 4, 5, 7, 8, 6, 9, 10, 11
*SOLID SECTION, ELSET=EALL, MATERIAL=MAT1,
ORIENTATION=ORIENT1
1.0
*UEL PROPERTY, ELSET=ALL
1.65, 1.0, 0.5, 0.15, 1.0, 1000.0, 1.0, 3
1
*MATERIAL, name=mat1
*ELASTIC, TYPE=ENGINEERING CONSTANTS
41.5E3, 9.5E3, 9.5E3, 0.3, 0.3, 0.3, 15.8E3, 3.65E3
3.65E3
orientation, name=orient1
1.0, 0.0, 0.0, 0.0, 1.0, 0.0
1, 0.
*BOUNDARY
1, 1, 2
2, 2, 2
3, 2, 2
4, 1, 1
11, 1, 1
8, 1, 1

```
*STEP, INC=100, NLGEOM
*STATIC
0.01, 1.0, 0.01
*MONITOR, DOF=2, NODE=4
*CONTROLS, PARAMETERS=TIME INCREMENTATION
7, 10, 9, 16, 10, 4, 20, 10, 6
*BOUNDARY
8, 2, 2, 1.0
7, 2, 2, 1.0
10, 2, 2, 1.0
*OUTPUT, FIELD, FREQ=1
*ELEMENT OUTPUT
S,
E,
*NODE OUTPUT
U,
RF,
*OUTPUT, HISTORY, FREQ=1
*NODE OUTPUT, NSET=ALL
U2,
RF2
*end step
```

APPENDIX B

INPUT FILE FOR 51 mm INITIAL CRACK

*HEADING
*Node, input=.\PREPARE51.2\ABA_ND.DAT
*NSET, NSET=TOP_POINT
1
*NSET, NSET=BOT_POINT
20370
*NSET, NSET=FIXED
2, 1018, 1019, 1020, 1021, 1022, 1023, 1024, 1025, 1026,
1027, 1028, 1029, 1030, 1031, 1032, 1033, 1034, 1035, 1036,
1037, 1038, 1039, 1040, 1041, 19331, 20347, 20348, 20349, 20350,
20351, 20352, 20353, 20354, 20355, 20356, 20357, 20358, 20359, 20360,
20361, 20362, 20363, 20364, 20365, 20366, 20367, 20368, 20369
*Nset, nset=CZ_TOP
*include,input=.\PREPARE\CZ_TOP.DAT
*user element, type=U6, nodes=6, coordinates=2, i properties=2, properties=7,
variables=30
1, 2
*ELEMENT, TYPE=CPE8, input=.\PREPARE\ABA_EL_TOP.DAT,
ELSET=TOP_ARM
*ELEMENT, TYPE=CPE8, input=.\PREPARE\ABA_EL_BOT.DAT,
ELSET=BOT_ARM
*ELEMENT, TYPE=U6, input=.\PREPARE\ABA_EL_COH.DAT,
ELSET=COHESIVE
*SOLID SECTION, ELSET=TOP_ARM, MATERIAL=MAT1,
ORIENTATION=ORIENT1
25.0
*SOLID SECTION, ELSET=BOT_ARM, MATERIAL=MAT1,
ORIENTATION=ORIENT1
25.0
*UEL PROPERTY, ELSET=COHESIVE
***number JssUo   U1   J0   Kfac
*** ref1   272   6.679   0.782   206   9.180
272e-3, 6.679, 0.782, 206e-3, 9.18, 1000.0, 25.0, 6
1
*MATERIAL, name=mat1
*ELASTIC, TYPE=ENGINEERING CONSTANTS
146.0E3, 8.214E3, 8.214E3, 0.332, 0.332, 0.332, 4.53E3, 4.53E3
4.53E3
*orientation, name=orient1

```
1.0, 0.0, 0.0, 0.0, 1.0, 0.0
1, 0.
*orientation, name=orient2
1.0, 0.0, 0.0, 0.0, -1.0, 0.0
1, 0.
*BOUNDARY
FIXED, 1, 2
*STEP, INC=100, NLGEOM
*STATIC
0.01, 1., 1e-08, 0.01
*MONITOR, DOF=2, NODE=TOP_POINT
*CONTROLS, PARAMETERS=TIME INCREMENTATION
7, 10, 9, 16, 10, 4, 20, 10, 6
*BOUNDARY
TOP_POINT, 2, 2, 10.0
BOT_POINT, 2, 2, -10.0
*OUTPUT, FIELD, FREQ=1
*ELEMENT OUTPUT
S,
E
*NODE OUTPUT
COORD,
U,
RF
*Element Output, ELSET=COHESIVE, directions=YES
SDV
*El print, ELSET=COHESIVE
SDV
*OUTPUT, HISTORY, FREQ=1
*NODE OUTPUT, NSET=TOP_POINT
U2,
RF2
*NODE OUTPUT, NSET=BOT_POINT
U2,
RF2
***NODE OUTPUT, NSET=CZ_TOP
***COORD,
***U2
*end step
```

INPUT FILE FOR 76.2 mm INITIAL CRACK

*HEADING
*Node, input=.\PREPARE_762\ABA_ND.DAT
*NSET, NSET=TOP_POINT
13860
*NSET, NSET=BOT_POINT
32208
*NSET, NSET=FIXED
1,714, 715, 716, 717, 718, 719, 720, 721, 722,
723, 724, 725, 726, 727, 728, 729, 730, 731, 732,
733, 734, 735, 736, 737, 19368, 20081, 20082, 20083, 20084,
20085, 20086, 20087, 20088, 20089, 20090, 20091, 20092, 20093, 20094,
20095, 20096, 20097, 20098, 20099, 20100, 20101, 20102, 20103
*Nset, nset=CZ_TOP
*include,input=.\PREPARE_762\CZ_TOP.DAT
*user element, type=U6, nodes=6, coordinates=2, i properties=2, properties=7, variables=30
1, 2
*ELEMENT, TYPE=CPE8, input=.\PREPARE_762\ABA_EL_TOP.DAT, ELSET=TOP_ARM
*ELEMENT, TYPE=CPE8, input=.\PREPARE_762\ABA_EL_BOT.DAT, ELSET=BOT_ARM
*ELEMENT, TYPE=U6, input=.\PREPARE_762\ABA_EL_COH.DAT, ELSET=COHESIVE
*SOLID SECTION, ELSET=TOP_ARM, MATERIAL=MAT1, ORIENTATION=ORIENT1
25.0
*SOLID SECTION, ELSET=BOT_ARM, MATERIAL=MAT1, ORIENTATION=ORIENT1
25.0
*UEL PROPERTY, ELSET=COHESIVE
***number JssUo   U1   J0   Kfac
*** ref1   272   6.679 0.782 206   9.180
272e-3, 6.679, 0.782, 206e-3, 9.18, 1000.0, 25.0, 6
1
*MATERIAL, name=mat1
*ELASTIC, TYPE=ENGINEERING CONSTANTS
146.0E3, 8.214E3, 8.214E3, 0.332, 0.332, 0.332, 4.53E3, 4.53E3
4.53E3
*orientation, name=orient1
1.0, 0.0, 0.0, 0.0, 1.0, 0.0
1, 0.
*orientation, name=orient2
1.0, 0.0, 0.0, 0.0, -1.0, 0.0
1, 0.
*BOUNDARY

FIXED, 1, 2
*STEP, INC=100, NLGEOM
*STATIC
0.01, 1., 1e-08, 0.01
*CONTROLS, PARAMETERS=TIME INCREMENTATION
7, 10, 9, 16, 10, 4, 20, 10, 6
*BOUNDARY
TOP_POINT, 2, 2, 7.5
BOT_POINT, 2, 2, -7.5
*OUTPUT, FIELD, FREQ=1
*ELEMENT OUTPUT
S,
E
*NODE OUTPUT
COORD,
U,
RF
*Element Output, ELSET=COHESIVE, directions=YES
SDV
*El print, ELSET=COHESIVE
SDV
*OUTPUT, HISTORY, FREQ=1
*NODE OUTPUT, NSET=TOP_POINT
U2,
RF2
*NODE OUTPUT, NSET=BOT_POINT
U2,
RF2
***NODE OUTPUT, NSET=CZ_TOP
***COORD,
***U2
*end step

COHESIVE ELEMENT CODE

```fortran
      SUBROUTINE
      UEL(RHS,AMATRX,SVARS,ENERGY,NDOFEL,NRHS,NSVARS,
     1 PROPS,NPROPS,COORDS,MCRD,NNODE,U,DU,V,A,JTYPE,TIME,DTIME,
     2 KSTEP,KINC,JELEM,PARAMS,NDLOAD,JDLTYP,ADLMAG,PREDEF,
     3
      NPREDF,LFLAGS,MLVARX,DDLMAG,MDLOAD,PNEWDT,JPROPS,NJPROP,
     4 PERIOD)
C
       INCLUDE 'ABA_PARAM.INC'
       PARAMETER (ZERO = 0.D0, HALF=0.5D0, ONE= 1.0D0, TWO=2.0d0,
     1 THREE= 3.0d0, TOL=-1E-5)

         LOGICAL::exists
         CHARACTER (len=200) outFilepath

       DIMENSION RHS(MLVARX,*),AMATRX(NDOFEL,NDOFEL),
     1 SVARS(NSVARS),ENERGY(8),PROPS(*),COORDS(MCRD,NNODE),
     2 U(NDOFEL),DU(MLVARX,*),V(NDOFEL),A(NDOFEL),TIME(2),
     3 PARAMS(3),JDLTYP(MDLOAD,*),ADLMAG(MDLOAD,*),
     4 DDLMAG(MDLOAD,*),PREDEF(2,NPREDF,NNODE),LFLAGS(*),
     5 JPROPS(*)

C GENERAL ELEMENT VALUES
         DIMENSION STRESS(MCRD)
      DIMENSION DDSDDR(MCRD,MCRD)

C GAUSS INTEGRATION VARIABLES (3 INTEG POINT)
      DIMENSION GAUSS3(3), WEIGHT3(3), COTNEW(3), CWEIGHT(3)
         DIMENSION GAUSS6(6), WEIGHT6(6), COTNEW6(6), CW6(6)
      DIMENSION GAUSS12(12), WEIGHT12(12), COTNEW12(12), CW12(12)

C ARRAYS FOR QUADRATIC LINE ELEMENT
         DIMENSION DNDXI(3), DELTA_U(6), DU_CONT(MCRD),
      DU_LOC(MCRD)
         DIMENSION H(MCRD,6), C_COOR(MCRD,NNODE), PSI(6,NDOFEL)
         DIMENSION B(MCRD, NDOFEL), BT(NDOFEL, MCRD)
         DIMENSION A1(NDOFEL, MCRD), A2(NDOFEL, NDOFEL)
         DIMENSION AV_COOR(MCRD, 3), V_XI(MCRD), V_N(MCRD)
         DIMENSION THETA(MCRD, MCRD), STR_GLOB(MCRD)
         DIMENSION D_GLOB(MCRD, MCRD), DD1(MCRD, MCRD)

         data iuel/0/
         save iuel
         outFilepath = 'D:\verify.out'
      CALL KASET2(AMATRX, NDOFEL, NDOFEL)
```

```fortran
      IF (NHRS.EQ.1) THEN
        CALL KASET1(RHS, MLVARX)
      ELSE
        CALL KASET2(RHS, MLVARX, NRHS)
      END IF

      CALL KASET2(PSI, 6, NDOFEL)
    CALL KASET2(H, MCRD, 6)
      CALL KASET2(AV_COOR, MCRD, 3)
      CALL KASET1(V_XI, MCRD)
      CALL KASET1(V_N, MCRD)
      CALL KASET2(THETA, MCRD, MCRD)

      CALL KASET2(DDSDDR, MCRD, MCRD)
    CALL KASET2(D_GLOB, MCRD, MCRD)

      CALL KASET1(STRESS, MCRD)
      CALL KASET1(STR_GLOB, MCRD)

C   REAL INPUT PROPERTIES
      WIDTH = PROPS(7) ! Width of elements (same as solid section width for
solid elements)
C   INTEGER INPUT PROPERTIES
      NINTP = JPROPS(1) ! Number of integration points
    INTS = JPROPS(2) ! Integration point scheme (1: gauss, 2: newton cotes)
C INFORMATION OUTPUT AND CHECK
    IF (iuel.EQ.0) THEN
              INQUIRE(file=outFilepath, exist=exists)

C CHECKING FOR THE RIGHT NUMBER OF NODES
      IF (NNODE.NE.6) THEN
          CALL STDB_ABQERR (-3, '6 nodes required for interface element:
   1 specified number of nodes is incorrect',0,0.0,' ')
      END IF

C Checking for number of state variables
    minnum = NINTP*5
    IF (NSVARS.LT.minnum) THEN
    CALL STDB_ABQERR(-3, 'Number of state variables too small for
   1 chosen number of integration points!',MINNUM,0.0,' ')
    END IF
              IUEL = 1
    END IF
C DEFINE DELTA_U=U_TOP - U_BOTTOM
    DO  K = 1, NDOFEL/2
      PSI(K, K) = -ONE
```

```fortran
         PSI(K, K+NDOFEL/2) = ONE
      END DO
C Compute nodal coordinates in deformed state
C ADD PROPER COORDINATE TRANSFORMATION LATER
      DO  I=1,MCRD
        DO  J=1, NNODE
           NN=I+(J-1)*MCRD
           C_COOR(I,J)=COORDS(I,J) + U(NN)
        END DO
      END DO
c Reference coordinate system (midpoint averages)
      DO  I=1, MCRD
        DO  J=1, NNODE/2
           AV_COOR(I,J)=ONE/TWO*(C_COOR(I,J)+C_COOR(I,J+NNODE/2))
        END DO
      END DO
c Gaussian integration (3 gauss points)
      GAUSS3(1) = -SQRT(0.6)
      GAUSS3(2) = ZERO
      GAUSS3(3) = SQRT(0.6)

      WEIGHT3(1) = 0.55555555555555
      WEIGHT3(2) = 0.88888888888888
      WEIGHT3(3) = 0.55555555555555

c Gaussian integration (6 gauss points)
      GAUSS6(1) = -0.932469514203152
      GAUSS6(2) = -0.6612093864662646
      GAUSS6(3) = -0.2386191860831968
      GAUSS6(4) = 0.2386191860831968
      GAUSS6(5) = 0.6612093864662646
      GAUSS6(6) = 0.932469514203152

      WEIGHT6(1) = 0.1713244923791709
      WEIGHT6(2) = 0.3607615730481379
      WEIGHT6(3) = 0.4679139345726913
      WEIGHT6(4) = 0.4679139345726913
      WEIGHT6(5) = 0.3607615730481379
      WEIGHT6(6) = 0.1713244923791709

c Gaussian integration (12 gauss points)
      GAUSS12(1) = -0.981560634246732
      GAUSS12(2) = -0.904117256370452
      GAUSS12(3) = -0.7699026741943177
      GAUSS12(4) = -0.5873179542866143
      GAUSS12(5) = -0.3678314989981804
      GAUSS12(6) = -0.12523340851114688
```

```
GAUSS12(7) = 0.12523340851114688
GAUSS12(8) = 0.3678314989981804
GAUSS12(9) = 0.5873179542866143
GAUSS12(10) = 0.7699026741943177
GAUSS12(11) = 0.904117256370452
GAUSS12(12) = 0.981560634246732

WEIGHT12(1) = 0.04717533638647547
WEIGHT12(2) = 0.1069393259953637
WEIGHT12(3) = 0.1600783285433586
WEIGHT12(4) = 0.2031674267230672
WEIGHT12(5) = 0.2334925365383534
WEIGHT12(6) = 0.2491470458134027
WEIGHT12(7) = 0.2491470458134027
WEIGHT12(8) = 0.2334925365383534
WEIGHT12(9) = 0.2031674267230672
WEIGHT12(10) = 0.1600783285433586
WEIGHT12(11) = 0.1069393259953637
WEIGHT12(12) = 0.04717533638647547

c Newton Cotes integration (3 integration points)
    COTNEW(1) = -ONE
    COTNEW(2) = ZERO
    COTNEW(3) = ONE

    CWEIGHT(1) = ONE/THREE
    CWEIGHT(2) = ONE + ONE/THREE
    CWEIGHT(3) = ONE/THREE

c Newton Cotes integration (6 integration points)

    COTNEW6(1) = -ONE
    COTNEW6(2) = -3.0d0/5.0d0
    COTNEW6(3) = -1.0d0/5.0d0
    COTNEW6(4) = 1.0d0/5.0d0
    COTNEW6(5) = 3.0d0/5.0d0
    COTNEW6(6) = ONE

    CW6(1) = 19.0d0/144.0d0
    CW6(2) = 75.0d0/144.0d0
    CW6(3) = 50.0d0/144.0d0
    CW6(4) = 50.0d0/144.0d0
    CW6(5) = 75.0d0/144.0d0
    CW6(6) = 19.0d0/144.0d0

c Newton Cotes integration (12 integration points)
    COTNEW12(1) = -ONE
```

```
COTNEW12(2) = -9.0d0/11.0d0
COTNEW12(3) = -7.0d0/11.0d0
COTNEW12(4) = -5.0d0/11.0d0
COTNEW12(5) = -3.0d0/11.0d0
COTNEW12(6) = -1.0d0/11.0d0
COTNEW12(7) = 1.0d0/11.0d0
COTNEW12(8) = 3.0d0/11.0d0
COTNEW12(9) = 5.0d0/11.0d0
COTNEW12(10) = 7.0d0/11.0d0
COTNEW12(11) = 9.0d0/11.0d0
COTNEW12(12) = ONE

CW12(1) = 2171465.0d0/43545600.0d0
CW12(2) = 13486539.0d0/43545600.0d0
CW12(3) = -3237113.0d0/43545600.0d0
CW12(4) = 25226685.0d0/43545600.0d0
CW12(5) = -9595542.0d0/43545600.0d0
CW12(6) = 15493566.0d0/43545600.0d0
CW12(7) = 15493566 .0d0/43545600.0d0
CW12(8) = -9595542.0d0/43545600.0d0
CW12(9) = 25226685.0d0/43545600.0d0
CW12(10) = -3237113.0d0/43545600.0d0
CW12(11) = 13486539.0d0/43545600.0d0
CW12(12) = 2171465.0d0/43545600.0d0


    IF (LFLAGS(3).EQ.1) THEN
C Normal incrementation (RHS and AMATRX required)
      IF (LFLAGS(1).EQ.1.OR.LFLAGS(1).EQ.2) THEN
C *STATIC AND *STATIC, DIRECT
C LOOP OVER INTEGRATION POINTS
        DO  IINTP = 1,NINTP
          IF (NINTP.EQ.3.AND.INTS.EQ.1) THEN

            POINT = GAUSS3(IINTP)
            WEIGHT = WEIGHT3(IINTP)

          ELSE IF (NINTP.EQ.6.AND.INTS.EQ.1) THEN

            POINT = GAUSS6(IINTP)
            WEIGHT = WEIGHT6(IINTP)

          ELSE IF (NINTP.EQ.12.AND.INTS.EQ.1) THEN

            POINT = GAUSS12(IINTP)
            WEIGHT = WEIGHT12(IINTP)

          ELSE IF (NINTP.EQ.3.AND.INTS.EQ.2) THEN
```

```
              POINT = COTNEW(IINTP)
              WEIGHT = CWEIGHT(IINTP)

          ELSE IF (NINTP.EQ.6.AND.INTS.EQ.2) THEN

              POINT = COTNEW6(IINTP)
              WEIGHT = CW6(IINTP)

          ELSE IF (NINTP.EQ.12.AND.INTS.EQ.2) THEN

              POINT = COTNEW12(IINTP)
              WEIGHT = CW12(IINTP)

          ELSE

C                 WRITE(15,*) 'Unspecified integration required'
C                 CALL FLUSH(15)
                  CALL XIT
              END IF
C Shape function value
              H1 = ONE/TWO*(-POINT + POINT**TWO)
              H2 = ONE/TWO*( POINT + POINT**TWO)
              H3 = ONE - POINT**TWO

C DERIVATIVE OF SHAPE FUNCTION VALUE (3X1 MATRIX)
              DNDXI(1) = -ONE/TWO + POINT
              DNDXI(2) = ONE/TWO + POINT
              DNDXI(3) = -TWO*POINT

C H matrix
              H(1,1) = H1
              H(2,2) = H1
              H(1,3) = H2
              H(2,4) = H2
              H(1,5) = H3
              H(2,6) = H3

C       write(15,*) 'Starting loop over integration points'
C       write(15,*) 'INTP POINT and WEIGHT', IINTP, POINT, WEIGHT
C       call flush(15)
      CALL KASET2(B, MCRD, NDOFEL)
      DO  I=1, MCRD
        DO  J=1, NDOFEL
          DO  K=1, NDOFEL/2

              B(I,J) = B(I,J) + H(I,K)*PSI(K,J)
```

82

```
      END DO
     END DO
    END DO
C TRANSPOSED B MATRIX
   DO  I=1, MCRD
     DO  J=1, NDOFEL
       BT(J,I) = B(I,J)
     END DO
    END DO
C CALCULATE GLOBAL DISPLACEMENT AT INTEGRATION POINT
C FROM CONTINUOUS DISPLACEMENT
    CALL KASET1(DU_CONT, MCRD)
    DO  I=1, MCRD
      DO  J=1, NDOFEL

        DU_CONT(I) = DU_CONT(I) + B(I,J)*U(J)

      END DO
    END DO
C LOCAL COORDINATE SYSTEM
C (USE AVERAGE OF DEFORMED X-POSITIONS OF TOP AND BOTTOM)
   X_xi = ZERO
   Y_xi = ZERO
   DO  I=1,3
     X_xi = X_xi +
   1 DNDXI(I)*AV_COOR(1,I)
     Y_xi = Y_xi +
   1 DNDXI(I)*AV_COOR(2,I)
    END DO
c Jacobian (vector length in xi-direction)
   DETJ = sqrt(X_xi**TWO + Y_xi**TWO)
   IF (DETJ.LT.ZERO) THEN
C    write(15,*) 'Negative Jacobian encountered!
C    1 Check element and nodal definition for elem', JELEM
   CALL XIT
   END IF
C Local coordinate vector
   V_XI(1) = X_XI/DETJ
   V_XI(2) = Y_XI/DETJ

C Normal vector in 90 degree angle
   V_N(1) = - V_XI(2)
   V_N(2) = V_XI(1)

c Rotational matrix
   THETA(1,1) = V_XI(1)
```

```fortran
      THETA(2,1) = V_XI(2)
      THETA(1,2) = V_N(1)
      THETA(2,2) = V_N(2)

c Relative displacement in local coordinate system

      CALL KASET1(DU_LOC, MCRD)
      DO I=1, MCRD
        DO  J=1, MCRD

           DU_LOC(I) = DU_LOC(I) + THETA(J,I)*DU_CONT(J)

        END DO
      END DO
c over-closure check (can be used as re-start criterion - see uinter)
      IF (DU_LOC(2).LT.TOL) THEN
C     write(15,*) 'Over-closure at element', JELEM
      END IF
C       write (15,*) 'DU_LOC:', DU_LOC(1), DU_LOC(2), IINTP
C         CALL FLUSH(15)
C         CALCULATE STRESS AND TRACTION STIFFNESS BASED ON
RELATIVE DISPLACEMENT
      CALL KTRACN(DU_LOC, PROPS, STRESS, DDSDDR,
     1 MCRD, SVARS, NSVARS, IINTP, NINTP, KINC, JELEM)

      DDSDDR(1,1) = 10000
C RHS ASSEMBLY
C CHECK FOR APPLIED LOADS ON STRUCTURE
      IF (NDLOAD.NE.0) THEN
C         WRITE(15,*) 'Element loads not implemented'
C         CALL FLUSH(15)
        CALL XIT
      END IF

C Stiffness matrix
c Transformation
      CALL KASET2(DD1, MCRD, MCRD)
      DO  I=1, MCRD
        DO  J=1, MCRD
          DO  K=1, MCRD

             DD1(I,J) = DD1(I,J) + DDSDDR(I,K)*THETA(J,K)

          END DO
        END DO
      END DO
```

```fortran
      CALL KASET2(D_GLOB, MCRD, MCRD)
      DO  I=1, MCRD
        DO  J=1, MCRD
          DO  K=1, MCRD

            D_GLOB(I,J) = D_GLOB(I,J) + THETA(I,K)*DD1(K,J)

          END DO
        END DO
      END DO

      CALL KASET2 (A1, NDOFEL, MCRD)
      DO  I=1, NDOFEL
        DO  J=1, MCRD
          DO  K=1, MCRD

            A1(I,J) = A1(I,J) + BT(I,K)*D_GLOB(K,J)

          END DO
        END DO
      END DO

      CALL KASET2 (A2, NDOFEL, NDOFEL)
      DO  I=1, NDOFEL
        DO  J=1, NDOFEL
          DO  K=1, MCRD

            A2(I,J) = A2(I,J) + A1(I,K)*B(K,J)

          END DO
        END DO
      END DO

      DO  I=1, NDOFEL
        DO  J=1, NDOFEL

          AMATRX(I,J) = AMATRX(I,J) +
     1 WIDTH*WEIGHT*DETJ*A2(I,J)

        END DO
      END DO
C Right hand side
C Transformation
      CALL KASET1(STR_GLOB, MCRD)
      DO  I=1, MCRD
        DO  J=1, MCRD
```

```fortran
          STR_GLOB(I) = STR_GLOB(I) + THETA(I,J)*STRESS(J)

          END DO
       END DO
      DO  I=1, NDOFEL
        DO  K=1,MCRD

          RHS(I,1) = RHS(I,1) +
     1 DETJ*WIDTH*WEIGHT*BT(I,K)*STR_GLOB(K)

          END DO
        END DO

      IF (NRHS.EQ.2) THEN
C       WRITE(15,*) 'Riks solution not supported by element'
C       CALL FLUSH(15)
        CALL XIT
      END IF

      IF (LFLAGS(4).EQ.1) THEN
C PERTURBATION STEP
C       WRITE(15,*) 'Perturbation step not supported by element'
C       CALL FLUSH(15)
        CALL XIT
      END IF
C SAVE OPENING AND STRESSES AT INTEGRATION POINT AS STATE
VARIABLES
      SVARS(IINTP+NINTP) = DU_LOC(1)
      SVARS(IINTP+2*NINTP) = DU_LOC(2)
      SVARS(IINTP+3*NINTP) = STRESS(1)
      SVARS(IINTP+4*NINTP) = STRESS(2)

      END DO

        ELSE
C         WRITE(15,*) 'Only static procedure supported by element'
C         CALL FLUSH(15)
          CALL XIT
      END IF

      ELSE IF (LFLAGS(3).EQ.4) THEN

        DO I=1, NDOFEL

          AMATRX(I,I)= 1.0d0
        END DO
```

86

```fortran
      ELSE

c            WRITE(15,*) 'Only normal incrementation supported by element'
c            CALL FLUSH(15)
             CALL XIT

         END IF
         RETURN
         END
C-------------------------------------------------------------------------------
      subroutine ktracn(RDISP, PROPS, STRESS, DDSDDR, MCRD, SVARS,
     1 NSVARS, IINTP, NINTP, KINC, JELEM)

      INCLUDE 'ABA_PARAM.INC'

      PARAMETER (ZERO = 0.D0, TWO=2.0D0, ONE= 1.0D0, THREE= 3.0d0)

      DIMENSION PROPS(*), RDISP(MCRD), STRESS(MCRD), DDSDDR(MCRD,
     MCRD)
      DIMENSION SVARS(NSVARS)

      data ifirst/0/
      data iopen/0/
      data iclose/0/
      save ifirst, nodefirst, iopen, iclose

c REAL INPUT PROPERTIES
C TEST MATERIAL from stochastic papaper
C  6.2 Numerical bridging results with finite stress value
      dJss = props(1) !Increase in fracture toughness
      deltac = props(2) !Max crack bridging opening
      delta1 = props(3) !Initial linear decrease/increase, softening afterwards
      dJ0 = props(4) !Value of J0 (from measurements)
      fac1 = props(5) !Stress increase factor for power law
      penalty = props(6) !Penalty factor on contact
C        write(15,*) 'ktracn call. Properties array'
C     WRITE(15,*) 'dJss =', props(1),' deltac =', props(2),'delta1 = ',props(3),' dJ0 =
     ',props(4),' fac1 = ',props(5),' penalty = ',props(6)
      flush(15)
C Sigma0, in the paper we have a different equation
         sigma0 = 1.5d0*dJss/delta1*sqrt(delta1/deltac)
      slope1 = -dJss/(delta1*deltac*sqrt(delta1/deltac))
      fac = dJss/(two*sqrt(deltac))
C Sigma1 this is similar to the pa
         sigma1 = fac/sqrt(delta1)
      slope = sigma1/delta1
c J0 is included separately now
```

```fortran
c with zero start power law
      alpha = 100.0
      delta2 = dJ0/(sigma0*fac1)*(alpha+1)/alpha
C get values from state variables
      iold = SVARS(IINTP)
      stressold = SVARS(IINTP + 4*NINTP)
      rdispold = SVARS(IINTP + 2*NINTP)
c Checks for opening/closing behaviour
      IF (ifirst.eq.0) THEN
         ifirst = 1
         NODEFIRST = NODE
C        write(15,*) dJss, deltac, delta1, dJ0, fac1, penalty
C        write(15,*) sigma0, sigma1, slope, slope1, delta2, fac
      END IF
c new increment detection (includes restart) to count contact changes
      IF (NODE.EQ.NODEFIRST.AND.KIT.EQ.1) THEN
         iopen = 0
         iclose = 0
      END IF
c Not included right now (KINC.GE.1000)
      IF (rdisp(2).LT.rdispold.AND.rdisp(2).GT.delta2.AND.
     1 KINC.GE.1000) THEN
c Elastic unloading and reloading
      stress(2) = stressold/rdispold*rdisp(2)
      ddsddr(2,2) = stressold/rdispold
C     write(15,*) 'Elastic unloading encountered'
      ELSE
c Check for penetration of surfaces and indicate status
       if (rdisp(2).LT.zero) then
C                    write(15,*) 'Area I'
      stress(2) = penalty*slope*rdisp(2)
      ddsddr(2,2) = penalty*slope
      lOpenClose = 0
c Stresses will be negative (tension)
c First slope bit (different from square root law)
      else if (rdisp(2).GE.zero.and.rdisp(2).LT.delta2) then
c Initial increase
C                 write(15,*) 'Area II'
      stress(2) = fac1*sigma0*
     1    (1.0-((delta2-rdisp(2))/delta2)**alpha)
      ddsddr(2,2) = fac1*alpha*sigma0/delta2*
     1 (((delta2-rdisp(2))/delta2)**(alpha-1))
      lOpenClose = 1
      c Softening behaviour
         else if (rdisp(2).GE.delta2.and.
     1 rdisp(2).LT.(delta1+delta2)) then
C                 write(15,*) 'Area III'
```

88

```fortran
      stress(2) = sigma0 + slope1*(rdisp(2)-delta2)
      ddsddr(2,2) = slope1
      lOpenClose = 2
      else if (rdisp(2).GE.(delta1+delta2).
   1 and.rdisp(2).LT.(deltac+delta2)) then
C              write(15,*) 'Area IV'
        stress(2) = fac/sqrt((rdisp(2)-delta2))
        ddsddr(2,2) = -fac/2*((rdisp(2)-delta2))**(-3.d0/2.d0)
        lOpenClose = 3
        else if (rdisp(2).GT.(deltac+delta2)) then
C              write(15,*) 'Area V'
          stress(2) = 0
          ddsddr(2,2) = 0
          lOpenClose = 4
      end if
      END IF
         IF (lOpenClose.NE.iold.AND.iold.EQ.0.AND.KINC.GT.3) THEN
C Restart if more than one contact pair opens (iold=0) in 2nd call
         IF (KIT.EQ.2) THEN
      iopen = iopen + 1
         END IF
C        write(15,*) 'Status: iopen=', iopen, 'at int point', IINTP,
C    1 'in element', JELEM, 'and increment', KINC
C        write(15,*) 'lOpenClose =',lOpenclose,'iold=',iold,'KIT=', KIT
c Possible restart procedure
         IF (iopen.gt.1) THEN
C        write(15,*) 'Too many contact openings: reduce increment'
         END IF
       END IF
c Restart if one contact pair closes (iold=1/lOpenClose=0)
      IF (lOpenClose.EQ.0.AND.iold.EQ.1.AND.KINC.GE.2) THEN
         iclose = iclose + 1
C        write(15,*) 'Status: iclose=', iclose, 'at int point', IINTP,
C    1 'in element', JELEM, 'and increment', KINC
C        write(15,*) 'lOpenClose =',lOpenclose,'iold=',iold,'KIT=', KIT
         IF (iclose.gt.0) THEN
C          write(15,*) 'Elastic unloading possible: reduce increment'
         END IF
      END IF
c Restart with PNEWDT (if PNEWDT less than 1)
      IF (iclose.gt.0) THEN
         PNEWDT = 1.0
      ELSE IF (iopen.gt.4) THEN
         PNEWDT = 1.0
      END IF
c Stiffness matrix according to ABAQUS definition: -dF/du!!
         stress(2) = - stress(2)
```

```fortran
      SVARS(IINTP) = lOpenClose
      return
      end
C-----------------------------------------------------------------------
      subroutine KASET1(DMATRIX, IDIMX)
      INCLUDE 'ABA_PARAM.INC'
      PARAMETER (ZERO = 0.0D0)
      DIMENSION DMATRIX(IDIMX)
      DO i=1, IDIMX
         DMATRIX(i) = ZERO
      END DO
      RETURN
      END
C-----------------------------------------------------------------------
      subroutine KASET2(DMATRIX, IDIMX, IDIMY)
      INCLUDE 'ABA_PARAM.INC'
      PARAMETER (ZERO = 0.0D0)
      DIMENSION DMATRIX(IDIMX, IDIMY)
      DO I = 1, IDIMX
         DO J = 1, IDIMY
            DMATRIX(I,J) = ZERO
         END DO
      END DO
      RETURN
      END
```

REFERENCES

Abunima, H., Teh, J., Lai, C.M. and Jabir, H. (2018). "A systematic review of reliability studies on composite power systems: A coherent taxonomy motivations, open challenges, recommendations, and new research directions." *Energies*, 11(9), 1–37.

Alexandrov, N.M., Dennis, J.E., Lewis, R.M. and Torczon, V. (1998). "A trust-region framework for managing the use of approximation models in optimization." *Structural Optimization*, 15(1), 16–23.

Alfano, G. (2006). "On the influence of the shape of the interface law on the application of cohesive-zone models." *Composites Science and Technology*, 66(6), 723–730.

Alfano, G. and Crisfield, M. (2001). "Finite element interface models for the delamination analysis of laminated composites: mechanical and computational issues." *International Journal for Numerical Methods in Engineering*, 50(7), 1701–1736.

Alış, Ö.F. and Rabitz, H. (2001). "Efficient implementation of high dimensional model representations." *Journal of Mathematical Chemistry,* 29(2), 127–142.

Allix, O. and Corigliano, A. (1996). "Modeling and simulation of crack propagation in mixed-modes interlaminar fracture specimens." *International Journal of Fracture*, 77(2), 111–140.

Anderson, T.L. (2017). *Fracture Mechanics: fundamentals and applications*, CRC press, Florida.

Andrews, D.J. (1976). "Rupture velocity of plane strain shear cracks." *Journal of Geophysical Research*, 81(32), 5679–5687.

Arregui-Mena, J.D., Margetts, L. and Mummery, P.M. (2016). "Practical application of the stochastic finite element method." *Archives of Computational Methods in Engineering*, 23(1), 171–190.

Atluri, S.N., Kobayashi, A.S. and Nakagaki, M. (1975). "An assumed displacement hybrid finite element model for linear fracture mechanics." *International Journal of Fracture*, 11(2), 257–271.

Balabanov, V.O., Giunta, A.A., Golovidov, O., Grossman, B., Mason, W.H., Watson, L.T. and Haftka, R.T. (1999). "Reasonable design space approach to response surface approximation." *Journal of Aircraft*, 36(1), 308–315.

Balu, A.S. and Rao, B.N. (2011). "Explicit fuzzy analysis of systems with imprecise properties." *International Journal of Mechanics and Materials in Design,* 7(4), 283–289.

Balu, A.S. and Rao, B.N. (2012). "High dimensional model representation based formulations for fuzzy finite element analysis of structures." *Finite Elements in Analysis and Design*, 50, 17–230.

Balu, A.S. and Rao, B.N. (2012). "Inverse structural reliability analysis under mixed uncertainties using high dimensional model representation and fast fourier transform." *Engineering Structures*, 37, 224–234.

Balu, A.S. and Rao, B.N. (2013). "Confidence bounds on design variables using high-dimensional model representation – based inverse reliability analysis." *Journal of Structural Engineering*, 139(6), 985–996.

Balu, A.S. and Rao, B.N. (2014). "Efficient assessment of structural reliability in presence of random and fuzzy uncertainties." *Journal of Mechanical Design*, 136(5), 051008-11.

Bao, G., Ho, S., Suo, Z. and Fan, B. (1992). "The role of material orthotropy in fracture specimens for composites." *International Journal of Solids and Structures*, 29(9), 1105–1116.

Baran, I., Cinar, K., Ersoy, N., Akkerman, R. and Hattel, J.H. (2017). "A review on the mechanical modeling of composite manufacturing processes." *Archives of Computational Methods in Engineering*, 24(2), 365–395.

Barenblatt, G.I. (1959). "The formation of equilibrium cracks during brittle fracture. General ideas and hypotheses: axially-symmetric cracks." *Journal of Applied Mathematics and Mechanics*, 23(3), 622–636.

Barenblatt, G.I. (1962). "The mathematical theory of equilibrium cracks in brittle fracture." *Advances in Applied Mechanics*, 7, 55–129.

Behroozinia, P., Taheri, S. and Mirzaeifar, R. (2018). "An investigation of intelligent tires using multiscale modeling of cord-rubber composites." *Mechanics Based Design of Structures and Machines*, 46(2), 168–183.

Bolotin, V. V. (2001). "Mechanics of delaminations in laminate composite structures." *Mechanics of Composite Materials*, 37(5-6), 367–380.

Bolotin, V.V. (1996). "Delaminations in composite structures: its origin, buckling, growth and stability." *Composites Part B: Engineering*, 27(2), 129–145.

Booker, A.J., Dennis, J.E., Frank, P.D., Serafini, D.B., Torczon, V. and Trosset, M.W. (1999). "A rigorous framework for optimization of expensive functions by surrogates." *Structural Optimization*, 17(1), 1–13.

Carlsson, L.A., Gillespie Jr, J.W. and Pipes, R.B. (1986). "On the analysis and design of the end notched flexure (ENF) specimen for mode II testing." *Journal of Composite Materials*, 20(6), 594–604.

Chang, T.P., Hu, C.Y. and Jane, K.C. (1998). "Vibration analysis of delaminated composite plates under axial load." *Journal of Structural Mechanics*, 26(2), 195–218.

Chaves, F.J., Da Silva, L.F.M., De Moura, M.F.S.F., Dillard, D.A. and Esteves, V.H.C. (2014). "Fracture mechanics tests in adhesively bonded joints: a literature review." *The Journal of Adhesion*, 90(12), 955–992.

Chen, G. and Baker, G. (2005). "One-dimensional nonlinear model for prediction of crack spacing in concrete pavements." *Advances in Structural Engineering,* 8(6), 595–602.

Chen, J., Crisfield, M., Kinloch, A.J., Busso, E.P., Matthews, F.L. and Qiu, Y. (1999). "Predicting progressive delamination of composite material specimens via interface elements." *Mechanics of Composite Materials and Structures*, 6(4), 301–317.

Chowdhury, R. and Adhikari, S. (2010). "High dimensional model representation for stochastic finite element analysis." *Applied Mathematical Modelling*, 34(12), 3917–3932.

Clarke, S.M., Griebsch, J.H. and Simpson, T.W. (2005). "Analysis of support vector regression for approximation of complex engineering analyses." *Journal of Mechanical Design*, 127(6), 1077–1087.

Cox, B.N. and Marshall, D.B. (1991). "The determination of crack bridging forces." *International Journal of Fracture*, 49(3), 159–176.

Cramer, G.M., Ford, R.A. and Hall, R.L. (1976). "Estimation of toxic hazard—a decision tree approach." *Food and cosmetics toxicology*, 16(3), 255–276.

Davidson, B.D. and Sundararaman, V. (1996a). "A single leg bending test for interracial fracture toughness determination." *International Journal of Fracture*, 78(2), 193–210.

Davidson, B.D., Hu, H. and Schapery, R.A. (1995). "An analytical crack-tip element for layered elastic structures." *Journal of Applied Mechanics*, 62(2), 294–305.

De Dear, R. and Brager, G.S. (2001). "The adaptive model of thermal comfort and energy conservation in the built environment." *International journal of biometeorology*, 45(2), 100–108.

Dennis, J.E. and Torczon, V. (1997). "Managing approximation models in optimization." *Multidisciplinary Design Optimization: State-of-the-Art*, 330–347.

Desai, C.K., Basu, S. and Parameswaran, V. (2016). "Determination of traction separation law for interfacial failure in adhesive joints at different loading rates." *The Journal of Adhesion*, 92(10), 819–839.

Devitt, D.F. (1980). "A method for determining the mode I delamination fracture toughness of elastic and viscoelastic materials." *Journal of Composite Materials*, 14, 270–285.

Dey, S., Mukhopadhyay, T. and Adhikari, S. (2017). "Metamodel based high-fidelity stochastic analysis of composite laminates: a concise review with critical comparative assessment." *Composite Structures,* 171, 227–250.

Dey, S., Mukhopadhyay, T., Spickenheuer, A., Adhikari, S. and Heinrich, G. (2016). "Bottom up surrogate based approach for stochastic frequency response analysis of laminated composite plates." *Composite Structures*, 140, 712–727.

Di Landro, L., Montalto, A., Bettini, P., Guerra, S., Montagnoli, F. and Rigamonti, M. (2017). "Detection of voids in carbon/epoxy laminates and their influence on mechanical properties." *Polymers and Polymer Composites*, 25(5), 371–380.

Dugdale, D.S. (1960). "Yielding of steel sheets containing slits." *Journal of the Mechanics and Physics of Solids*, 8(2), 100–104.

Durrleman, S. and Simon, R. (1989). "Flexible regression models with cubic splines." *Statistics in medicine*, 8(5), 551–561.

Dyn, N., Levin, D. and Rippa, S. (1986). "Numerical procedures for surface fitting of scattered data by radial functions." *SIAM Journal on Scientific and Statistical Computing*, 7(2), 639–659.

Elices, M.G.G.V., Guinea, G.V., Gomez, J. and Planas, J. (2002). "The cohesive zone model: advantages, limitations and challenges." *Engineering Fracture Mechanics*, 69(2), 137–163.

Feih, S. (2006). "Development of a user element in ABAQUS for modeling of cohesive laws in composite structures." Riso national laboratory, Roskilde, Denmark.

Feih, S., Wei, J., Kingshott, P. and Sørensen, B.F. (2005). "The influence of fibre sizing on the strength and fracture toughness of glass fibre composites." *Composites Part A: Applied Science and Manufacturing,* 36(2), 245–255.

Feraren, P. and Jensen, H.M. (2004). "Cohesive zone modeling of interface fracture near flaws in adhesive joints." *Engineering Fracture Mechanics*, 71(15), 2125–2142.

Friedman, J.H. (1991). "Multivariate adaptive regression splines." *The Annals of Statistics*, 19(1), 1–67.

Frossard, G., Cugnoni, J., Gmür, T. and Botsis, J. (2017). "An efficient method for fiber bridging traction identification based on the R-curve: Formulation and experimental validation." *Composite Structures*, 175, 135–144.

Gain, A.L., Carroll, J., Paulino, G.H., and Lambros, J. (2011). "A hybrid experimental/numerical technique to extract cohesive fracture properties for mode-I fracture of quasi-brittle materials." *International Journal of Fracture*, 169(2), 113–131.

Gao, Z. H., Wang, C., and Huang, J. (2015). "HDMR-based Surrogate Model for High Dimensional Aerodynamic Design Problems." In *16th AIAA/ISSMO Multidisciplinary Analysis and Optimization Conference* (p. 3094).

Ghanem, R. and Spanos, P.D. (1990). "Polynomial chaos in stochastic finite elements." *Journal of Applied Mechanics*, 57(1), 197–202.

Ghobadi, A. (2017). "Common type of damages in composites and their inspections." *World Journal of Mechanics*, 7(2), 1–24.

Giunta, A. and Watson, L. (1998). "A comparison of approximation modeling techniques-polynomial versus interpolating models." *AIAA/USAF/NASA/ISSMO Symposium on Multidisciplinary Analysis and Optimization* (p. 4758).

Giunta, A., Wojtkiewicz, S. and Eldred, M. (2003). "Overview of modern design of experiments methods for computational simulations." *Aerospace Sciences Meeting and Exhibit,* 649.

Giunta, A.A., Balabanov, V., Haim, D., Grossman, B., Mason, W.H., Watson, L.T. and Haftka, R.T. (1997). "Multidisciplinary optimisation of a supersonic transport using design of experiments theory and response surface modeling." *The Aeronautical Journal*, 101(1008), 347–356.

Goldberger, A.S. (1962). "Best linear unbiased prediction in the generalized linear regression model." *Journal of the American Statistical Association*, 57(298), 369–375.

Gowrishankar, S., Mei, H., Liechti, K. M. and Huang, R. (2012). "A comparison of direct and iterative methods for determining traction-separation relations." *International Journal of Fracture*, 177(2), 109–128.

Griffith, A. (1921). "The phenomena of rupture and flow in solids." *Philosophical Transactions of the Royal Society of London. Series A, Containing Papers of a Mathematical or Physical Character,* 221, 163–198.

Heidari-Rarani, M., Shokrieh, M.M. and Camanho, P.P. (2013). "Finite element modeling of mode I delamination growth in laminated DCB specimens with R-curve effects." *Composites Part B: Engineering*, 45(1), 897–903.

Hillerborg, A., Modéer, M. and Petersson, P.E. (1976). "Analysis of crack formation and crack growth in concrete by means of fracture mechanics and finite elements." *Cement Concrete Research*, 6(6), 773–781.

Högberg, J.L., Sørensen, B.F. and Stigh, U. (2007). "Constitutive behavior of mixed mode loaded adhesive layer." *International Journal of Solids and Structures*, 44(25-26), 8335–8354.

Hutchinson, J.W. and Evans, A.G. (2000). "Mechanics of materials: top-down approaches to fracture." *Acta Materialia*, 48(1), 125–135.

Hutchinson, J.W. and Suo, Z. (1991). "Mixed mode cracking in layered materials." *Advances in Applied Mechanics*, 29, 63–191.

Irwin, G.R. (1957). "Analysis of stresses and strains near the end of a crack traversing a plate." *Journal of Applied Mechanics,* 24, 361–366.

Ivens, J., Albertsen, H., Wevers, M., Verpoest, I. and Peters, P. (1995). "Interlaminar fracture toughness of CFRP influenced by fibre surface treatment: part 2. modeling of the interface effect." *Composites Science and Technology*, 54(2), 147–159.

Jacobsen, T.K. and Sørensen, B.F. (2001). "Mode I intra-laminar crack growth in composites—modelling of R-curves from measured bridging laws." *Composites Part A: Applied Science and Manufacturing*, 32(1), 1–11.

Jiang, L. and Li, X. (2015). "Multi-element least square HDMR methods and their applications for stochastic multiscale model reduction." *Journal of Compututational Physics*, 294, 439–461.

Jin, R., Chen, W. and Simpson, T.W. (2001). "Comparative studies of metamodeling techniques under multiple modeling criteria." *Structural and Multidisciplinary Optimization*, 23(1), 1–13.

Jin, Z.H. and Sun, C.T. (2005). "Cohesive zone modeling of interface fracture in elastic bi-materials." *Engineering Fracture Mechanics*, 72(12), 1805–1817.

Jin, Z.H. and Sun, C.T. (2006). "A comparison of cohesive zone modeling and classical fracture mechanics based on near tip stress field." *International Journal of Solids and Structures*, 43(5), 1047–1060.

Johnson, W.S. and Mangalgiri, P.D. (1987). "Investigation of fiber bridging in double cantilever beam specimens." *Journal of Composites, Technology and Research*, 9(1), 10–13.

Kim, B.S., Lee, Y.B. and Choi, D.H. (2009). "Comparison study on the accuracy of metamodeling technique for non-convex functions." *Journal of Mechanical Science and Technology*, 23(4), 1175–1181.

Kim, C., Wang, S., Kang, E. and Lee, K. (2006). "New design process for reliability-based topology optimization of a laser scanned model." *Mechanics Based Design of Structures and Machines*, 34(3), 325–347.

Kim, J.K. and Mai, Y.W. (1991). "High strength, high fracture toughness fibre composites with interface control-a review." *Composites Science and Technology*, 41(4), 333–378.

Kleijnen, J.P.C. (1987). *Statistical tools for simulation practitioners*. New York: Marcel Dekker.

Koch, P.N., Simpson, T.W., Allen, J.K. and Mistree, F. (1999). "Statistical approximations for multidisciplinary design optimization: the problem of size." *Journal of Aircraft*, 36(1), 275–286.

Koehler, J.R. (1998). "Estimating the response, derivatives, and transmitted variance using computer experiments." *Computing Science and Statistics*, 25–32.

Kossakowski, P.G. (2007). "Influence of anisotropy on the energy release rate GI for highly orthotropic materials." *Journal of Theoretical and Applied Mechanics*, 45, 739–752.

Koziel, S. and Yang, X.S. (Eds.). (2011). *Computational optimization, methods and algorithms* (Vol. 356). Springer.

Krueger, R. (2002). *The virtual crack closure technique: history, approach and 369 applications* (No. 370, p. 10). Technical Report NASA/CR-2002-211628 ICASE Report.

Lancaster, P. and Salkauskas, K. (1981). "Surfaces generated by moving least squares methods." *Mathematics of computation*, 37(155), 141–158.

Langley, P. and Simon, H.A. (1995). "Applications of machine learning and rule induction." *Communications of the ACM*, 38(11), 54–64.

Leary, S.J., Bhaskar, A. and Keane, A.J. (2003). A knowledge-based approach to response surface modeling in multi-fidelity optimization." *Journal of Global Optimization*, 26(3), 297–319.

Lee, M.J., Cho, T.M., Kim, W.S., Lee, B.C. and Lee, J.J. (2010). "Determination of cohesive parameters for a mixed-mode cohesive zone model." *International Journal of Adhesion and Adhesives*, 30(5), 322–328.

Lee, T.T. and Jeng, J.T. (1998). "The Chebyshev-polynomials-based unified model neural networks for function approximation." *IEEE Transactions on Systems, Man, and Cybernetics, Part B (Cybernetics)*, 28(6), 925–935.

Li, G., Wang, S.W., Rosenthal, C. and Rabitz, H. (2001). "High dimensional model representations generated from low dimensional data samples. I. mp-Cut-HDMR." *Journal of Mathematical Chemistry*, 30(1), 1–30.

Li, G., Wang, S.W., Rabitz, H., Wang, S. and Jaffé, P. (2002). "Global uncertainty assessments by high dimensional model representations (HDMR)." *Chemical Engineering Science*, 57(21), 4445–4460.

Li, G., Xing, X., Welsh, W. and Rabitz, H. (2017). "High dimensional model representation constructed by support vector regression. I. independent variables with known probability distributions." *Journal of Mathematical Chemistry,* 55(1), 278–303.

Li, G.Y., Rosenthal, C. and Rabitz, H. (2001). "High dimensional model representations." *The Journal of Physical Chemistry A*, 105(33), 7765–7777.

Li, S. and Thouless, M.D. (2006). "Mixed-mode cohesive-zone models for fracture of an adhesively bonded polymer—matrix composite." *Engineering Fracture Mechanics*, 73(1), 64–78.

Li, S., Thouless, M.D., Waas, A.M., Schroeder, J.A. and Zavattieri, P.D. (2005a). "Use of a cohesive-zone model to analyze the fracture of a fiber-reinforced polymer-matrix composite." *Composites Science and Technology*, 65(3–4), 537–549.

Li, S., Thouless, M.D., Waas, A.M., Schroeder, J.A. and Zavattieri, P.D. (2005b). "Use of mode-I cohesive-zone models to describe the fracture of an adhesively-bonded polymer-matrix composite." *Composites Science and Technology*, 65(2), 281–293.

Li, Y.F., Ng, S.H., Xie, M. and Goh, T.N. (2010). "A systematic comparison of metamodeling techniques for simulation optimization in decision support systems." *Applied Soft Computing*, 10(4), 1257–1273.

Liechti, K.M. and Chai, Y.S. (1992). "Asymmetric shielding in interfacial fracture under in-plane shear." *Journal of Applied Mechanics*, 59(2), 295–304.

Liu, X., Duddu, R. and Waisman, H. (2012). "Discrete damage zone model for fracture initiation and propagation." *Engineering Fracture Mechanics*, 92, 1–18.

Lu, X., Lapusta, N. and Rosakis, A.J. (2010). "Pulse-like and crack-like dynamic shear ruptures on frictional interfaces: experimental evidence, numerical modeling, and implications." *International Journal of Fracture*, 163(1–2), 27–39.

Maleque, M.A. and Salit, M.S. (2013). *Materials selection and design*. Springer Singapore.

Mangalgiri, P.D. (1999). "Composite materials for aerospace applications." *Bulletin of Materials Science*, 22(3), 657–664.

Manshadi, B.D., Farmand-Ashtiani, E., Botsis, J. and Vassilopoulos, A.P. (2014). "An iterative analytical/experimental study of bridging in delamination of the double cantilever beam specimen." *Composites Part A: Applied Science and Manufacturing*, 61, 43–50.

Martin, J.D. and Simpson, T.W. (2005). "Use of kriging models to approximate deterministic computer models." *American Institute of Aeronautics and Astronautics*, 43(4), 853–863.

Mello, A.W. and Liechti K.M. (2006). "The effect of self-assembled monolayers on interfacial fracture." *Journal of Applied Mechanics*, 73(5), 860–870.

Mohammed, I. and Liechti, K.M. (2000). "Cohesive zone modeling of crack nucleation at bimaterial corners." *Journal of the Mechanics and Physics of Solids*, 48(4), 735–764.

Moroni, F. and Pirondi, A. (2011). "Cohesive zone model simulation of fatigue debonding along interfaces." *Procedia Engineering*, 10, 1829–1834.

Morris, M.D., Mitchell, T.J. and Ylvisaker, D. (1993). "Bayesian design and analysis of computer experiments: use of derivatives in surface prediction." *Technometrics*, 35(3), 243–255.

Mukhopadhyay, T., Chowdhury, R. and Chakrabarti, A. (2016). "Structural damage identification: a random sampling-high dimensional model representation approach." *Advances in Structural Engineering*, 19(6), 908–927.

Mukhopadhyaya, T., Dey, T.K., Chowdhury, R., Chakrabarti, A. and Adhikari, S. (2015). "Optimum design of FRP bridge deck: an efficient RS-HDMR based approach." *Structural and Multidisciplinary Optimization*, 52(3), 459–477.

Mullur, A.A. and Messac, A. (2005). "Extended radial basis functions: more flexible and effective metamodeling." *American Institute of Aeronautics and Astronautics*, 43(6), 1306–1315.

Myers, D.E. (1982). "Matrix formulation of co-kriging." *Journal of the International Association for Mathematical Geology*, 14(3), 249–257.

Naveen, B.O. and Balu, A.S. (2017). "HDMR-Based model update in structural damage identification." *International Journal of Computational Methods*, 15(2), 1840004.

Needleman, A. (1987). "A continuum model for void nucleation by inclusion debonding." *Journal of Applied Mechanics*, 54(3), 525–531.

Needleman, A. (1990). "An analysis of decohesion along an imperfect interface." *Non-Linear Fracture*, Springer, Dordrecht, 21–40.

O'Brien, T.K. (1998). "Interlaminar fracture toughness: the long and winding road to standardization." *Composites Part B: Engineering*, 29(1), 57–62.

Oliveira, J.M., de Moura, M. F. and Morais, J.J. (2009). "Application of the end loaded split and single-leg bending tests to the mixed-mode fracture characterization of wood." *Holzforschung*, 63(5), 597–602.

Osio, I.G. and Amon, C.H. (1996). "An engineering design methodology with multistage bayesian surrogates and optimal sampling." *Research in Engineering Design*, 8(4), 189–206.

Ouyang, Z. and Wan, B. (2009). "An analytical model of FRP-concrete bond deterioration in moist environment." *Advances in Structural Engineering*, 12(6), 761–769.

Papadrakakis, M., Lagaros, N.D. and Tsompanakis, Y. (1998). "Structural optimization using evolution strategies and neural networks." *Computer Methods in Applied Mechanics and Engineering*, 156(1–4), 309–333.

Pappas, G. and Botsis, J. (2016). "Intralaminar fracture of unidirectional carbon/epoxy composite: experimental results and numerical analysis." *International Journal of Solids and Structures*, 85, 114–124.

Pappas, G., Joncas, S., Michaud, V. and Botsis, J. (2017). "The influence of through-thickness reinforcement geometry and pattern on delamination of fiber-reinforced composites: Part II–Modeling." *Composite Structures*, 181, 379–390.

Park, J. and Sandberg, I.W. (1991). "Universal approximation using radial-basis-function networks." *Neural computation*, 3(2), 246–257.

Park, K. and Paulino, G.H. (2012). "Computational implementation of the PPR potential-based cohesive model in ABAQUS: educational perspective." *Engineering Fracture Mechanics*, 93, 239–262.

Park, S. and Dillard, D.A. (2007). "Development of a simple mixed-mode fracture test and the resulting fracture energy envelope for an adhesive bond." *International Journal of Fracture*, 148(3), 261–271.

Parks, D.M. (1974). "A stiffness derivative finite element technique for determination of crack tip stress intensity factors." *International Journal of Fracture*, 10(4), 487–502.

Parmigiani, J.P. and Thouless, M.D. (2007). "The effects of cohesive strength and toughness on mixed-mode delamination of beam-like geometries." *Engineering*

Fracture Mechanics, 74(17), 2675–2699.

Pirondi, A., Giuliese, G., Moroni, F., Bernasconi, A. and Jamil, A. (2014). "Comparative study of cohesive zone and virtual crack closure techniques for three-dimensional fatigue debonding." *The Journal of Adhesion*, 90, 457–481.

Rabitz, H., Aliş, Ö.F., Shorter, J. and Shim, K. (1999). "Efficient input-output model representations." *Computer Physics Communications*, 117(1–2), 11–20.

Rafiee, R. and Ghorbanhosseini, A. (2018). "Predicting mechanical properties of fuzzy fiber reinforced composites: radially grown carbon nanotubes on the carbon fiber." *International Journal of Mechanics and Materials in Design*, 14(1), 37–50.

Raju, I.S. (1987). "Calculation of strain-energy release rates with higher order and singular finite elements." *Engineering Fracture Mechanics*, 28(3), 251–274.

Rasmussen, J. (1998). "Nonlinear programming by cumulative approximation refinement." *Structural optimization*, 15(1), 1–7.

Razavi, S.M.J., Aliha, M.R.M. and Berto, F. (2018). "Application of an average strain energy density criterion to obtain the mixed mode fracture load of granite rock tested with the cracked asymmetric four-point bend specimens." *Theoretical and Applied Fracture Mechanics*, 97, 419–425.

Reeder, J.R. and Crews, J.H. (1990). "Mixed-mode bending method for delamination testing." *American Institute of Aeronautics and Astronautics*, 28(7), 1270–1276.

Reeder, J.R. and Crews, J.H. (1992). "Redesign of the mixed-mode bending delamination test to reduce nonlinear effects." *Journal of Composites, Technology and Research*, 14(1), 12–19.

Renaud, J.E. and Gabriele, G.A. (1994). "Approximation in nonhierarchic system optimization." *American Institute of Aeronautics and Astronautics*, 32(1), 198–205.

Rice, J.R. (1968). "A path independent integral and the approximate analysis of strain concentration by notches and cracks." *Journal of Applied Mechanics*, 35(2), 379–386.

Roe, K.L. and Siegmund, T. (2003). "An irreversible cohesive zone model for interface fatigue crack growth simulation." *Engineering fracture mechanics*, 70(2), 209–232.

Robinson, P. and Song, D.Q. (1992). "A modified DCB specimen for mode-I testing of multidirectional laminates." *Journal of Composite Materials*, 26(11), 1554–1577.

Rosakis, A.J. (2002). "Intersonic shear cracks and fault ruptures." Advances in Physics, 51(4), 1189–1257.

Ruppert, D. and Wand, M.P. (1994). "Multivariate locally weighted least squares regression." *The annals of statistics*, 1346–1370.

Russell, A.J. and Street, K.N. (1985). "Moisture and temperature effects on the mixed-mode delamination fracture of unidirectional graphite/epoxy." *Delamination and Debonding of Materials*, 349–370.

Rybicki, E.F. and Kanninen, M.F. (1977). "A finite element calculation of stress intensity factors by a modified crack closure integral." *Engineering Fracture Mechanics*, 9(4), 931–938.

Sacks, J., Schiller, S.B. and Welch, W.J. (1989a). "Designs for computer experiments." *Technometrics*, 31(1), 41–47.

Sacks, J., Welch, W.J., Mitchell, T.J. and Wynn, H.P. (1989b). "Design and analysis of computer experiments." *Statistical Science*, 4(4), 409–435.

Salih, S., Davey, K. and Zou, Z. (2019). "A computationally efficient cohesive zone model for fatigue." *Fatigue & Fracture of Engineering Materials & Structures*, 1–15. DOI: 10.1111/ffe.12927

Schellekens, J.C.J. and De Borst, R. (1993). "On the numerical integration of interface elements." *International Journal for Numerical Methods in Engineering*, 36(1), 43–66.

Segurado, J. and Llorca, J. (2004). "A new three-dimensional interface finite element to simulate fracture in composites." *International Journal of Solids and Structures*, 41(11–12), 2977–2993.

Sela, N. and Ishai, O. (1989). "Interlaminar fracture toughness and toughening of laminated composite materials: a review." *Composites*, 20(5), 423–435.

Shabir, Z., Van Der Giessen, E., Duarte, C.A. and Simone, A. (2011). "The role of cohesive properties on intergranular crack propagation in brittle polycrystals." *Modeling and Simulation in Materials Science and Engineering*, 19(3), 035006.

Shanmugam, V., Penmetsa, R. and Tuegel, E. (2012). "Calibration of a probabilistic cohesive zone model for generating a fracture nomograph." *Fatigue and Fracture of Engineering Materials and Structures*, 35(4), 328–346.

Shanmugam, V., Penmetsa, R., Tuegel, E. and Clay, S. (2013). "Stochastic modeling of delamination growth in unidirectional composite DCB specimens using cohesive zone models." *Composite Structures*, 102, 38–60.

Sheppard, A., Kelly, D. and Tong, L. (1998). "A damage zone model for the failure analysis of adhesively bonded joints." *International Journal of Adhesion and Adhesives*, 18(6), 385–400.

Shet, C. and Chandra, N. (2002). "Analysis of energy balance when using cohesive zone models to simulate fracture processes." *Journal of Engineering Materials and Technology*, 124(4), 440–450.

Shi, Z., Needleman, A. and Ben-Zion, Y. (2010). "Slip modes and partitioning of energy during dynamic frictional sliding between identical elastic–viscoplastic solids." *International Journal of Fracture*, 162(1–2), 51–67.

Shih, C.F. (1991). "Cracks on bimaterial interfaces: elasticity and plasticity aspects." *Materials Science and Engineering: A*, 143(1–2), 77–90.

Shin, Y.S. and Grandhi, R.V. (2001). "A global structural optimization technique using an interval method." *Structural and Multidisciplinary Optimization*, 22(5), 351–363.

Shirani, A. and Liechti, K.M. (1998). "A calibrated fracture process zone model for thin film blistering." *Recent Advances in Fracture Mechanics*, 93, 281–314.

Shymchenko, A.V., Tereshchenko, V.V., Ryabov, Y.A., Salkutsan, S.V. and Borovkov, A.I. (2017). "Review of the computational approaches to advanced materials simulation in accordance with modern advanced manufacturing trends." *Materials Physics and Mechanics*, 32(3), 328–352.

Simpson, T.W., Mauery, T.M., Korte, J.J. and Mistree, F. (2001b). "Kriging models for global approximation in simulation-based multidisciplinary design optimization." *American Institute of Aeronautics and Astronautics*, 39(12), 2233–2241.

Simpson, T.W., Poplinski, J.D., Koch, P.N. and Allen, J.K. (2001c). "Metamodels for computer-based engineering design: survey and recommendations." *Engineering with Computers*, 17(2), 129–150.

Smith, R.A. (2009). "Composite defects and their detection." *Materials Science and Engineering*, 3, 103–143.

Song, K., Dávila, C.G. and Rose, C.A. (2008). "Guidelines and parameter selection for the simulation of progressive delamination." ABAQUS User's Conference 41, 43–44.

Sørensen, B.F. and Jacobsen, T.K. (1998). "Large-scale bridging in composites: R-curves and bridging laws." *Composites Part A: Applied Science and Manufacturing*, 29, 1443–1451.

Sørensen, B.F. and Jacobsen, T.K. (2000). "Crack growth in composites applicability of R-curves and bridging laws." *Plastics, Rubber and Composites*, 29(3), 119–133.

Sorensen, L., Botsis, J., Gmür, T. and Cugnoni, J. (2007). "Delamination detection and characterisation of bridging tractions using long FBG optical sensors." *Composites Part A: Applied Science and Manufacturing*, 38, 2087–2096.

Sorensen, L., Botsis, J., Gmür, T. and Humbert, L. (2008). "Bridging tractions in mode I delamination: measurements and simulations." *Composites Science and Technology*, 68(12), 2350–2358.

Spearing, S.M. and Evans, A.G. (1992). "The role of fiber bridging in the delamination resistance of fiber-reinforced composites." *Acta Metallurgica et Materialia*, 40(9), 2191–2199.

Spring, D.W. and Paulino, G.H. (2014). "A growing library of three-dimensional cohesive elements for use in ABAQUS." *Engineering Fracture Mechanics*, 126, 190–216.

Stumpf, H. and Le, K.C. (1990). "Variational principles of nonlinear fracture mechanics." *Acta Mechanica*, 83(1-2), 25–37.

Sundararaman, V. and Davidson, B.D. (1997). "An unsymmetric double cantilever beam test for interfacial fracture toughness determination." *International Journal of Solids and Structures*, 34(7), 799–817.

Suo, Z., Bao, G. and Fan, B. (1992). "Delamination R-curve phenomena due to damage." *Journal of the Mechanics and Physics of Solids*, 40(1), 1–16.

Suykens, J. A. and Vandewalle, J. (1999). "Least squares support vector machine classifiers." *Neural processing letters*, 9(3), 293–300.

Szekrényes, A. and Uj, J. (2006). "Comparison of some improved solutions for mixed-mode composite delamination coupons." *Composite Structures*, 72(3), 321–329.

Tan, H., Liu, C., Huang, Y. and Geubelle, P.H. (2005). "The cohesive law for the particle/matrix interfaces in high explosives." *Journal of the Mechanics and Physics of Solids*, 53(8), 1892–1917.

Tong, L. and Steven, G.P. (1999). "Analysis and design of structural bonded joints." Univ. of Sydney, New South Wales (AU).

Toropov, V.V., Filatov, A.A. and Polynkin, A.A. (1993). "Multiparameter structural optimization using FEM and multipoint explicit approximations." *Structural Optimization*, 6(1), 7–14.

Tsai, C.L., Guan, Y.L., Ohanehi, D.C., Dillard, J.G., Dillard, D.A. and Batra, R.C. (2014). "Analysis of cohesive failure in adhesively bonded joints with the SSPH meshless method." *International Journal of Adhesion and Adhesives*, 51, 67–80.

Turon T.A. (2006). "Simulation of delamination in composites under quasi-static and fatigue loading using cohesive zone models." Ph.D. thesis, Universitat de Girona, Girona, Catalonia, Spain.

Tvergaard, V. and Hutchinson, J.W. (1992). "The relation between crack growth resistance and fracture process parameters in elastic-plastic solids." *Journal of the Mechanics and Physics of Solids*, 40(6), 1377–1397.

Tvergaard, V. and Hutchinson, J.W. (1993). "The influence of plasticity on mixed mode interface toughness." *Journal of the Mechanics and Physics of Solids*, 41(6), 1119–1135.

Valoroso, N. and Champaney, L. (2006). "A damage-mechanics-based approach for modeling decohesion in adhesively bonded assemblies." *Engineering Fracture Mechanics*, 73(18), 2774–2801.

Van Beers, W.C. and Kleijnen, J.P.C. (2003). "Kriging for interpolation in random simulation." *Journal of the Operational Research Society*, 54(3), 255–262.

Varadarajan, S., Chen, W.E.I. and Pelka, C.J. (2000). "Robust concept exploration of propulsion systems with enhanced model approximation capabilities." *Engineering Optimization*, 32, 309–334.

Victor, L.C., Chan, C.M. and Leung, C.K. (1987). "Experimental determination of the tension-softening curve in cementitious composites." *Cement and Concrete Research,* 17, 441–452.

Vossen, B.G., Schreurs, P.J., Van der sluis, O. and Geers, M.G.D (2014). "Multi-scale modeling of delamination through fibrillation." *Journal of the Mechanics and Physics of Solids*, 66, 117–132.

Wang, A.S.D., Chou, P.C. and Lei, S.C. (1984). "A stochastic model for the growth of matrix cracks in composite laminates." *Journal of Composite Materials*, 18(3), 239–254.

Wang, G.G. (2003). "Adaptive response surface method using inherited latin hypercube design points." *Journal of Mechanical Design*, 125(2), 210–220.

Wang, G.G., and Simpson, T.W. (2004). "Fuzzy clustering based hierarchical metamodeling for space reduction and design optimization." *Journal of Engineering Optimization*, 36(3), 313–335.

Wang, L., Grandhi, R.V. and Canfield, R.A. (1996). "Multivariate hermite approximation for design optimization." *International Journal for Numerical Methods in Engineering*, 39(5), 787–803.

Wang, S.W., Levy, H., Li, G. and Rabitz, H. (1999). "Fully equivalent operational models for atmospheric chemical kinetics within global chemistry-transport models." *Journal of Geophysical Research: Atmospheres*, 104(D23), 30417.

Wei, H.X., Li, Y.D., Zhao, H. and Guan, Y. (2017). "Fracture analysis on a layered multiferroic smart structure containing non-periodic interfacial cracks under magnetic/electric and mechanical loadings." *Mechanics Based Design of Structures and Machines*, 45(2), 253–270.

Welch, W.J., Buck, R.J., Sacks, J., Wynn, H.P., Mitchell, T.J. and Morris, M.D. (1992). "Screening, predicting, and computer experiments." *Technometrics*, 34(1), 15–25.

Whitney, J.M. and Pagano, N.J. (1989). "Interlaminar response of composite materials." Vol. 5, eds 1, North Holland.

Wujek, B.A. and Renaud, J.E. (1998a). "New adaptive move-limit management strategy for approximate optimization, part 1." *American Institute of Aeronautics and Astronautics*, 36(10), 1911–1921.

Wujek, B.A. and Renaud, J.E. (1998b). "New adaptive move-limit management strategy for approximate optimization, part 2." *American Institute of Aeronautics and Astronautics*, 36(10), 1922–1934.

Xu, X.P. and Needleman, A. (1994). "Numerical simulations of fast crack growth in brittle solids." *Journal of the Mechanics and Physics of Solids*, 42(9), 1397–1434.

Yao, X. (1999). "Evolving artificial neural networks." *Proceedings of the IEEE*, 87(9), 1423–1447.

Zhu, Y., Liechti, K.M. and Ravi-Chandar, K. (2009). "Direct extraction of rate-dependent traction–separation laws for polyurea/steel interfaces." *International Journal of Solids and Structures*, 46(1), 31–51.

Zou, Z., Reid, S.R., and Li, S. (2003). "A continuum damage model for delaminations in laminated composites." *Journal of the Mechanics and Physics of Solids*, 51(2), 333–356.

Zou, Z., Reid, S.R., Soden, P.D. and Li, S. (2001). "Mode separation of energy release rate for delamination in composite laminates using sub-laminates." *International Journal of Solids and Structures*, 38(15), 2597–2613.

PUBLICATIONS

INTERNATIONAL JOURNALS

1. Kesava Rao, B. and Balu, A.S. (2018). "Modeling of delamination in fiber reinforced composite using high dimensional model representation based cohesive zone model." *Journal of the Brazilian Society of Mechanical Sciences and Engineering*, Springer. (SCIE & Scopus).

2. Kesava Rao, B. and Balu, A.S. (2019). "Assessment of cohesive parameters using high dimensional model representation for mixed mode cohesive zone model." *Structures*, 19, 156–160. (Scopus).

3. Kesava Rao, B. and Balu, A.S. (2018). "Application of high dimensional model representation for fracture characterization of composite beam." *Journal of Engineering Technology*, 7, 322–336. (SCIE & Scopus).

4. Kesava Rao, B. and Balu, A.S. (2018). "Efficient simulation of single leg bending joint for mixed mode fracture." *Engineering Fracture Mechanics,* Elsevier. (SCI & Scopus) (under review).

5. Kesava Rao, B. and Balu, A.S. (2018). "Modeling crack growth in composite double cantilever beam using HDMR based cohesive zone model." *Journal of Strength, Fracture and Complexity,* IOS Press. (Scopus) (under review).

INTERNATIONAL CONFERENCES

1. Kesava Rao, B. and Balu, A.S. (2016). "Fracture characterization of bone using crack equivalent concept." *Structural Engineering Convention (SEC 2016)*, December 21–23, SERC–CSIR, Chennai, India.

2. Kesava Rao, B and Balu, A.S. (2017). "Modeling of delamination growth in composite using high dimensional model representation based cohesive zone model." *International Conference on Composite Materials and Structures (ICCMS 2017)*, December 27–29, IIT Hyderabad, India.

3. Kesava Rao, B. and Balu, A.S. (2017). "Fracture characterization of composite using high dimensional model representation based cohesive zone model." *International Conference on Theoretical Applied Computational and Experimental Mechanics (ICTACEM 2017)*, December 28–30, IIT Kharagpur, India.

4. Kesava Rao, B. and Balu, A.S. (2018). "Simulation of an experimentally investigated single leg bending joint for mixed mode fracture." *Structural Engineering Convention (SEC 2018)*, December 19–21, Kolkata, India.

CURRICULUM VITAE

1. NAME   : KESAVA RAO BATTENA.

2. DATE OF BIRTH   : September 17, 1987

3. EDUCATIONAL QUALIFICATIONS

    Degree   : Diploma
    Specialization   : Civil Engineering
    Institute   : Jawaharlal Nehru Govt. Polytechnique,
                             Ramanthapur, Hyderabad,
                             under S.B.T.E, India
    Year   : 2006

    Degree   : Bachelor of Engineering Technology (B.Tech.)
    Specialization   : Civil Engineering
    Institute   : Bapatla Engineering College, Bapatla,
                             under Acharya Nagarjuna University,
                             Guntur, India
    Year   : 2010

    Degree   : Master of Engineering Technology (M.Tech.)
    Specialization   : Structural Engineering
    Institute   : J.N.T.U. College of Engineering, Kakinada, India.
    Year   : 2012

    Degree   : Doctor of Philosophy (Ph.D)
    Specialization   : Structural Engineering
    Institute   : National Institute of Technology Karnataka, Surathkal,
                             India
    Registration Date   : January 05, 2015

4. ADDRESS   : S/o B. Srinivasa Rao,
                             #61-13-8, Krishnaveni Road, Ramalingeswara Nagar,
                             Vijayawada - 520 013, Andhra Pradesh, India
                             Mobile: +91 8123740325/9493447208
                             Email: kesava.battena@gmail.com